UNIVERSITY OF SOUTHAMPTON

Nonlinear Optics of Light-induced Structural Transitions in Confined Gallium

by

Kevin Francis MacDonald

A thesis submitted for the degree of
Doctor of Philosophy

Department of Physics and Astronomy
Faculty of Science

April 2002

UNIVERSITY OF SOUTHAMPTON

ABSTRACT

FACULTY OF SCIENCE
DEPARTMENT OF PHYSICS AND ASTRONOMY

Doctor of Philosophy

NONLINEAR OPTICS OF LIGHT-INDUCED STRUCTURAL TRANSITIONS IN CONFINED GALLIUM

by Kevin Francis MacDonald

An ultra-high-vacuum system has been constructed to facilitate atomic-beam deposition of gallium on cryogenically cooled substrates, including optical fibre tips. Alongside this, a fibre-optic pump-probe diagnostic system, based on semiconductor lasers, has been developed to perform in-situ measurements of the linear and transient nonlinear optical properties of gallium nanostructures, both during and after deposition. This unique combination of deposition and optical diagnostic techniques has provided a new means of studying the growth and optical characteristics of gallium nanostructures under highly controlled conditions.

The linear and nonlinear optical properties of a new material structure, namely gallium/glass interfaces prepared by ultrafast pulsed laser deposition (UPLD), have been studied for the first time. The reflectivity characteristics of these high-quality interfaces were measured under varying conditions of temperature and light intensity at 810 nm: At temperatures several degrees below gallium's melting point T_m, excitation intensities of just a few kW.cm^{-2} were seen to induce reflectivity changes of more than 30%. Experiments performed with a nanosecond optical parametric oscillator have illustrated that UPLD gallium/silica interfaces show a nonlinear response to optical excitation in the 440-680 nm wavelength range: Fluences of less than 10 mJ.cm^{-2} were seen to induce reflectivity changes of up to 35%, even at temperatures 15° below T_m.

It has been found that low power (17 μW average) laser illumination of cryogenically cooled substrates during atomic-beam deposition of gallium leads to the formation of uniformly sized gallium nanoparticles. This phenomenon is believed to be the result of a non-thermal light-assisted particle self-assembly process.

Gallium nanoparticles have been seen to show a strongly temperature-dependent nonlinear response to low intensity, infrared (1550 nm) optical excitation: 1 μs pulses with peak intensities in the kW.cm^{-2} range induced reversible reflectivity changes with a magnitude of as much as several percent (in the vicinity of the phase transition temperatures) and a typical relaxation time of ~0.5 μs.

These various experiments have illustrated that the modification of gallium's transitional properties, brought about by confinement, facilitates the achievement of a large optical nonlinearity via light-induced structural transformations in the metal. The studies of UPLD interfaces have shown that bulk gallium's nonlinearity is exceptionally broadband, that its response time can be as short as a few picoseconds, and that its relaxation time is typically in the nano- to microsecond range. Furthermore, the data collected have enabled the development and quantitative testing of theories to describe the thermal and non-thermal metallization mechanisms underlying the nonlinearity. The nanoparticles' nonlinear response shares certain characteristics with that of the bulk interfaces but the experimental data suggest that, in contrast to the bulk nonlinearity, it is not derived from a structural transition involving gallium's α phase.

CONTENTS

ACKNOWLEDGEMENTS

I would like to thank my supervisor Professor Nikolay Zheludev for his guidance, assistance and encouragement throughout my time as a research student. I would also like to express my gratitude to those with whom I worked, both in Southampton and at other institutions, in particular V. Albanis, P. J. Bennett, P. Besnard, R. T. Bratfalean, W. S. Brocklesby, S. Dhanjal, V. I. Emel'yanov, V. A. Fedotov, D. C. Hanna, R. J. Knize, L. Lefort, A. Mihaescu, P. Petropoulos, K. Peuch, S. Pochon, D. J. Richardson, A. V. Rode, K. J. Ross, G. C. Stevens and B. V. Zhdanov. Furthermore, I would like to thank the technical and administrative staff at the Department of Physics and Astronomy for the help afforded to me over the years. I would like to acknowledge the EPSRC* for providing my maintenance grant and, in conjunction with the EOARD†, the Institute of Physics and the British Council, for funding my attendance at conferences and my visits to the United States Air Force Academy (Colorado Springs, U.S.A.) and the Ecole National Supérieure de Sciences Appliquées et de Technologie (Lannion, France). I would like to thank my father for his assistance in preparing this thesis, and finally, I would like to thank Jane and all of my family and friends for their unstinting support and encouragement.

* Engineering and Physical Sciences Research Council, UK.
† European Office of Aerospace Research and Development, United States Air Force.

Chapter 1

Introduction

1.1 Introduction

The first observation of a nonlinear optical effect was reported in 1926 by Vavilov and Lewshin [1]. They found that the absorption of uranium-doped glass decreased with increasing light intensity - demonstrating for the first time that light could change the optical properties of a medium through which it was passing. In 1950, still more than ten years before the invention of the laser, Vavilov introduced the concept of 'nonlinear optics' when he wrote: "An absorbing medium must exhibit a 'nonlinearity' not only with respect to absorption. The latter is related to dispersion, and therefore the velocity of light propagation in a medium must generally depend on the light power, too. For the same reason other optical properties of a medium - birefringence, dichroism, rotation capacity, and so on - must generally exhibit a dependence on the light power, that is, a violation of the superposition principle." [2].

Since the emergence of the laser in the early sixties, the quest for materials with larger and faster nonlinearities has been pursued vigorously and there have been some great successes in finding and engineering such materials [3]. Nevertheless, devices based on these materials generally rely on optical resonators and extended interaction lengths to achieve nonlinear effects of the requisite magnitude. This will not be possible in the nanoscale photonic devices which are likely to be required in the near future if current trends continue. Highly integrated nanoscale electronic devices are now commonplace (e.g. computer processors), and in recent years the mass production of micron-scale

optical devices has also become viable [4, 5]. These MEMS's (Micro-Electro-Mechanical Systems) are typically based on arrays of passive elements (mirrors, lenses, etc.) and their functionality is derived from their electro-mechanical nature. Efforts to further miniaturise these devices (i.e. to replace micro- with nano-) will continue, but if an extensive range of nanoscale photonic devices is to be realised, materials with exceptionally large nonlinearities will be required. It will be necessary to control one beam of light with another in a nanoscale layer, or in a single nanoparticle of material. In addition, according to Gibbs [6], such devices should operate at room temperature with switching energies of less than a femtojoule and switching times of less than one picosecond (although millisecond response times may be acceptable for some applications). The question is, is it (even in principle) possible to substantially change the intensity or phase of a signal beam by causing it to interact with a pump beam in such a small volume of material?

Consider a nonlinear material in which the complex refractive index for the signal wave is $N = n + i\kappa$, and Δn and $\Delta\kappa$ denote changes to the real and imaginary parts of that index, induced by the pump beam. To achieve a strong induced phase-retardation effect on transmission through a layer of material with thickness L, one should satisfy the condition $\Delta n\, L \approx \lambda/2$, where λ is the signal wavelength. Similarly, to significantly change the signal intensity, one should fulfil the condition that $\Delta\alpha\, L \approx 1$ (where α is the medium's absorption coefficient), or in terms of the complex refractive index, $\Delta\kappa\, L \approx \lambda/4\pi$. For reflective effects the requirements are more complex, but in general, if a strong transmissive nonlinearity is achieved, the reflective effect will also be strong. By rearranging this last condition, for a transmissive effect on probe intensity, one can obtain the following expression for L:

$$L \approx \frac{\lambda}{4\pi\Delta\kappa} = \left(\frac{\lambda}{4\pi}\right)\left(\frac{1}{\kappa}\right)\left(\frac{\kappa}{\Delta\kappa}\right)$$

The components of this expression indicate that in order to achieve interaction lengths in the nanometre range, one requires materials with high values of κ, in which the pump-induced change $\Delta\kappa$ can achieve a magnitude equal to a significant fraction of κ.

For example, at a wavelength of 1550 nm, an interaction length of just 46 nm could be achieved in a medium where $\kappa = 8$ and $\Delta\kappa = \kappa/3$.

Conventionally, optical nonlinearities arise as result of nonlinear components in the restoring force acting on electrons displaced by interaction with a light-wave's electric field. The optical properties of metals, prime examples of materials with large κ values, are determined primarily by the response of free electrons. Consequently, they were not expected to show any significant optical nonlinearity in bulk form because this restoring force does not exist for ideally 'free' electrons. Nevertheless, electronic nonlinearities resulting from multipole interactions, the dependence of electron mass and relaxation time on energy, and spin-flipping [7], have been seen in metals, but these are very small effects and therefore of little use for practical applications.

However, in recent years a novel means of achieving optical nonlinearities has emerged, a means that relies on the interaction between a material's optical electrons and its crystal lattice. The technique is fundamentally very simple: If optical excitation induces a transition between phases of a material with markedly different optical properties, and if the original phase (and associated properties) are recovered on removal of the excitation, the medium's response can be considered nonlinear.

Given the general perception that metallic elements all have very similar optical properties (i.e. they are highly reflective) and that these properties are essentially independent of phase, this concept may not seem applicable to metals. There are, however, exceptions to this 'rule' – gallium being one of the most notable. It is a remarkably polymorphic material given its elemental nature: At least nine different phases have been identified [8], with properties ranging from those of the semi-metallic α-phase (the stable bulk solid form) [9, 10] through to those of the liquid and amorphous solid phases, which are, to all intents and purposes, free-electron metals [11, 12]. Consequently, a significant change in optical properties is associated with some of the transitions between these phases. Gallium also has the added advantage that its solid-liquid transition occurs at the easily accessible temperature of 29.8°C.

The requirement that any light-induced changes are reversible is potentially more problematic than it sounds. Phase changes in bulk materials are typically sharp, first

order transitions and are often hysteretic. So for example, if optical excitation initiates a transition by heating a material, removing the excitation and reversing the temperature increase may not reverse the transition. However, placing materials in confining geometries can convert the abrupt transformations between phases into dynamic equilibria [13]. Consequently, when a confined solid is brought to the verge of what, in bulk, would be a first order phase transition, its sensitivity to external stimulation is dramatically increased, leading to an enhancement of any optical nonlinearities. Moreover, the nonlinearity will be reversible because the structural transition in the confined material is continuous and reversible.

Indeed, this is exactly what happens in gallium. Nanoparticles of the metal exist in a temperature-dependent mixture of phases [14] and the one-dimensional confinement of bulk gallium (i.e. the formation of an interface with another medium such as vacuum or glass) leads via surface melting [15] to a softening of the solid-liquid transition in the material close to the interface.

The study of laser-induced phase transitions first generated considerable interest in the 1970's following the discovery of the laser annealing process for semiconductors [16], wherein crystalline defects in a material are repaired by using short pulse laser irradiation to induce structural changes. Thermal transitions induced by nano- and picosecond laser pulses were subsequently studied in detail [17-19]. Interest in this subject area was renewed following the introduction of femtosecond lasers in the mid-1980's. Pulses lasting less than 100 fs made it possible to deposit energy in a material on a time scale much shorter than the electron-lattice equilibration time (typically a few picoseconds), and so to create the conditions necessary for electronically driven ultrafast structural changes. Such transitions have since been studied in various semiconductors and metals [20-28]. In recent years, the study of laser-induced phase transitions has begun to attract considerable attention once more, for several reasons. Firstly, the development of sub-picosecond x-ray sources [29] has facilitated a range of new 'laser pump, x-ray diffraction probe' experiments in physics, chemistry and biology wherein atomic re-arrangement following laser excitation can be directly measured with sub-nanometre resolution [30-34]. Secondly, within the rapidly growing field of nanoparticle research, it has been found that laser-induced transformations can

be employed to manipulate the morphology and phase composition of particles [35-40]. Finally, because phase transitions are often accompanied by abrupt changes in optical, electrical and magnetic properties, there is growing interest in the potential switching applications of light-induced structural transformations [41-48].

It was first reported in 1997 that a large optical nonlinearity could be achieved at very low light intensities (a few $kW.cm^{-2}$) as the result of a light-induced transition in bulk gallium interfaced with glass and brought to a temperature near its melting point [49]. It was subsequently demonstrated that this phenomenon could form the basis of cross-wavelength optical switching devices [50] and could be used to passively Q-switch fibre lasers [51]. These early experiments demonstrated the potential of gallium as a material for nonlinear optics. They were the foundation of a successful international patent application [52] and they initiated a program of research dedicated to exploring gallium's nonlinear optical properties and the physical processes behind them. Chapters 2 and 3 of this thesis will describe a range of experiments performed as a part of that program.

As noted above, nanoscience is a rapidly growing area of research – a fact evidenced by the United States' recent implementation of a 'National Nanotechnology Initiative' [53, 54] and by the growing number of journals and conferences dedicated to the subject (See, for example, References 55-59). Within this field, the preparation of monodisperse metallic nanoparticles is a challenge that has received considerable attention in recent years due to their extensive range of potential applications [60-69]. Numerous laser-based techniques, relying on thermally-induced evaporation and fragmentation or non-thermal light-induced desorption, have been developed to tailor the shape and size of nanoparticles after the growth/deposition process [37-39, 70-73]. Recently, Wenzel *et al.* have demonstrated that size-selective laser-induced evaporation can be used to control the growth of silver nanoparticles during deposition [74]. Chapters 4 and 5 of this thesis will describe work relating to the formation and optical study of gallium nanoparticles.

1.2 Thesis plan

This thesis is divided into six chapters:

This first chapter is an introduction to the subject areas that have been investigated, with a brief outline of the subsequent chapters.

Chapters 2 and 3 describe studies wherein bulk gallium/glass interfaces were subjected to various regimes of optical excitation. The results of these experiments have facilitated the development of a theory to describe the thermal and non-thermal microscopic mechanisms underlying the nonlinear optical properties of such interfaces.

Chapter 4 describes a novel light-assisted self-assembly technique for preparing gallium nanoparticles. The procedure achieves control over nanoparticle growth through non-thermal processes and has enabled the fabrication of particles directly on the ends of optical fibres, in such a way that their optical properties can be probed both during and after growth.

Chapter 5 details experiments which demonstrate that a light-induced structural transformation can be the source of a large optical nonlinearity in gallium nanoparticles, as it is in bulk gallium films.

Chapter 6 concludes the thesis with a summary of the results reported in previous chapters and a discussion of ongoing and potential research work.

The work reported in this thesis was carried out while the author was registered as a postgraduate student in the Department of Physics and Astronomy at the University of Southampton, UK. It is, unless otherwise indicated, the original work of the author. In particular, the data shown in Figure 2.8 were collected by S. Dhanjal and P. Petropoulos, and were presented in their theses submitted for the degree of Doctor of Philosophy [75, 76].

1.3 References

1 S. J. Vavilov and W. L. Lewschin, Z. Phys. **35**, 920 (1926).

2 S. J. Vavilov, *Mikrostruktura Sveta (The Microstructure of Light)* (USSR Academy of Sciences Publishing, Moscow, 1950).

3 *Handbook of Advanced Electronic and Photonic Materials Vol. 9: Nonlinear Optical Materials* edited by H. S. Nalwa (Academic Press, San Diego, 2001).

4 E. L. Goldstein, L-Y. Lin and J. A. Walker, in *Optics and Photonics News*, 2001, Vol. 12, p. 60-65.

5 M. Roukes, in *Physics World*, 2001, Vol. 14, p. 25-31.

6 H. M. Gibbs, *Optical Bistability. Controlling Light with Light* (Academic Press, Orlando, 1985).

7 N. I. Zheludev, P. J. Bennett, H. Loh, S. V. Popov, I. R. Shatwell, Yu. P. Svirko, V. E. Gusev, V. F. Kamalov and E. V. Slobodchikov, Opt. Lett. **20**, 1368 (1995).

8 R. D. Heyding, W. Keeney and S. L. Segel, J. Phys. Chem. Solids **34**, 133 (1973).

9 M. Bernasconi, G. L. Chiarotti and E. Tosatti, Phys. Rev. B **52**, 9988 (1995).

10 R. Kofman, P. Cheyssac and J. Richard, Phys. Rev. B **16**, 5216 (1977).

11 N. R. Comins, Phil. Mag. **25**, 817 (1972).

12 O. Hunderi and R. Ryberg, J. Phys. F **4**, 2096 (1974).

13 R. S. Berry and B. M. Smirnov, J. Chem. Phys. **113**, 728 (2000).

14 A. Di Cicco, Phys. Rev. Lett. **81**, 2942 (1998).

15 G. Fritsch and E. Luscher, Phil. Mag. A **48**, 21 (1983).

[16] E. Shtyrkov, I. B. Khaibullin, M. M. Zaripov, M. F. Galyatudinov and R. M. Bayazitov, Sov. Phys. Semicond. **9**, 1309 (1976).

[17] *Pulsed Laser Processing of Semiconductors* edited by R. F. Wood, C. W. White and R. T. Young (Academic Press, New York, 1984).

[18] *Energy Beam-Solid Interactions and Transient Thermal Processing* edited by D. K. Biegelsen, G. A. Rozgonyi and C. V. Shank (Materials Research Society, Pittsburgh, 1985).

[19] M. von Allmen and A Blatter, *Laser-Beam Interactions with Materials*, 2nd Edition (Springer, Berlin, 1995).

[20] K. Sokolowski-Tinten, J. Bialkowski and D. von der Linde, Phys. Rev. B **51**, 14186 (1995).

[21] K. Sokolowski-Tinten, J. Bialkowski, M. Boing, A. Cavalleri and D. von der Linde, Phys. Rev. B **58**, R11805 (1998).

[22] P. Saeta, J-K. Wang, Y. Siegal, N. Bloembergen and E. Mazur, Phys. Rev. Lett. **67**, 1023 (1991).

[23] L. Huang, J. P. Callan, E. N. Glezer and E. Mazur, Phys. Rev. Lett. **80**, 185 (1998).

[24] C. V. Shank, R. Yen and C. Hirlimann, Phys. Rev. Lett. **50**, 454 (1983).

[25] H. W. K. Tom, G. D. Aumiller and C. H. Brito-Cruz, Phys. Rev. Lett. **60**, 1438 (1988).

[26] J. G. Fujimoto, J. M. Liu, E. P. Ippen and N. Bloembergen, Phys. Rev. Lett. **53**, 1837 (1984).

[27] H. E. Elsayed-Ali, T. B. Norris, M. A. Pessot and G. A. Mourou, Phys. Rev. Lett. **58**, 1212 (1987).

[28] C. Guo, G. Rodriguez, A. Lobad and A. J. Taylor, Phys. Rev. Lett. **84**, 4493 (2000).

[29] A. Cavalleri, C. W. Siders, K. Sokolowski-Tinten, C. Toth, C. Blome, J. A. Squier, D. von der Linde, C. P. J. Barty and K. R. Wilson, in *Optics and Photonics News*, 2001, Vol. 12, p. 28-33.

[30] A. Cavalleri, Cs. Toth, C. W. Siders, J. A. Squier, F. Raksi, P. Forget and J. C. Kieffer, Phys. Rev. Lett. **87**, 237401 (2001).

[31] C. W. Siders, A. Cavalleri, K. Sokolowski-Tinten, Cs. Toth, T. Guo, M. Kammler, M. Horn von Hoegen, K. R. Wilson, D. von der Linde and C. P. J. Barty, Science **286**, 1340 (1999).

[32] C. Rose-Petruck, R. Jimenez, T. Guo, A. Cavalleri, C. W. Siders, F. Rksi, J. A. Squier, B Walker, C., K. R. Wilson and C. P. J. Barty, Nature (London) **398**, 310 (1999).

[33] C. Rischel, A. Rousse, I. Uschmann, P-A. Albouy, J-P. Geindre, P. Audebert, J-C. Gauthier, E. Fröster, J-L. Martin and A. Antonetti, Nature (London) **390**, 490 (1997).

[34] A. H. Chin, R. W. Schoenlein, T. E. Glover, P. Balling, W. P. W. P. Leemans and C. V. Shank, Phys. Rev. Lett. **83**, 336 (1999).

[35] V. V. Yakovlev, V. Lazarov, J. Reynolds and M. Gajdardziska-Josifovska, Appl. Phys. Lett. **76**, 2050 (2000).

[36] M. Gajdardziska-Josifovska, V. Lazarov, J. Reynolds and V. V. Yakovlev, Appl. Phys. Lett. **78**, 3298 (2001).

[37] A. L. Stepanov, D. E. Hole, A. A. Bukharaev, P. D. Townsend and N. I. Nurgazizov, Appl. Surf. Sci. **136**, 298 (1998).

[38] M. Kaempfe, T. Rainer, K-J. Berg, G. Seifert and H. Graener, Appl. Phys. Lett. **74**, 1200 (1999).

[39] S. Link, C. Burda, B. Nikoobakht and M. A. El-Sayed, J. Phys. Chem. B **104**, 6152 (2000).

[40] S. Link, Z. L. Wang and M. A. El-Sayed, J. Phys. Chem. B **104**, 7867 (2000).

[41] H-K. Leea, K. Doia, A. Kanazawaa, T. Shionoa, T. Ikedaa, T. Fujisawab, M. Aizawab and B. Leec, Polymer **41**, 1757 (2000).

[42] T. Matsui, K. Nakayama, M. Ozaki and K. Yoshino, Appl. Phys. Lett. **76**, 1228 (2000).

[43] T. Yamamoto, A. Ohashi, S. Yoneyama, M. Hasegawa, O. Tsutsumi, A. Kanazawa, T. Shiono and T. Ikeda, J. Phys. Chem. B **105**, 2308 (2001).

[44] M. Nishino and S. Miyashita, Phys. Rev. B **63**, 174404 (2001).

[45] O. Sato, T. Iyoda, A. Fujishima and K. Hashimoto, Science **272**, 704 (1996).

[46] F. Wang, G. H. Haertling and K. K. Li, Proc. SPIE **2338**, 168 (1994).

[47] S. A. Pollack, D. B. Chang, F. A. Chudnovky and I. A. Khakhaev, J. Appl. Phys. **78**, 3592 (1995).

[48] R. Lopez, L. A. Boatner, T. E. Haynes, R. F. Haglund Jr. and L. C. Feldman, Appl. Phys. Lett. **79**, 3161 (2001).

[49] S. Dhanjal, I. R. Shatwell, Yu. P. Svirko and N. I. Zheludev, in *Quantum Electronic and Laser Science 1997*, Technical digest (Opt. Soc. Am., Washington DC, USA, 1997).

[50] P. J. Bennett, S. Dhanjal, P. Petropoulos, D. J. Richardson, N. I. Zheludev and V. I. Emel'yanov, Appl. Phys. Lett. **73**, 1787 (1998).

[51] P. Petropoulos, H. L. Offerhaus, D. J. Richardson, S. Dhanjal and N. I. Zheludev, Appl. Phys. Lett. **74**, 3619 (1999).

[52] N. I. Zheludev, D. J. Richardson and S. Dhanjal, WO99/26106, *assigned to* University of Southampton, 27 May 1999.

[53] http://nano.gov

[54] M. C. Roco, J. Nanopart. Res. **3**, 5 (2001).

[55] *Nanotechnology* (Institute of Physics, London, 1990-).

[56] *Journal of Nanoparticle Research* (Kluwer Academic Publishers, Dordrecht, 1999-).

[57] *Journal of Nanoscience and Nanotechnology* (American Scientific Publishers, California, 2001-).

[58] *1st IEEE Conference on Nanotechnology* (Maui, USA, 2001).

[59] *Ninth Foresight Conference on Molecular Nanotechnology* (Santa Clara, USA, 2001).

[60] D. J. Maxwell, J. T. Krug II and S. Nie, Proc. SPIE **3913**, 112 (2000).

[61] C. Sonnichsen, S. Geier, N. E. Hecker, G. von Plessen, J. Feldmann, H. Ditlbacher, B. Lamprecht, J. R. Krenn, F. R. Aussenegg, V. Z-H. Chan, J. P. Spatz and M. Moller, Appl. Phys. Lett. **77**, 2949 (2000).

[62] L. Ansheng, A. Rahmani, G. W. Bryant, L. J. Richter and S. J. Stranick, J. Opt. Soc. Am. A **18**, 704 (2001).

[63] S. Kirkpatrick, M. E. McHenry, M. DeGraef, P. A. Smith, Y. Nakamura, D. E. Laughlin, E. M. Brunsman, J. H. Scott and S. A. Majetich, Scr. Metall. Mater. **33**, 1703 (1995).

[64] H. Ditlbacher, J. R. Krenn, B. Lamprecht, A. Leitner and F. R. Aussenegg, Opt. Lett. **25**, 563 (2000).

[65] M. Quinten, A. Leitner, J. R. Krenn and F. R. Aussenegg, Opt. Lett. **23**, 1331 (1998).

[66] H. R. Stuart and D. G. Hall, Appl. Phys. Lett. **69**, 2327 (1996).

[67] H. R. Stuart and D. G. Hall, Appl. Phys. Lett. **73**, 3815 (1998).

[68] M. Haruta, Catal. Today **36**, 153 (1997).

[69] G. A. Somorjai, Appl. Surf. Sci. **121/122**, 1 (1997).

[70] J. Bosbach, D. Martin, F. Stietz, T. Wenzel and F. Trager, Appl. Phys. Lett. **74**, 2605 (1999).

[71] M. Vollmer, R. Weidenauer, W. Hoheisel, U. Schulte and F. Trager, Phys. Rev. B **40**, 12509 (1989).

[72] W. Hoheisel, M. Vollmer and F. Trager, Phys. Rev. B **48**, 17463 (1993).

[73] H. Kurita, A. Takami and S. Koda, Appl. Phys. Lett. **72**, 789 (1998).

[74] T. Wenzel, J. Bosbach, A. Goldmann, F. Stietz and F. Trager, Appl. Phys. B **69**, 513 (1999).

[75] S. Dhanjal, Ph.D. thesis, University of Southampton, 1999.

[76] P. Petropoulos, Ph.D. thesis, University of Southampton, 2000.

Chapter 2

Non-thermal light-induced metallization and associated optical nonlinearity in gallium films

2.1 Synopsis

Gallium mirrors prepared on silica by ultrafast pulsed laser deposition show a fully reversible light-induced reflectivity increase. This effect cannot be fully accounted for by thermal phenomena and so a non-thermal mechanism for light-induced metallization of gallium at the interface is proposed.

The technique used to prepare high-quality gallium mirrors is outlined in Section 2.3. In Section 2.4, experiments performed on these gallium/glass interfaces, using a reflectometer based on a Ti:sapphire laser, and the results thereof, are described. An analysis of the results is presented in the following section. It illustrates the problems with a thermal explanation for the observations, and demonstrates that a model based on non-thermal light-induced metallization of gallium can successfully reproduce the experimental results. Further evidence in support of a non-thermal metallization process, derived from a study of the induced reflectivity change's nanosecond dynamics, is presented in Section 2.6.

2.2 Introduction

In recent years it has been found that gallium, confined at an interface with glass and brought to a temperature just below its melting point (29.8°C), shows a dramatic response to low-power optical excitation: Intensities of just a few $kW.cm^{-2}$ are seen to increase the interface's reflectivity by up to 30%. Indeed, potential applications of this remarkable phenomenon to all-optical cross-wavelength switching and laser Q-switching have already been demonstrated [1-3].

This work was performed using gallium/glass interfaces prepared either by squeezing molten gallium against a glass slide or by dipping a freshly cleaved optical fibre into a bead of the liquid metal. Whilst these techniques are both very quick and very simple, they are unsatisfactory for a number of reasons. These include the unpredictable quality and inhomogeneous structure of the interface, a high chance of contamination or oxidation, rapid degradation and, looking towards commercial applications, incompatibility with mass production techniques. A controlled, reproducible gallium deposition process would be preferable. Attempts have been made to deposit gallium on silica using electron-beam evaporation and RF sputtering, but in both cases the films produced were not in the normal crystalline α-phase, as required for the observation of the nonlinearity.

It has been found however, that high quality, thin α-gallium films can be prepared on glass by so-called 'ultrafast pulsed laser deposition' or UPLD (See Section 2.3). There are some subtle differences between the optical properties of UPLD interfaces and those of samples prepared by other means but they have, by virtue of their excellent quality and long-term stability, enabled the collection of accurate, reproducible data on the temperature and intensity dependencies of gallium/glass interface reflectivity (Section 2.4). It has thus been possible, for the first time, to quantitatively compare experimental results with microscopic models for the mechanisms underlying gallium's nonlinear optical response (Section 2.5).

2.3 Ultrafast pulsed laser deposition of gallium films

Pulsed laser deposition (PLD) has been employed for many years in the preparation of thin films [4]. However, when this process is applied in its conventional form, the deposition of particles/droplets on the film can be a major problem, particularly in relation to its optical quality. This section describes an adaptation of the PLD process that has allowed for the formation of high-quality, uniform, droplet-free gallium films on glass substrates.

In conventional PLD, high-energy excimer or solid-state lasers, which typically produce ~10 ns, 1 J pulses at rates of 10-100 Hz, are used to ablate material from a target. Under such conditions, the film that develops on a nearby substrate does so in a discontinuous manner (each laser pulse sends a short burst of material towards the substrate) and, as noted above, it can be spoilt by the deposition of particles and droplets. In recent years however, a modified version of the PLD process has been developed which overcomes these problems. Ultrafast PLD (UPLD), as it is known, achieves this by using low-energy (μJ-mJ) picosecond laser pulses and repetition rates of several tens of megahertz [5, 6]. The reduced pulse energies mean that the number of atoms evaporated per pulse is reduced by several orders of magnitude and it becomes impossible for droplets to be ejected from the target. In order to maintain a sensible deposition rate, the frequency of pulses is increased and a combination of pulse intensity and duration is selected (according the thermodynamic properties of the target) that optimises ablation. A secondary consequence of the high repetition rate is that the fastest atoms evaporated by one pulse catch up with the slower atoms produced by the previous pulse. As a result, the film grows continuously rather than in bursts.

A supply of UPLD gallium/glass interfaces was made available through a collaborative arrangement with one of the research groups that pioneered the development of the UPLD process at the Australian National University in Canberra. Samples were prepared in Australia and studied, at both the University of Southampton (UK) and in Canberra. As part of this collaboration, Prof. N. I. Zheludev travelled from Southampton to Canberra to take part in the deposition and characterisation of

interfaces, and Dr. A. V. Rode made the reverse journey on two occasions to participate in sample characterisation experiments.

At the UPLD facility in Canberra, in a chamber evacuated to ~2.7 x 10^{-6} mbar, 1-2 μm thick films were deposited over a period of several hours from 6N purity gallium targets onto flat, 1 mm thick glass substrates held approximately 10 cm from the target and cooled to ~170 K. A Q-switched mode-locked Nd:YAG laser (λ = 1.064 μm), producing 60 ps pulses at 76 MHz and giving an intensity of ~10^{11} W.cm^{-2} at the target, was used to evaporate the gallium. The emission spectrum of the plume of ablated material, in the range from 220 to 400 nm, was found to be rich in lines of atomic and singly ionised gallium. This process deposited gallium in an amorphous form, but after melting it re-solidified in the α phase. The samples produced were of uniformly high optical quality and have shown no degradation despite repeated heating and cooling across gallium's melting point over a period that now exceeds two years. This exceptional structural stability, which is considerably better than that of the 'squeezed gallium' and 'dipped fibre' interfaces described above, is attributed to the presence of a transitional region formed by the penetration of energetic gallium ions into the glass during deposition (See Figure 2.3). Optical measurements (See Sections 2.4 and 2.5) indicate that ions are implanted to a depth of ~3 nm, much deeper than would be expected for a thermal evaporation process. Numerical modelling performed in Canberra, using the well-known Monte Carlo simulation program TRIM (TRansport of Ions in Matter) developed by Ziegler *et al.* [7], showed that this required ions to have rather high kinetic energies, ~600 eV. However, an ion acceleration mechanism has been proposed that may give some ions energies of up to 1 keV during the laser ablation process [8], thus providing an explanation for the transitional region's origins.

2.4 Gallium/glass interface reflectivity measurements

A reflectometer based on a Ti:sapphire laser (See Figure 2.1) was assembled to investigate how the near-normal-incidence reflectivity of gallium/glass interfaces

depends on temperature and incident light intensity – the sort of characteristics that must be understood if the performance characteristics of gallium-based devices for applications such as Q-switching [3] are to be optimised.

The acquisition of this data in a simple, single-beam experiment was facilitated by the consistent high quality of the UPLD interfaces which, for the purposes of these studies, were mounted gallium-side-down on a thermostatic copper plate with a protective cover-glass in between (See Figure 2.1). The thermostat was based on a small Peltier heat pump and allowed the interface temperature to be controlled to an accuracy of ~0.1°C.

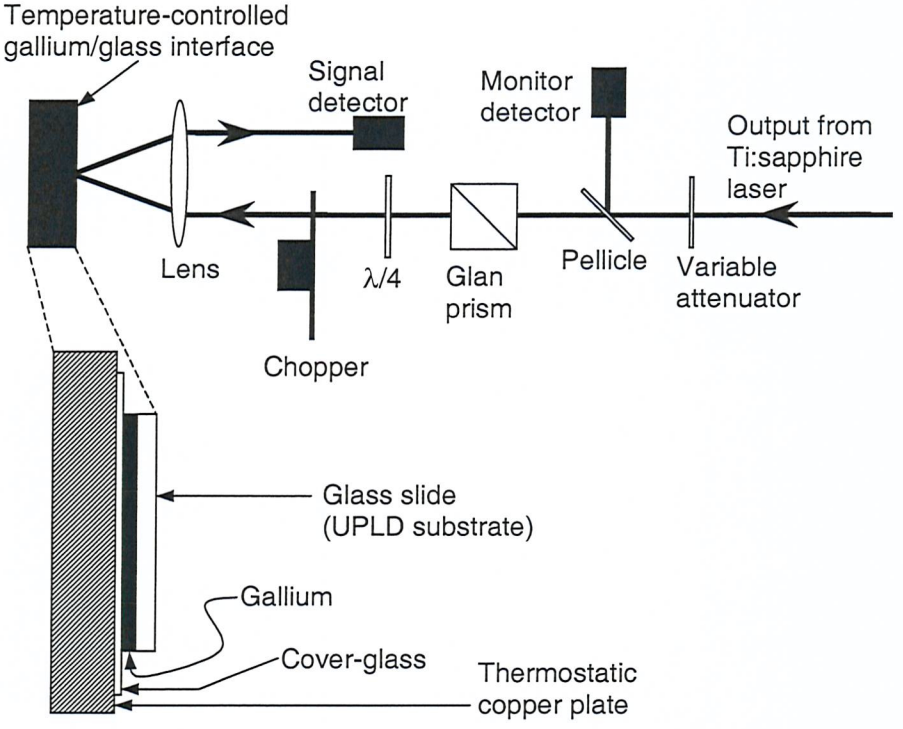

Figure 2.1: Schematic of the reflectometer, based on a Ti:sapphire laser, used to study the optical properties of gallium/glass interfaces prepared by UPLD. Detail of the configuration in which the samples were mounted on the thermostat is also shown.

In view of the fact that a femtosecond Ti:sapphire laser (wavelength = 810 nm) would be used to investigate the interfaces' ultrafast response dynamics (See Section 3.6), a similar laser was used for the present study. However, although the mode-locked regime (giving ~50 fs pulses at a rate of ~87 MHz) was retained for stability, the laser's

output was treated as though it were continuous, i.e. time-averaged parameters were measured and used in calculations. This assumption was made following preliminary pump-probe reflectivity measurements (See Section 3.6), in which the interface showed no response to individual pulses (or to be more precise, no response that could be resolved in the time between one pump pulse and the next), even at the maximum available laser power.

The beam from the laser was circularly polarised (to negate the effects of α-gallium's birefringence) and mechanically chopped at ~200 Hz to facilitate the use of a lock-in detection system. A pellicle directed a fraction of the beam to a reference photodetector, so that the signal reflected from the sample could be normalised against any variations in laser output. The main beam was focused, through the glass substrate, to a spot of ~20 μm diameter on the gallium/glass interface. (The FWHM beam diameter was measured prior to installing the gallium/glass sample by scanning a pinhole across the beam at the intended sample position and monitoring the transmitted light intensity). A variable attenuator was used to control the intensity of light incident on the sample. A computer was used to perform temperature-control and data-acquisition operations. Calibration experiments indicated that the reflectometer was accurate to ±2%.

At low intensities (≤ 220 W.cm^{-2}), reflectivity varies with temperature across gallium's melting point as shown by curves *i* and *i** in Figure 2.2a. Note the continuous change in the interface's reflectivity with increasing temperature just below the melting point. This behaviour is markedly different from that of interfaces formed simply by pressing gallium into contact with glass, where the change in reflectivity associated with melting is much more abrupt [1]. The smooth transition shown in Figure 2.2a indicates a pronounced 'surface melting' effect, whereby the gallium at the interface exists in a phase different from the α phase. This interfacial layer does not form because the interface is hotter than the bulk (although its thickness is a function of temperature) but because it is energetically preferable for it to do so [9-11]. We can immediately draw the conclusions that this phase is more reflective (more metallic) than α-gallium, and that the surface energy of the 'metallic-gallium'/glass interface is lower than that of an α-gallium/glass interface. Overcooling of liquid gallium causes a reflectivity hysteresis

with a width of ~3°C, which is stable against repeated melting and solidification. This confirms the high purity of the gallium film.

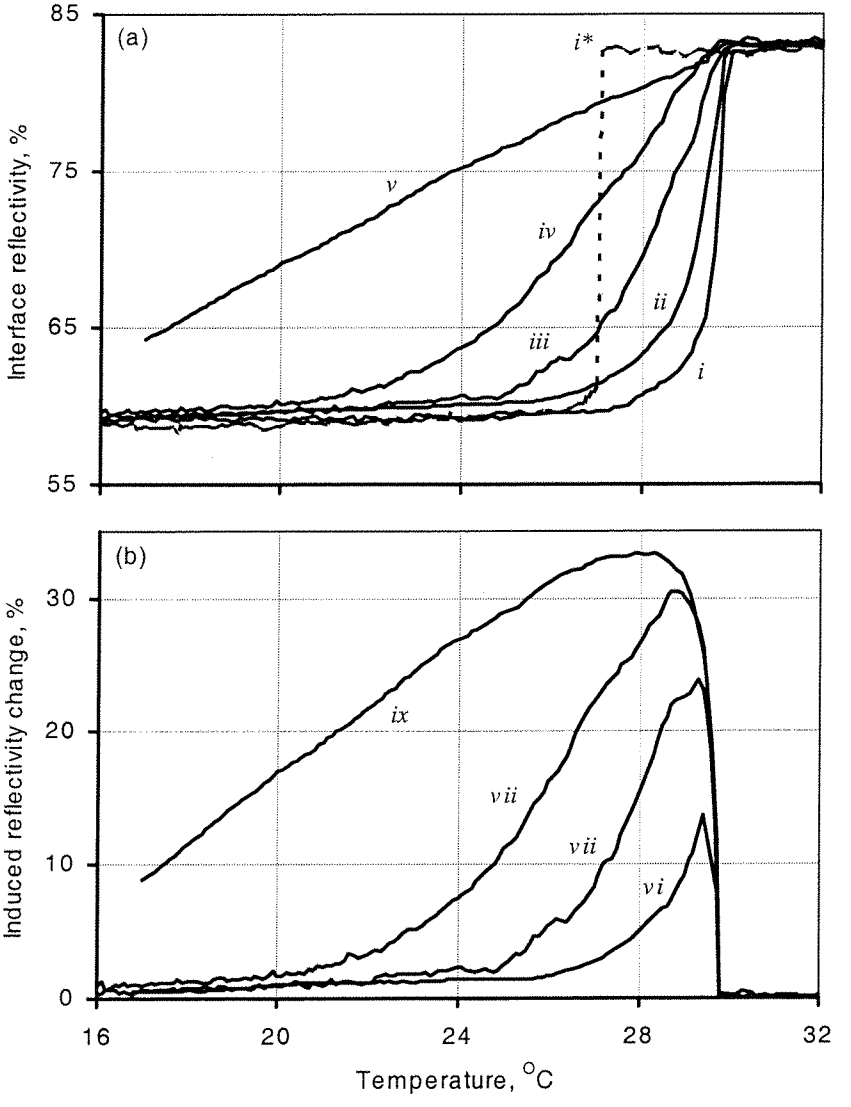

Figure 2.2: (a) Gallium/glass interface reflectivity as a function of increasing temperature for incident intensities of *i*: 220, *ii*: 320, *iii*: 950, *iv*: 2230, *v*: 3180 W.cm^{-2}, and *i**: as a function of decreasing temperature at 220 W.cm^{-2}. (b) Magnitude of the light-induced reflectivity change for intensities of *vi*: 320, *vii*: 950, *viii*: 2230, *ix*: 3180 W.cm^{-2}.

Curves *ii-v* show how the rising temperature part of this hysteresis changes with increasing intensity. The reflectivity change becomes less abrupt (i.e. the melting transition is softened) with increasing intensity but the temperature at which bulk melting of the gallium film occurs (the bend point at ~30°C) remains constant at all excitation levels.

Figure 2.2b shows the magnitude of the light-induced reflectivity change in the rising temperature parts of the hysteresis curves, calculated as the difference between curves *ii-v* and curve *i* as a percentage of the reflectivity level shown in curve *i*. This indicates that a considerable reflectivity change, ~30%, can be achieved with modest excitation intensities of just a few $kW.cm^{-2}$.

2.5 Non-thermal light-induced metallization of gallium

The collection of reliable data on the temperature and intensity dependencies of gallium/glass interface reflectivity made it possible to develop and assess theoretical models to describe the functionality of the structure. The data were analysed in conjunction with, amongst others, Prof. V. I. Emelyanov, a visiting fellow from Moscow State University (Russia) whose expertise lies in the theory of light-matter interactions, and V. A. Fedotov, a postgraduate at Southampton University, who performed numerical simulations of the samples' thermal and (proposed) non-thermal response to laser excitation. The first part of this analysis demonstrates that the behaviour of the interfaces' reflectivity is related to the 'metallization' of α-gallium but that this cannot be accounted for purely in terms of thermal phenomena. A non-thermal model is subsequently developed which can reproduce the experimentally observed dependencies of interface reflectivity on temperature and light intensity.

Given the fact that gallium is subject to surface melting, it is reasonable to conclude that a gallium/glass interface's optical properties change on illumination because laser excitation increases the thickness of a highly reflective surface-wetting layer between the glass and the low-reflectivity α-gallium bulk (See Figure 2.3).

The high-reflectivity phase involved may be liquid or amorphous gallium, both of which have approximately free-electron, metallic properties [12, 13]. It could also be one of gallium's numerous metastable solid phases, all of which are more 'metallic' than the α phase [14]. Whatever the metallic phase is, the thickness of the metallic layer, and thus the sample's reflectivity, increase with applied light intensity.

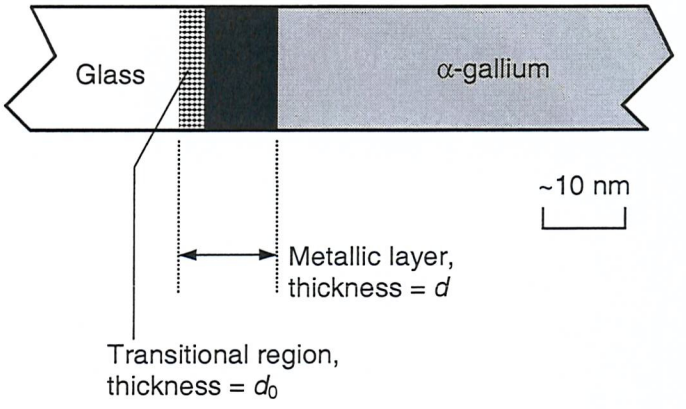

Figure 2.3: Schematic of the perceived gallium/glass interface structure relating to the surface metallization model for its response to optical excitation.

Assuming that the optical properties of the metallic layer are the same as those of free-electron (i.e. liquid) gallium and that there is a well-defined boundary between the metallic and α phases, the layer's thickness can be calculated from the reflectivity data shown in Figure 2.2a, using standard thin-film formulae (See Appendix A). Such analysis is complicated by the fact that α-gallium's optical properties are highly anisotropic. However, it has been established that gallium dimers in the liquid phase tend to be oriented perpendicular to an interface [15]. Therefore, one may expect that this orientation would prevail near the interface after solidification. Indeed, simultaneous measurements of the intensity and phase of light reflected from α-gallium/glass interfaces support this expectation [16]. So, in keeping with this crystalline orientation, for the purposes of the present study, which is based on circularly polarised light at 810 nm, the refractive index of α-gallium is taken to be 2.11 – 3.38i (based on values derived by Albanis [17] from dielectric coefficients measured by Kofman *et al.* [18]). Figure 2.4 shows the results of these metallic-layer thickness calculations.

The plot indicates, as discussed in Section 2.3, that a high-reflectivity layer, with a thickness d_0 of about 3 nm, is always present at the interface. It also shows that a metallic layer ~25 nm thick is sufficient to achieve the full 'liquid' reflectivity level. The curves fitted to the data in Figure 2.4 are all of the form

$$d = d_0 + \Delta \exp[-\mu(T_m - T)] \qquad (2.1)$$

where Δ and μ are fitting parameters, T is the thermostat temperature and T_m is gallium's melting temperature.

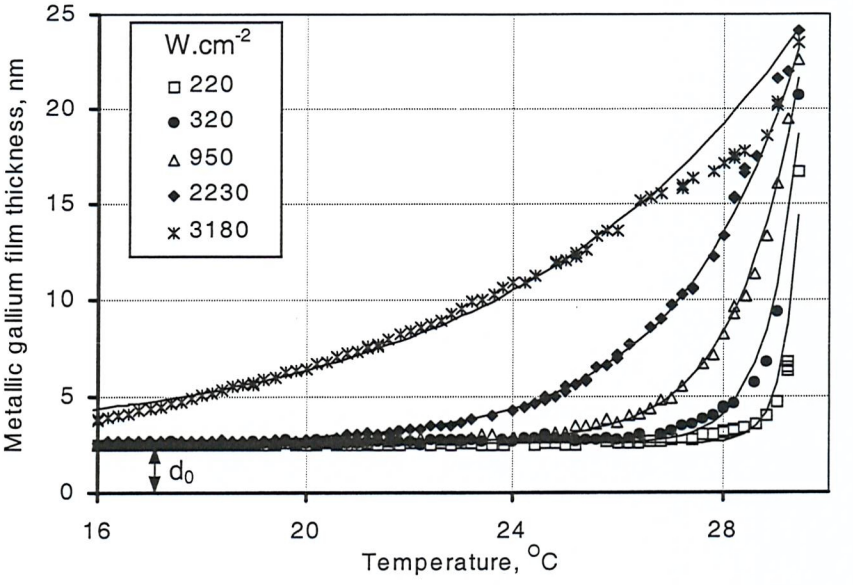

Figure 2.4: Metallic layer thickness required at an α-gallium/glass interface to account for the observed dependencies of reflectivity on temperature, for several different incident light intensities. The data points are derived from the reflectivity data presented in figure 2.2a. The fittings (lines) are of the form $d = d_0 + \Delta \exp (-\mu (T_m - T))$, where Δ and μ are fitting parameters, T is the thermostat temperature and T_m is gallium's melting temperature.

An exponential dependence on temperature of a surface layer's thickness has been obtained previously for a gallium/vacuum interface from measurements of specific heat capacity [11]. From Figure 2.4, it is clear that this dependence is also valid for optically excited gallium at an interface with glass, if the assumption is made that μ is a function of light intensity. This analysis demonstrates that the observed reflectivity increase may be interpreted as a light-induced 'surface-metallization' effect. However, the question remains as to what the mechanisms responsible for the metallization of α-gallium are.

A thermal mechanism, wherein the laser heats the gallium at the interface, causing it to melt, would perhaps be the simplest and most obvious explanation. To assess this possibility, the temperature distribution and heat-flow in the sample were modelled by numerically solving the 3D thermal conductivity equation for the sample structure and its immediate surroundings using a method based on Green's function [19]. The results of

this analysis, for a 1 μm thick gallium film on a thermostat at 26°C, subjected to a laser beam with an average intensity of 1115 W.cm^{-2} (2230 W.cm^{-2} chopped with a 50% duty cycle), are presented in Figure 2.5.

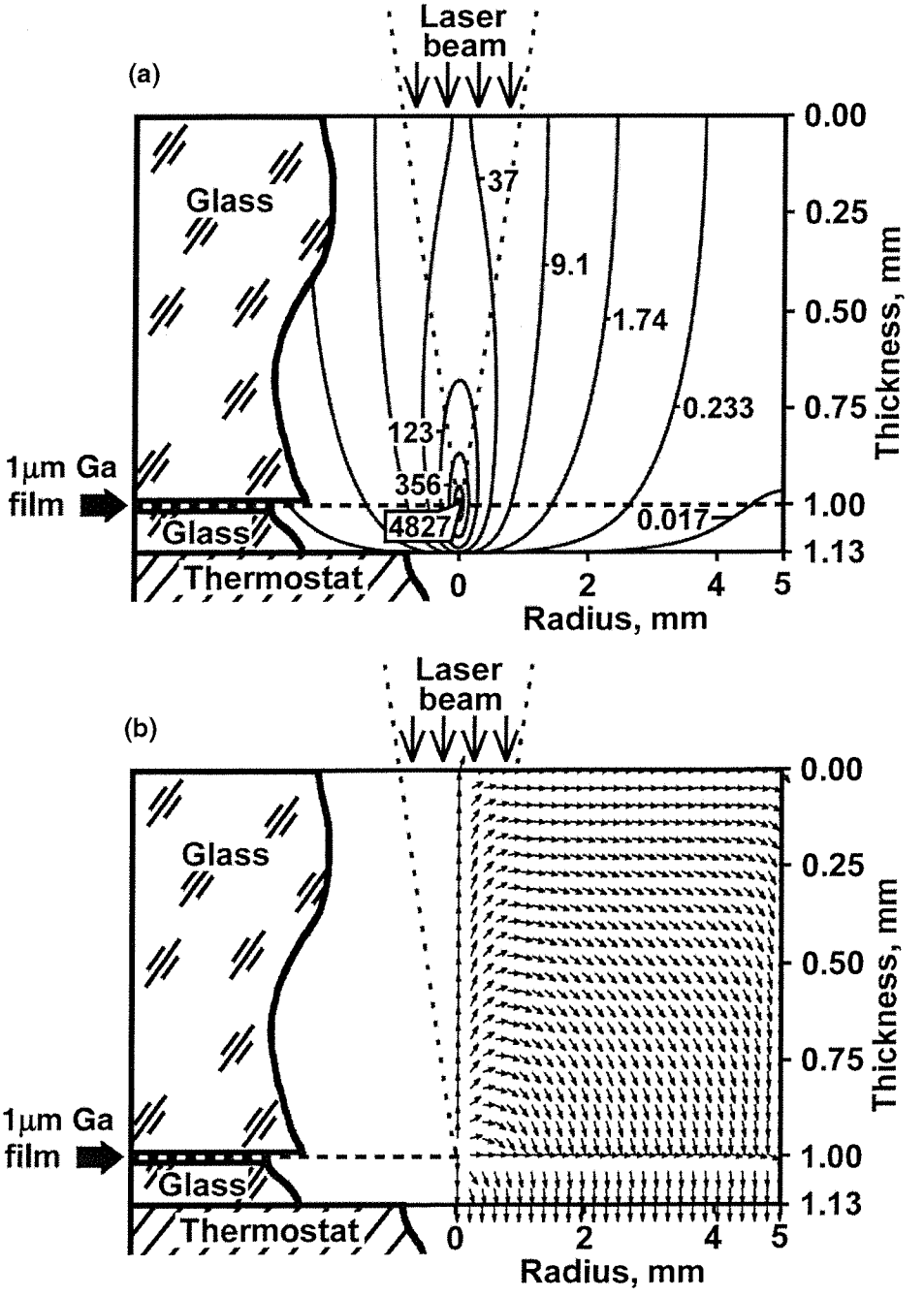

Figure 2.5: Sample cross-sections showing structure on the left, and on the right: (a) lines of constant laser-induced temperature increase (in thousandths of °C); (b) direction of heat flow. These temperature and heat-flow maps were calculated and prepared by V. A. Fedotov and are shown here for illustrative purposes.

The thermal properties of α-gallium are, like its optical properties, anisotropic. These calculations took account of that fact and assumed, in keeping with the crystal orientation described above, a thermal conductivity of 15.9 $W.m^{-1}K^{-1}$ perpendicular to the interface and 64.55 $W.m^{-1}K^{-1}$ in the plane of the interface (an average of the principal coefficients 40.8 and 88.3 $W.m^{-1}K^{-1}$) [20].

Figure 2.5a shows that under the conditions specified above, laser heating could increase the temperature at the focal point by ~4.8° – just enough to reach the melting point. However, in reality this increase is likely to be smaller because the calculations assume a relatively low value, 0.8 $W.m^{-1}K^{-1}$, for the thermal conductivity of glass and they ignore both radiative heat losses and losses from the sides of the sample. Nevertheless, this analysis does not completely eliminate the possibility that laser-induced thermal melting of bulk gallium could explain the experimental results described in Section 2.4.

However, an explanation based on thermal melting does have some serious difficulties: At the same time as giving a value for the laser-induced temperature increase, the numerical model indicates that the temperature difference across the gallium film is only ~0.5°C. Thus, if the laser were simply heating the gallium, it would melt the whole thickness of the film and, on scanning the thermostat temperature from 16 to 32°C and back, one would expect to see the low-intensity reflectivity hysteresis (curves *i* and *i** in Figure 2.2a) simply shifted down the temperature axis by an amount equal to the laser-induced temperature increase, ΔT. So with increasing incident intensity, and thus increasing ΔT, the observed melting and solidification temperatures would become lower and lower. Instead, we see that the melting temperature remains constant at any level of optical excitation, while the reflectivity's dependence on temperature becomes less steep with increasing intensity. In light of the fact that thermal effects cannot account fully for the experimental results, a non-thermal mechanism for the metallization of α-gallium can be considered.

This model (illustrated schematically in Figure 2.6) relies on the unique structure of α-gallium in which molecular and metallic properties coexist [14] - some bonds are covalent, forming Ga_2 dimers [21] and leading to an optical absorption band extending

from ~0.68 eV (1820 nm) to ~4 eV (310 nm) [22], and the remaining bonds are metallic. The model assumes that the absorption of light leads to highly localised excitation of gallium dimers from the bonding (*b*) to the anti-bonding (*a*) state, which in turn destabilises the surrounding crystalline cell.

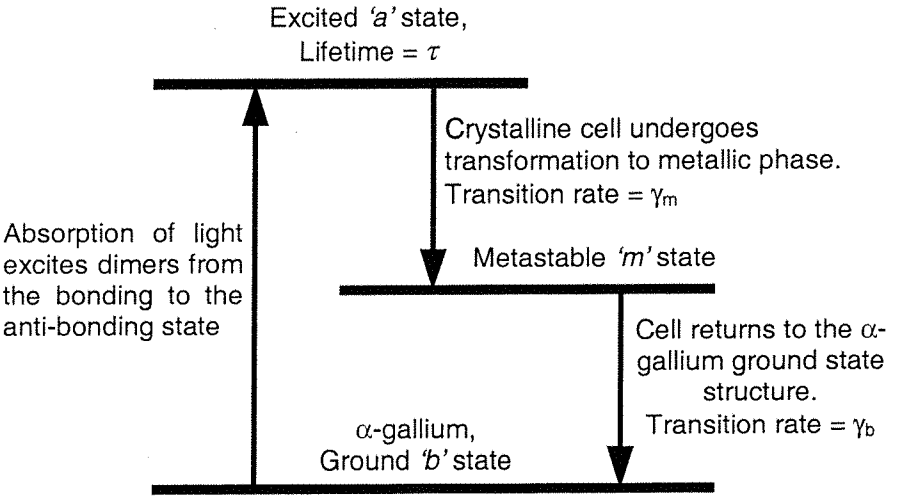

Figure 2.6: Schematic of the three-level, non-thermal light-induced metallization model.

The cell subsequently undergoes a transition to a new metastable 'metallic' configuration (the '*m*' state), thus creating a microscopic inclusion of this metastable phase (which may be crystalline or disordered) in the α-gallium bulk.

Using the standard equations for populations in a multi-level system it is possible to calculate the relative number density of crystal cells in the *m*-state, sustained by the presence of light:

$$\frac{n_m}{n} = \frac{\left(\frac{\gamma_m}{\gamma_b}\right)\Gamma}{2\Gamma + \tau^{-1} + \gamma_m\left(1 + \frac{\Gamma}{\gamma_b}\right)} \qquad (2.2)$$

where n is the number density of cells, γ_m and γ_b are, respectively, transition rates from the excited (*a*) to the metastable (*m*) state, and from the metastable to the ground (*b*) state, and τ is the lifetime of the excited state. Γ is defined as follows:

$$\Gamma = \frac{(1-R)I\alpha}{h\nu n} \qquad (2.3)$$

where R and α are the optical reflection and absorption coefficients of α-gallium respectively and I and ν are the intensity and the frequency of the laser light. Since the metallic state is metastable when $T < T_m$, the equilibrium number density of metallized cells can achieve a high value even at relatively low optical excitation levels. The presence of metallic-phase inclusions in the α-gallium shifts the delicate energy balance at the interface, leading to an increase in the thickness of the metallic layer. By minimising the free energy of the surface layer, an equation for its equilibrium thickness can be obtained:

$$d = d_0 + \Delta \exp\left[-\mu_0\left(1-\frac{n_m}{n}\right)(T_m - T)\right] \qquad (2.4)$$

Comparing this expression to formula 2.1, one can see that the factor μ is replaced with the intensity dependent $\mu_0(1-n_m/n)$. From here, the interface's reflectivity can be calculated using standard thin film formulae. Figure 2.7 shows that a good fit to the experimental reflectivity data is obtained for a wide range of light intensities and temperatures using this non-thermal light-induced metallization model.

The following parameters were used in these calculations: Number density of α-gallium crystal cells, n = 6.5 x 10^{21} cm^{-3}; reflectivity of an α-gallium/glass interface, R = 0.6; absorption coefficient, α = 4 x 10^5 cm^{-1}; lifetime of the excited state, τ = 10^{-8} s (typical for direct-gap semiconductors); transition rate from the excited to the metastable state, γ_m = 3.3 x 10^{10} s^{-1} (typical for metals); Δ = 18.4 nm and μ_0 = 16.5 (consistent with the exponential temperature dependence of surface layer thickness found by Fritsch *et al.* [11], as mentioned above). The only free parameter in these calculations is then the lifetime of the metastable state, γ_b^{-1}. A value of 5 x 10^3 s^{-1} was selected such that a curve of the correct form could be fitted to a plot of μ against incident light intensity (inset to Figure 2.7).

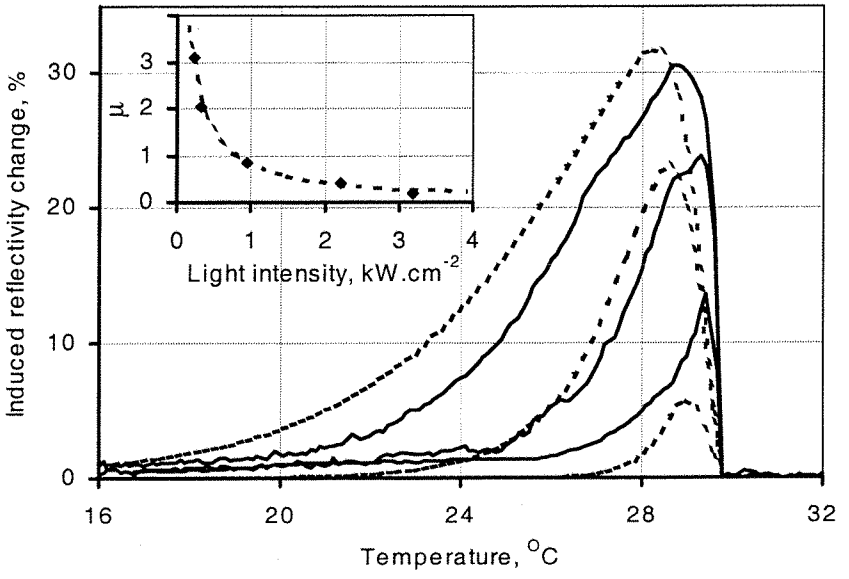

Figure 2.7: Magnitude of the light-induced reflectivity change for peak intensities of 320, 950 and 2230 W.cm^{-2} (solid lines, as shown in figure 2.2), with fittings (dashed lines) derived by V. A. Fedotov from the non-thermal light-induced metallization model and shown here for illustrative purposes. Inset is the intensity dependence of the fitting parameter μ.

2.6 Nanosecond dynamics of light-induced metallization

As part of the investigations into α-gallium metallization, experimental data on the nanosecond dynamics of the process were collected by P. Petropoulos and S. Dhanjal. An analysis of their results, carried out by, amongst others, Prof. V. I. Emel'yanov, Dr. D. J. Richardson, V. A. Fedotov and the author, provides further evidence in support of a non-thermal mechanism for α-gallium metallization.

These experiments utilized gallium/silica interfaces formed by dipping the cleaved end of an optical fibre into a small bead of molten gallium sitting on a thermostatic plate. As discussed in Section 2.1, this process is problematic but it can yield high quality interfaces. They have an advantage over other types of interface in that they are inherently coupled to the optical system used to probe their properties. Furthermore, they provide a sample structure in which the dimensions of the light-matter interaction

region are well defined: The size of the 'laser-spot' on the interface is simply the fibre's core area.

Interfaces were formed at the ends of single-mode optical fibres with mode radii of ~4 μm, and studied using a pump-probe technique: The reflectivity of the interface was monitored continuously using a low power beam from a diode laser operating at a wavelength of 1550 nm. Transient changes in the reflectivity were initiated by pump pulses generated using a combination of diode laser (with a wavelength of 1536 nm), erbium–doped fibre amplifier and acousto-optic modulator.

The dynamics of the reflectivity change induced at the gallium/glass interface by 100 ns pump pulses of varying peak power, at a thermostat temperature of 24°C, are shown in Figure 2.8a. The magnitude of this pump-induced reflectivity change is presented as a function of temperature for various pump power levels in Figure 2.8b. (Note the similarity to Figure 2.2b.) Figure 2.8c illustrates the fact that after termination of a pump pulse the reflectivity recovers to its original level in a time that, importantly, depends strongly on the thermostat temperature and on the peak power of the pulse.

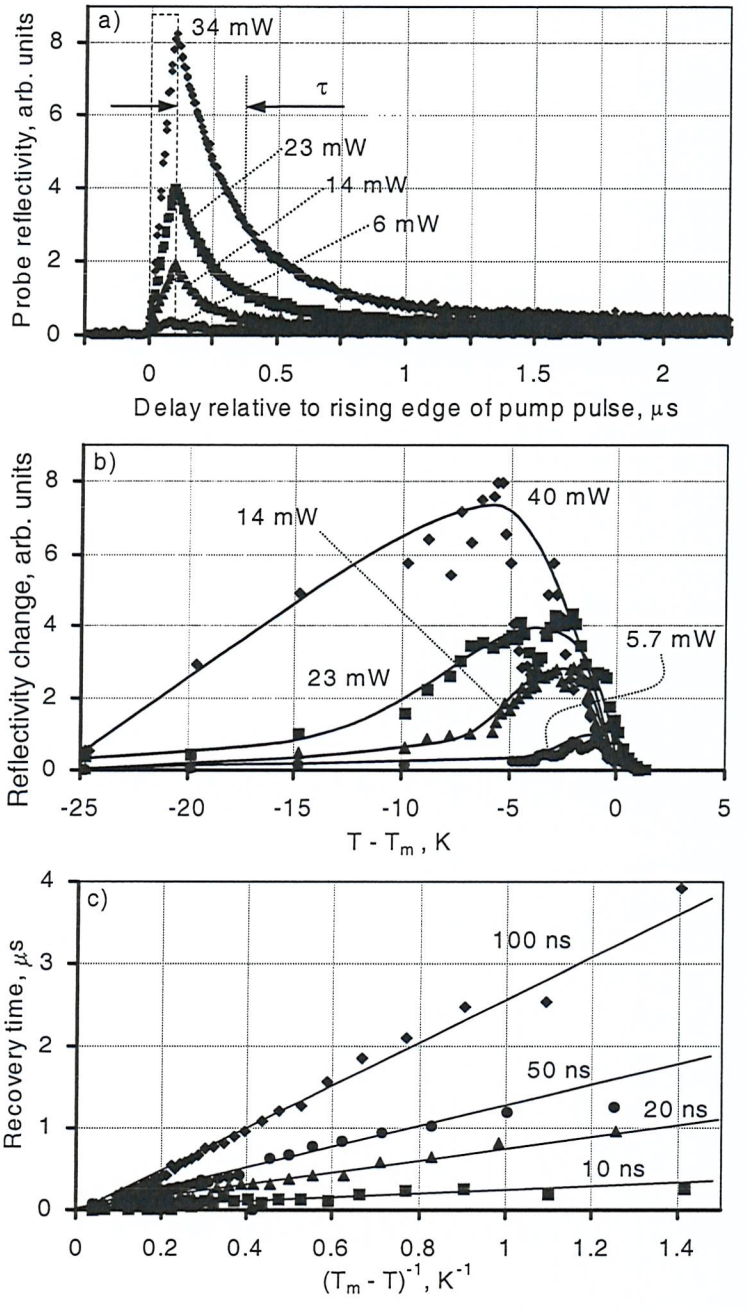

Figure 2.8: a) Dynamics of the reflectivity change induced by 100 ns pump pulses of varying peak power at a thermostat temperature of 24°C. (Pump timing is indicated by the dashed line.) b) Magnitude of pump-induced reflectivity change as a function of temperature *T*, relative to gallium's melting point T_m, for various peak power levels. c) Recovery time of reflectivity changes induced by 70 mW pump pulses of various durations, as a function of temperature *T*, relative to T_m. These data were collected by P. Petropoulos and S. Dhanjal and are shown here for illustrative purposes.

The conditions of these experiments were numerically modelled by V. A. Fedotov, using techniques similar to those described in Section 2.5. The laser power required to

achieve melting at the interface was calculated as a function of pulse duration and thermostat temperature (See Figure 2.9).

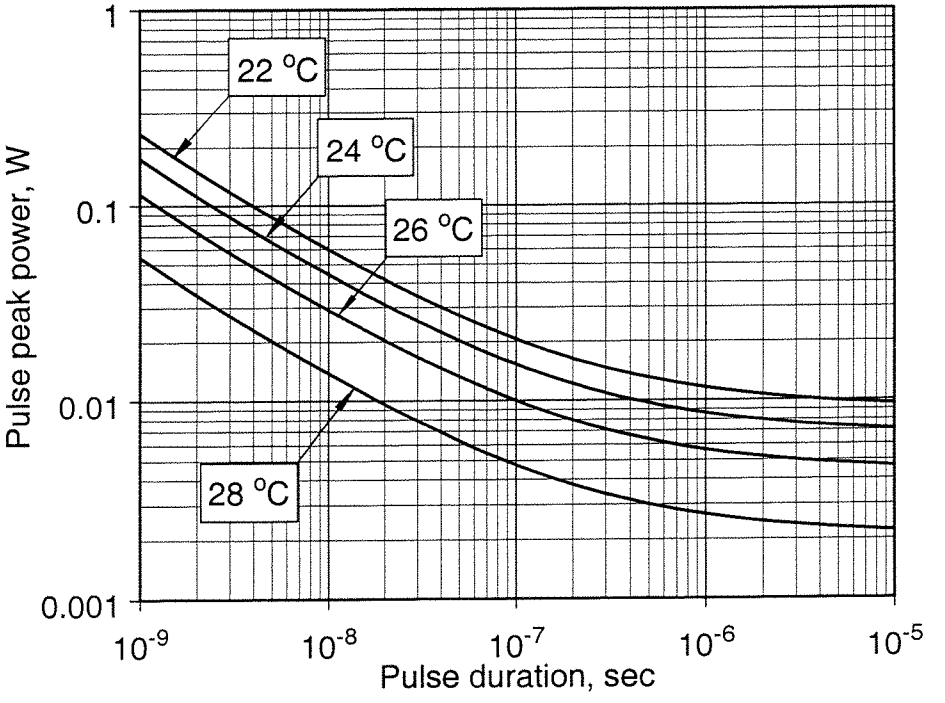

Figure 2.9: Duration and peak power of the optical excitation pulse required to achieve gallium's melting temperature (29.8°C) at the interface for different thermostat temperatures. This chart was derived by V. A. Fedotov from a numerical simulation of the samples' thermal and optical properties and is shown here for illustrative purposes.

These calculations did not account for the thermal conductivity of the optical fibre. Consequently, the pulse duration and peak power requirements for a given thermostat temperature are likely to have been underestimated. Nevertheless, Figure 2.9 demonstrates that laser-induced thermal melting is, once again, inadequate as an explanation for the experimental observations. For example, the calculations indicate that with a background temperature of 24°C and pulses lasting up to 100 ns, no reflectivity change should be seen at powers below 16 mW. However, Figure 2.8a shows that reflectivity changes are seen under such conditions, even with 6 mW pump pulses.

The recovery time data shown in Figure 2.8c also rule out a non-melting thermal explanation (wherein reflectivity is a function of temperature but no phase change

occurs). If such a mechanism were active, the reflectivity would relax with temperature after termination of a pump pulse, in a time that would be independent of the thermostat temperature and the pump power. However, the data indicate that relaxation time is temperature-dependent.

Therefore, a non-thermal metallization mechanism appears to be required once more. However, in this case the interface's response to individual optical pulses must be considered, rather than its steady-state response to quasi-continuous excitation. The energy difference between α-gallium and the metal's metastable metallic phases is of the order 1.3×10^{-20} J.atom^{-1} (Ref. 23). So, to completely transform the light-matter interaction volume (approximately $\pi r^2 \alpha^{-1} = 1.9 \times 10^{-18}$ m^3, where r is the radius of the fibre's core and α^{-1} is gallium's skin depth at a wavelength of 1550 nm, ~38 nm), which contains ~10^{11} atoms, a total energy of ~1.3 nJ is needed. Comparing this energy with the pulse energies used in the experiment (up to several nJ) indicates that non-thermal metallization is possible. As described in Section 2.5, optical excitation leads to the formation of metallic-phase inclusions in the α-gallium bulk. Reflectivity then increases with inclusion density or, if there is time during the pulse for a well-defined layer to form at the interface, with metallic layer thickness.

When the excitation is withdrawn, the metallic phase becomes unstable and recrystallizes back to the α-phase. The associated relaxation time is a function of the α-phase's growth velocity, v_r (i.e. of the rate at which energy is released due to solidification) and the rate of thermal diffusion. In the present case, the former is dominant because the characteristic thermal diffusion time is shorter than the recrystallization time. The growth velocity is a function of temperature: $v_r = F(1 - T/T_m)$, where F depends on the crystallization mechanism [24-26]. One would therefore expect longer relaxation times for higher light intensities (i.e. greater degrees of metallization) and temperatures closer to gallium's melting point. This is exactly what Figure 2.8c shows.

2.7 Summary and conclusions

A reflectometer was developed to study the optical response of gallium/glass interfaces to quasi-cw laser excitation at a wavelength of 810 nm, across a range of temperatures encompassing the metal's melting point. The quality and long-term stability of interfaces prepared by UPLD meant that reproducible data on the intensity and temperature dependencies of gallium's reflectivity hysteresis could be obtained. These data demonstrate that gallium/glass interfaces show a fully reversible light-induced reflectivity increase in response to optical pulses (lasting at least 10 ns) and quasi-cw optical excitation. In conjunction with numerical simulations of the interfaces' thermal and optical properties, the results illustrate that an explanation for this behaviour based on laser-induced heating is unsatisfactory, although a thermal contribution to the effect cannot be ruled out. Consequently, a model based on the non-thermal light-induced metallization of gallium has been proposed, and it has been shown that this model produces a reasonably good facsimile of the experimental results.

The non-thermal light-induced transition in gallium is different from those observed in semiconductors [27-33]and various metals [34-36]. To achieve non-thermal effects in these materials high-intensity femtosecond optical excitation is required. The results of such excitation are de-localised and the phase transition occurs through plasma-induced instability in the crystalline structure, typically on a sub-picosecond time scale. In gallium, the molecular character of the α-gallium structure leads to highly localised excitation of the dimers, resulting in a local transformation of the structure.

The experimental data are not sufficient to discern the nature of the metallic phase, i.e. whether it is solid or liquid, crystalline or amorphous. Transitions between different solid phases are certainly possible, as evidenced by the recent observation of a non-thermal light-induced transition between crystalline phases of vanadium dioxide [37] using simultaneous femtosecond optical and x-ray measurements [38]. Indeed, it has been suggested that even the simple melting of α-gallium is actually a continuous transition through several of the metal's crystalline phases [23]. Thus, the metallic phase could well be any (or perhaps a mixture) of gallium's liquid, amorphous and crystalline phases.

The model described in Section 2.5 could be improved, in particular by (a) taking more

accurate account of changes in the sample's reflectivity with intensity, which should give a better fit at higher intensities, (b) considering multiphoton absorption, and (c) allowing for the fact that the various transition rates may depend on temperature, and that the relaxation rates γ_m and γ_b for a given atom may depend on the state of neighbouring atoms [39]. More accurate reflectivity data, particularly at temperatures close to the melting point, would allow the various modelling parameters to be evaluated more precisely. However, the question remains as to whether the hypothesis of excitation localisation at the gallium dimers, which is crucial to the non-thermal model, is correct.

2.8 References

1 P. J. Bennett, S. Dhanjal, P. Petropoulos, D. J. Richardson, N. I. Zheludev and V. I. Emel'yanov, Appl. Phys. Lett. **73**, 1787 (1998).

2 S. Dhanjal, K. F. MacDonald, P. Petropoulos, D. J. Richardson and N. I. Zheludev, in *Conference on Lasers and Electro-optics 1999*, Technical digest (Opt. Soc. Am., Washington DC, USA, 1999), p. 282-283.

3 P. Petropoulos, H. L. Offerhaus, D. J. Richardson, S. Dhanjal and N. I. Zheludev, Appl. Phys. Lett. **74**, 3619 (1999).

4 D. B. Chrisey and G. K. Hubler, *Pulsed Laser Deposition of Thin Films* (Wiley, New York, 1994).

5 E. G. Gamaly, A. V. Rode and B. Luther-Davies, J. Appl. Phys. **85**, 4213 (1999).

6 A. V. Rode, B. Luther-Davies and E. G. Gamaly, J. Appl. Phys. **85**, 4222 (1999).

7 J. F. Ziegler, J. P. Biersack and U. Littmark, *The Stopping and Range of Ions in*

Solids, Vol. 1 (Pergamon Press, New York, 1985).

[8] E. G. Gamaly, A. V. Rode and B. Luther-Davies, Appl. Phys. A **69**, S121 (1999).

[9] J. G. Dash, Contemp. Phys. **30**, 89 (1989).

[10] B. Pluis, D. Frenkel and J. F. van der Veen, Surf. Sci. **239**, 282 (1990).

[11] G. Fritsch and E. Luscher, Phil. Mag. A **48**, 21 (1983).

[12] N. R. Comins, Phil. Mag. **25**, 817 (1972).

[13] O. Hunderi and R. Ryberg, J. Phys. F **4**, 2096 (1974).

[14] M. Bernasconi, G. L. Chiarotti and E. Tosatti, Phys. Rev. B **52**, 9988 (1995).

[15] W. J. Huisman, J. F. Peters, M. J. Zwanenburg, S. A. de Vries, T. E. Derry, D. Abernathy and J. F. van der Veen, Nature (London) **390**, 379 (1997).

[16] P. Petropoulos, H. S. Kim, D. J. Richardson and N. I. Zheludev, in *Conference on Lasers and Electro-optics 2000*, technical digest (Opt. Soc. Am., Washington DC USA, 2000), p. 320.

[17] V. Albanis, Ph.D. thesis, University of Southampton, 2001.

[18] R. Kofman, P. Cheyssac and J. Richard, Phys. Rev. B **16**, 5216 (1977).

[19] H. S. Carslaw and J. C. Jaeger, *Conduction of Heat in Solids*, 2nd edition (Clarendon Press, Oxford, 1959).

[20] C. Y. Ho, R. W. Powell and P. E. Liley, J. Phys. Chem. Ref. Data **1**, 279 (1972).

[21] O. Zuger and U. Durig, Phys. Rev. B **46**, 7319 (1992).

[22] X. G. Gong, G. L. Chiarotti, M. Parrinello and E. Tosatti, Phys. Rev. B **43**, 14277 (1991).

[23] H. G. von Schnering and R. Nesper, Acta Chem. Scand. **45**, 870 (1991).

[24] S. D. Peteves and R Abbaschian, Met. Trans. **22A**, 1259 (1991).

[25] S. D. Peteves and R Abbaschian, Met. Trans. **22A**, 1271 (1991).

[26] V. T. Borisov and Yu. E. Matveev, Sov. Phys. Crystallogr. **14**, 765 (1970).

[27] Y. Siegal, E. N. Glezer, L. Huang and E. Mazur, Annu. Rev. Mater. Sci. **25**, 223 (1995).

[28] K. Sokolowski-Tinten, J. Bialkowski and D. von der Linde, Phys. Rev. B **51**, 14186 (1995).

[29] K. Sokolowski-Tinten, J. Bialkowski, M. Boing, A. Cavalleri and D. von der Linde, Phys. Rev. B **58**, R11805 (1998).

[30] P. Saeta, J-K. Wang, Y. Siegal, N. Bloembergen and E. Mazur, Phys. Rev. Lett. **67**, 1023 (1991).

[31] L. Huang, J. P. Callan, E. N. Glezer and E. Mazur, Phys. Rev. Lett. **80**, 185 (1998).

[32] C. V. Shank, R. Yen and C. Hirlimann, Phys. Rev. Lett. **50**, 454 (1983).

[33] H. W. K. Tom, G. D. Aumiller and C. H. Brito-Cruz, Phys. Rev. Lett. **60**, 1438 (1988).

[34] J. G. Fujimoto, J. M. Liu, E. P. Ippen and N. Bloembergen, Phys. Rev. Lett. **53**, 1837 (1984).

[35] H. E. Elsayed-Ali, T. B. Norris, M. A. Pessot and G. A. Mourou, Phys. Rev. Lett. **58**, 1212 (1987).

[36] C. Guo, G. Rodriguez, A. Lobad and A. J. Taylor, Phys. Rev. Lett. **84**, 4493 (2000).

[37] A. Cavalleri, Cs. Toth, C. W. Siders, J. A. Squier, F. Raksi, P. Forget and J. C. Kieffer, Phys. Rev. Lett. **87**, 237401 (2001).

[38] A. Cavalleri, C. W. Siders, K. Sokolowski-Tinten, C. Toth, C. Blome, J. A. Squier, D. von der Linde, C. P. J. Barty and K. R. Wilson, in *Optics and Photonics News*, 2001, Vol. 12, p. 28-33.

[39] S. V. Demishev, T. V. Ischenko and S. J. Blundell, J. Phys.: Condens. Matter **7**, 9173 (1995).

Chapter 3

Thermal mechanisms for broadband, low-threshold reflectivity switching in gallium films

3.1 Synopsis

A laser-heating-induced structural phase transition in a nanoscale layer of gallium at an interface with silica can drive reversible changes in the optical properties of the interface across a very broad spectral range. Femtosecond pump-probe measurements reveal that gallium's nonlinear response to short-pulse excitation has a component with a response time of just a few picoseconds.

The response of gallium/silica interfaces to 3 ns excitation pulses at a range of visible wavelengths has been investigated. Details of this study and the results obtained are presented in Section 3.4. The analysis described in Section 3.5 demonstrates that the observations can be explained by the thermally-induced metallization of a layer of gallium just a few nanometres thick. Pump-probe measurements, wherein pico- and femtosecond pulses were used to study the dynamics of light-induced reflectivity changes, are described in Section 3.6.

3.2 Introduction

Chapter 2 described experiments that probed various aspects of gallium's nonlinear optical response to both quasi-continuous and long-pulse (duration ≥10 ns) laser excitation regimes. Under such circumstances, the heat generated by the absorption of light is efficiently removed from the light-matter interaction region by thermal diffusion, and the metallization of α-gallium proceeds primarily through a non-thermal mechanism. For shorter optical pulses, the process of thermal diffusion will be less efficient, very little of the heat generated will dissipate during the pulse and it may therefore be expected that laser-induced thermal phenomena will be the root cause of any interfacial response. Investigations based on nanosecond (and shorter) pulses are therefore required if the understanding of α-gallium metallization mechanisms is to be improved. Such studies may also illustrate potential opportunities (or limitations on) the development of devices based on gallium mirrors (e.g. Q-switches [1] and cross-wavelength optical modulators [2, 3]).

This chapter deals primarily with a study of changes induced in the reflectivity of gallium/silica interfaces by 3 ns laser pulses generated by an optical parametric oscillator (OPO). This laser system had the advantage of being wavelength-tuneable so, for the first time, it was also possible to subject the gallium/silica structure to the same regime of optical excitation at several different wavelengths. The results, in conjunction with numerical modelling, show that the interfaces' response to nanosecond pulses, across a broad spectral range, can be explained by a thermally-induced structural transition in a layer of gallium just a few nanometres thick.

Further evidence that thermal effects dominate the interfaces' response to short optical pulses is provided by a study, performed in collaboration with the Australian National University in Canberra, using pico- and femtosecond laser pulses. Perhaps more importantly, these measurements reveal the details of gallium's ultrafast response dynamics - indicating that that there is a component of the induced reflectivity change which occurs on a picosecond time scale.

3.3 Interface fabrication

For the purposes of the experiments described below, gallium/silica interfaces were prepared directly on the surfaces of miniature Peltier devices.

Gallium was deposited simultaneously on the surfaces of a silica flat and a Peltier heat pump using the ultrafast pulsed laser deposition technique described in Section 2.3. These components were subsequently joined by pressing the two gallium-coated surfaces together, then melting and re-solidifying the metal. The join was sealed with epoxy to prevent the silica flat from sliding across the surface of the Peltier device on subsequent melting of the gallium. A small thermistor was attached to the surface of the Peltier device and the whole sample was mounted on the base of a 'TO-3 can' (typically used as a housing for electronic components) through which the electrical connections to the Peltier device and the thermistor were made. A high-quality α-gallium/silica interface, in optimum contact with a thermostatic temperature controller and in a compact, robust package, was thus formed (See Figure 3.1). This integrated structure enabled control of the interfaces' 'background' temperature (ignoring local changes due to laser illumination), to an accuracy of 0.05°C.

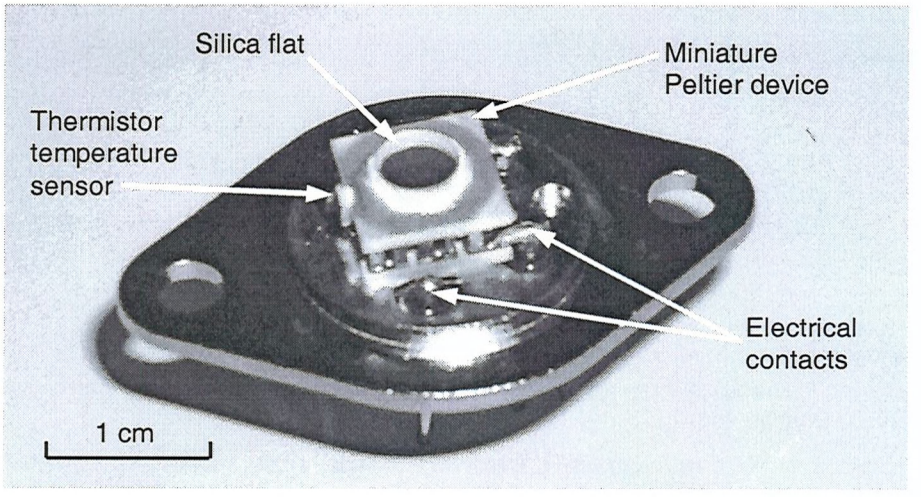

Figure 3.1: Integrated sample structure comprising the gallium/silica interface, Peltier device and temperature sensor on a TO-3 base.

3.4 Broadband, nanosecond pump-probe measurements

A study of gallium/silica interface response to nanosecond optical pulses, at a broad range of wavelengths, was considered to be important to the development of a complete understanding of the structure's functionality, and of its potential applications. However, the facilities required to perform such a study were not available in Southampton. A collaboration was therefore entered into with Prof. R. J. Knize and Dr. B. V. Zhdanov of the Laser and Optics Research Center at the United States Air Force Academy in Colorado. With financial support from the EPSRC* and EOARD†, the author was able to visit the Academy and make use of a Coherent Infinity-XPO optical parametric oscillator system. The XPO is a single-crystal BaB_2O_4 (BBO) device pumped by the third harmonic of an Infinity YAG laser. It has a computerised control system and produces pulses lasting ~3 ns across a tuning range that extends from 420 to 2200 nm. Due to constraints of time, the experiments described below were performed using only the 'signal' output range (420-709 nm).

Pump-probe measurements of light-induced changes in gallium/silica interface reflectivity were performed at four different wavelengths within the XPO's signal range, using a pulse repetition rate of 50 Hz. To negate the effects of α-gallium's birefringence, the laser light was circularly polarized using a Fresnel rhomb. It then passed through two pellicle beam-splitters, one of which sent a fraction of the beam to a reference photodetector whilst the other split the beam into pump and probe components. The pump beam was directed past a mechanical shutter, through a 3 mm aperture and onto the gallium/silica interface at near-normal incidence. The probe beam was maintained at an average power (measured with a pyroelectric power meter immediately in front of the gallium mirror) of not more than 0.01 mW (fluence ≤ 0.03 mJ.cm^{-2}) using a variable neutral density filter. It was directed through a 1 mm aperture to a point on the gallium/silica interface at the centre of the pump spot, at an angle of approximately 9°. Probe pulses arrived at the interface approximately 2.2 ns after the corresponding pump pulse. Reflected probe light was collected by a second photodetector. A schematic of this experimental arrangement is shown in Figure 3.2.

---

* Engineering and Physical Sciences Research Council, UK.
† European Office of Aerospace Research and Development, United States Air Force.

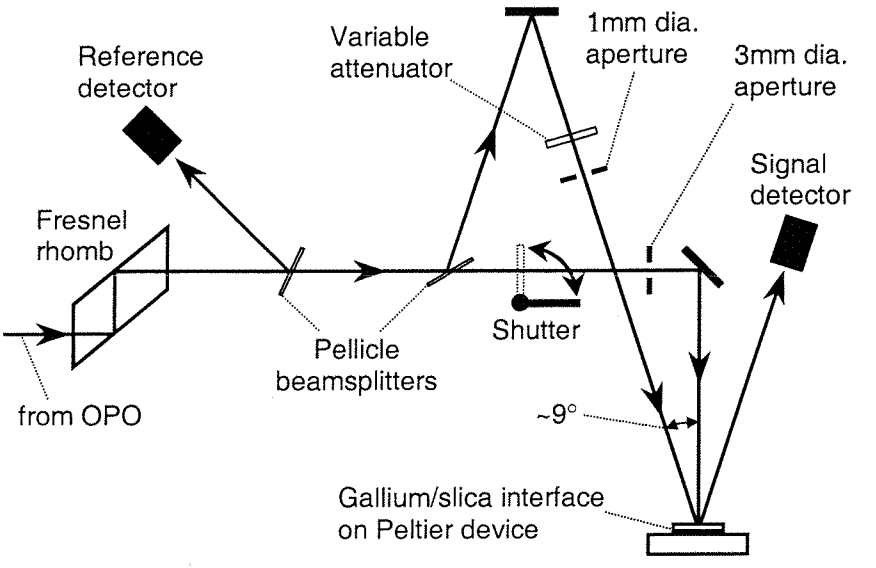

Figure 3.2: Schematic of the experimental arrangement for pump-probe reflectivity measurements at wavelengths between 440 and 680 nm using nanosecond pulses from a optical parametric oscillator.

The reference detector served two functions. Firstly, it enabled the data acquisition system to ignore pulses whose energy (before interaction with the sample) differed from a pre-set value by more than 1%. This considerably reduced the noise arising from the fact that the output energy of the OPO fluctuated from one pulse to the next. Secondly, for pulses accepted by this filter, it provided a means of normalising the reflected signal against small variations in laser output. Pump-induced reflectivity change was calculated by comparing probe signals, averaged over ten acceptable pulses, obtained first in the absence of pump light (i.e. with the shutter closed), and then with the pump present (shutter open). To avoid any possibility of measurements being affected by the movement of the shutter, the acquisition system paused for one second each time the shutter changed position.

Pump-induced reflectivity change was measured as a function of pump fluence at a constant temperature of 26°C (~4° below gallium's melting point, T_m = 29.8°C), at wavelengths of 680, 600, 520 and 440 nm (See Figure 3.3a). At each wavelength, the induced change increases with fluence, reaching a wavelength-dependent saturation level at around 6 mJ.cm^{-2}. The saturation levels are, in each case, approximately half of the maximum possible reflectivity change, i.e. the difference between the solid and liquid reflectivity levels. However, these reduced saturation levels are to be expected

(See Figure 3.3b) given that a transitional metallic gallium layer is known to exist at the interface as a consequence of the UPLD process (See Section 2.3).

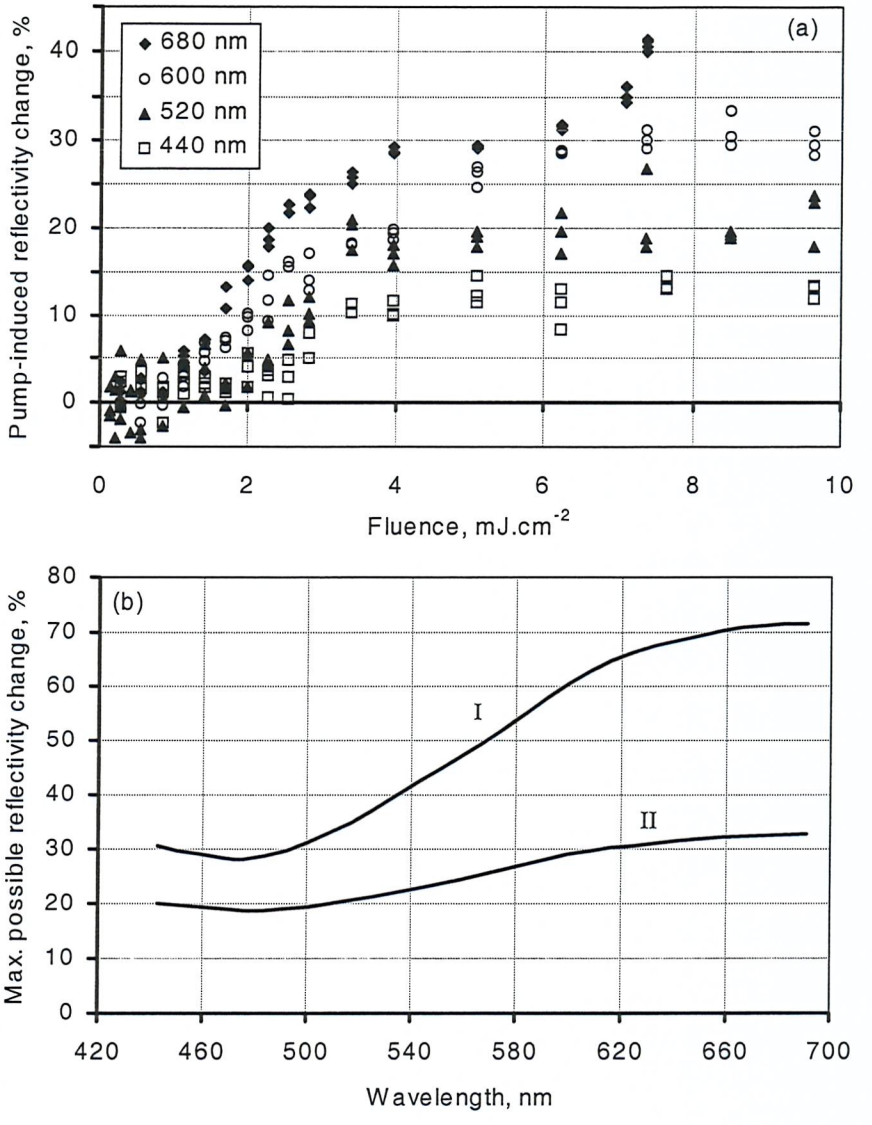

Figure 3.3: (a) Change induced in gallium/silica interface reflectivity by 3 ns pump pulses at 26°C as a function of pump fluence for four different wavelengths; (b) Maximum possible pump-induced reflectivity change as a function of wavelength for: I) an ideal α-gallium/silica interface; II) an α-gallium/silica interface at which a 3.8 nm metallic gallium layer exists prior to laser excitation.

The data also suggest that there may be a wavelength-independent threshold fluence, of ~1 $mJ.cm^{-2}$, required for the observation of a pump-induced reflectivity change. This would be consistent with a thermal metallization process: The threshold fluence would relate to the specific and latent heat required to bring the gallium from the thermostat

temperature to the phase transition temperature and then to effect a phase change. Indeed, a fluence of 1 $mJ.cm^{-2}$ is certainly consistent, for a starting temperature of 26°C, with the energy required to heat and then begin to melt a nanoscale layer of α-gallium. (The optical skin depth at visible wavelengths is ~17 nm.)

At the same four wavelengths, the magnitude of the induced reflectivity change was measured as a function of increasing interface temperature at constant pump fluence. Such data were recorded at high energy densities, above the saturation level, and at much lower levels on the rising parts of the curves shown in Figure 3.3a. A representative set of results is shown in Figure 3.4.

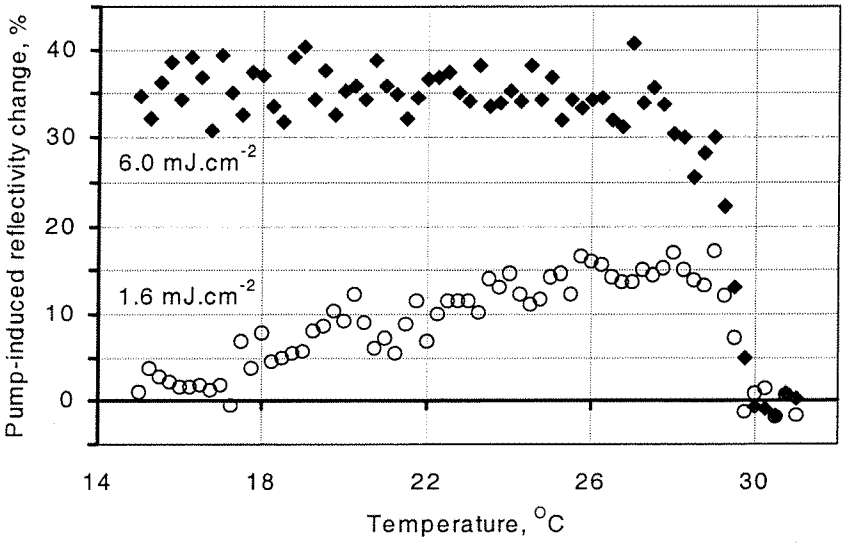

Figure 3.4: Change induced in gallium/silica interface reflectivity by 3 ns pump pulses at 680 nm as a function of interface temperature at different pump fluences.

At the lower pump fluence, the magnitude of the induced reflectivity change increases with temperature until ~28°C (approximately 2° below T_m). This is because the fraction of the pump energy required to bring the gallium to its transition temperature decreases as the thermostat temperature increases. Consequently, more energy can go into the metallization transition itself. For the higher pump fluence, the pump pulses supply more than enough energy to saturate the induced reflectivity change, even at temperatures some 15° below T_m. In both cases, the magnitude of the induced change falls between 28°C and T_m (~30°C). This is a consequence of the surface melting effect

mentioned in Section 2.4: As the thermostat temperature approaches T_m, the 'ground-state' reflectivity of the interface increases (See curve *i* in Figure 2.2a). The maximum change that can be achieved by laser excitation subsequently decreases. No pump-induced reflectivity change is seen at temperatures above 30°C because the entire gallium bulk is then in a high-reflectivity state (specifically the liquid state) regardless of any laser excitation.

3.5 Thermally-induced metallization of α-gallium

It was established in Chapter 2 that the light-induced reflectivity increase observed at gallium/glass interfaces is the result of optically-induced metallization of α-gallium. However, the mechanisms of metallization that dominate under a regime of nanosecond optical pulses are expected to be somewhat different from those underlying the response to cw excitation. Indeed, as discussed in the previous section, certain features of the response curves suggest that the induced reflectivity changes are primarily a result of laser-induced heating. A numerical simulation of the experiment, outlined below, demonstrates very clearly that this is indeed the case.

Thermal diffusion removes energy very effectively from the skin layer when the optical excitation is continuous or in the form of long pulses because the characteristic thermal diffusion length is much longer than the skin depth. For example, in the 100 ns, 1550 nm pulse experiments described in Section 2.6, the diffusion length $\sqrt{\chi\tau_p}$ ~850 nm, where $\chi = 7.3 \times 10^{-6}$ m^2.s^{-1} is the thermal diffusivity in the direction perpendicular to the interface [4] (assuming a crystalline orientation as described in Section 2.5), and τ_p is the pulse duration. The skin depth at 1550 nm is ~38 nm. Under these circumstances, metallization results from crystalline cells undergoing a non-thermal transition to a metastable metallic state. With very short pump pulses (~picoseconds), there would be negligible thermal diffusion during the pulse and the excitation energy would be confined to the skin layer, leading to thermal melting of the metal. For the nanosecond pulses used in the experiments described above, there will be a certain amount of

thermal diffusion, but during the pulses it cannot be expected to completely dissipate the pump energy absorbed within the skin layer. Consequently, a thermally-induced structural transition is likely to be the dominant mechanism of metallization, and is believed to proceed along the following lines: A pump pulse incident on the gallium/silica interface penetrates the metal, with an exponentially decreasing intensity profile, to a depth of several tens of nanometres. The absorption of laser radiation leads to an increase in the gallium's temperature and, if more energy is absorbed than is required to reach a phase transition temperature, any excess energy contributes towards the transition itself. So for a given thermostat temperature and pump fluence (below the saturation level), the energy deposited in the first few nanometres of gallium will be sufficient to achieve complete metallization. Further from the interface, there will still be enough energy to bring the gallium to its transition temperature, but metallization will be incomplete. The extent of metallization will decrease with increasing distance from the interface up to the point where the energy absorbed is not enough to achieve the transition temperature. The net result of this process, in terms of the reflectivity seen by the probe beam, is essentially the same as that arising from the non-thermal metallization process described in Section 2.5, i.e. the reflectivity of the interface depends on the thickness of a metallic gallium 'layer' where that thickness is a function of thermostat temperature and incident laser fluence.

To substantiate this thermal metallization model, a numerical simulation was performed by V. A. Fedotov. It was based on the assumption that the metallic phase was liquid gallium, i.e. the induced structural change was simply melting. This is not to say that the metallic phase really is liquid gallium: As detailed in Section 2.7, the 'melting' of α-gallium is probably more than a simple solid-to-liquid transition, given that several crystalline phases, which are energetically close to the liquid and have very similar properties, are known to exist. The liquid was chosen for the purposes of the following calculations simply because data on its physical and optical properties is readily available.

Optical absorption by electrons leads to heating of the crystalline lattice within the skin layer through electron-phonon relaxation. The electron and lattice temperatures

equilibrate rapidly because the pulse duration is much longer than the electron-phonon energy relaxation time $\tau_{e\text{-}ph}$, which is given by the formula [5]

$$\tau_{e-ph} \approx \frac{h\omega}{2\pi\omega_{ph}k_bT\lambda} \sim 1 \text{ ps} \qquad (3.1)$$

where $\omega_{ph} = 8 \times 10^{12}$ s^{-1} is the optical phonon frequency of gallium dimer vibrations, $\lambda = 0.4$ is the dimensionless electron-phonon coupling constant for gallium [5] and typical experimental values of $T = 300$ K and $\omega = 4.71 \times 10^{15}$ s^{-1} are used. Since $\tau_p >> \tau_{e\text{-}ph}$, and the thermal diffusion length in the plane of the interface (~0.3 μm) is much smaller than the beam diameter (3 mm), the problem can be reduced to a one-dimensional thermal conductivity problem in the direction perpendicular to the interface (See Figure 3.5). It can therefore be expressed in terms of the temperature distribution $T(x,t)$:

$$\rho c \frac{\partial T(x,t)}{\partial t} - \frac{\partial}{\partial x}\left(\lambda \frac{\partial T(x,t)}{\partial x}\right) = A(x,t) \qquad (3.2)$$

where the heat source $A(x,t)$ describes a supply of energy from the absorption of laser radiation.

It was assumed that the reflectivity changed continuously during irradiation and that the density ρ, heat capacity c, thermal conductivity λ and dielectric properties of gallium were functions of state (solid or molten). To apply the finite-difference integration scheme, a set of nodes, separated by a minimum increment of 8×10^{-10} m, was introduced along the x-axis and a small volume of material was associated with each node (Figure 3.5b). The time increment used was 3×10^{-14} s, as determined by von Neumann stability analysis. The temperature at each node was constantly monitored and if the gallium at a given node reached its melting point, T_m, it was maintained at that temperature until the net heat accumulated equalled or exceeded the latent heat of melting. After melting, the properties of the gallium at that node were changed from those of solid gallium to those of the liquid. Nodes where the melting point was reached, but where the heat supplied was not enough to achieve a complete transition, were assumed to contain a two-phase mixture with properties between those of the

solid and molten phases (the composition of the mixture and resultant optical properties being proportional to the fraction of the latent heat supplied). The reflectivity of the interface (integrated over the pulse duration) was evaluated using a matrix technique that considered the set of nodal volumes as a set of layers with different optical properties (Figure 3.5c). Refractive index data for solid and liquid gallium were taken from Kofman *et al.* [6] (via Albanis [7]) and from Teshev and Shebzukhov [8] respectively.

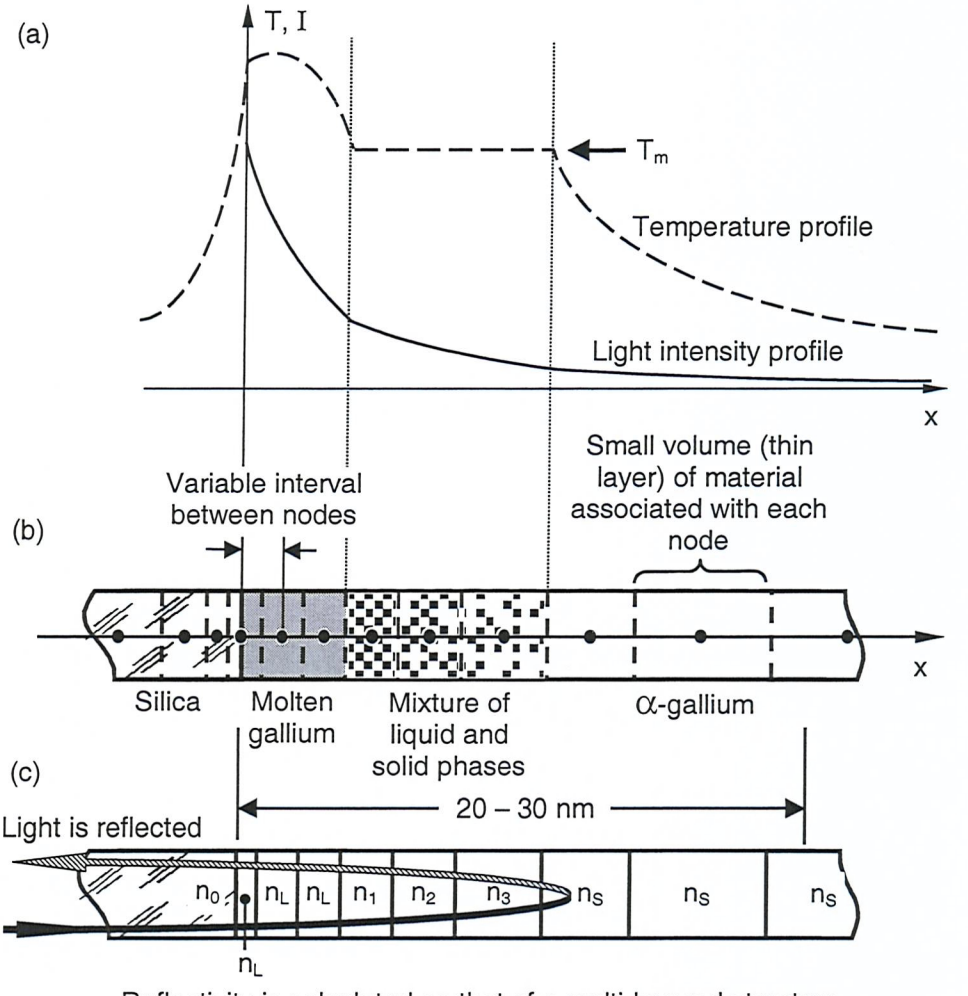

Figure 3.5: Schematic representation of the laser-induced melting model for metallization of α-gallium at an interface with silica. (a) Pump intensity, and resultant temperature profiles in gallium near to the interface; (b) The energy absorbed causes complete melting of gallium close to the interface and partial melting further into the gallium bulk. The structure is divided into 'nodes' to facilitate a numerical simulation of the metallization process; (c) The reflectivity of the interface is determined by the refractive index profile generated as a result of light-induced melting: n_0 = silica, n_S = solid gallium, n_L = liquid gallium, $n_{1,2,3,}$ = value between n_S and n_L depending on the phase composition of the node. [Illustrations prepared by V. A. Fedotov.]

This simulation produces a good facsimile of the experimental data (See Figure 3.6) if account is taken of the fact that a transitional metallic layer a few nanometres thick is present at the UPLD gallium/silica interface even in the absence of optical excitation (See Section 2.3).

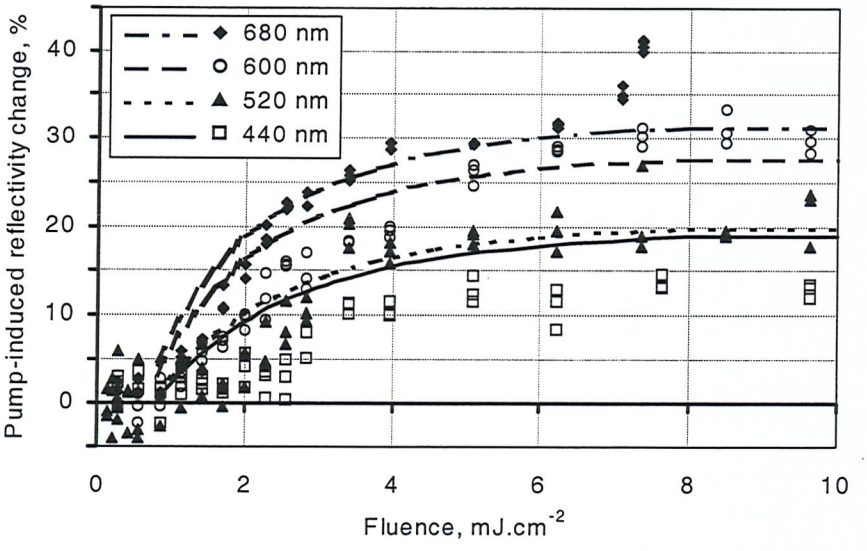

Figure 3.6: Change induced in gallium/silica interface reflectivity by 3 ns pump pulses at 26°C as a function of pump fluence. Experimental data (from figure 3.3a) are shown as points. Fittings derived by V. A. Fedotov from a numerical simulation of the experiment are shown, for illustrative purposes, as lines.

The numerical model verifies the existence of a temperature-dependent fluence threshold for the observation of a pump-induced effect and, as Figure 3.7 shows, correctly predicts the form of the temperature dependence curves for the induced reflectivity change. Note, however, that this purely thermal model underestimates the magnitude of the nonlinear response at temperatures more than a few degrees below the melting point. This discrepancy may be an indication that the non-thermal metallization process still makes a tangible contribution to the response under an excitation regime of nanosecond pulses.

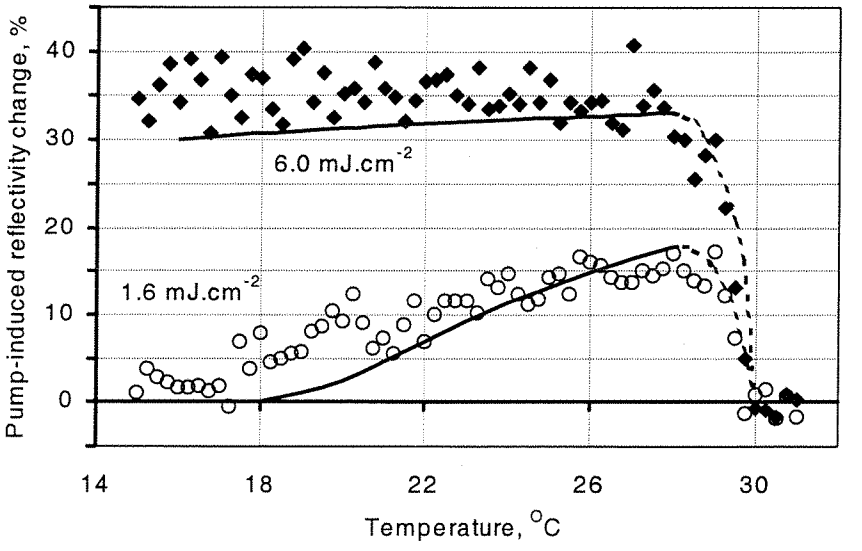

Figure 3.7: Change induced in gallium/silica interface reflectivity by 3 ns pump pulses at 680 nm as a function of interface temperature. Experimental data (from figure 3.3b) are shown as points. Fittings derived by V. A. Fedotov from a numerical simulation of the experiment are shown, for illustrative purposes, as lines. The dashed lines were added by hand because, close to T_m, the 'ground state' (pre-excitation) reflectivity of the interface changes rapidly with temperature (as a result of surface melting) and the numerical model can only qualitatively predict the drop in magnitude.

3.6 Ultrafast dynamics of reflectivity switching in gallium

Since the introduction of femtosecond lasers in the mid-1980's, the study of ultrafast, laser-induced phase transitions has generated considerable interest. Motivated by potential applications in materials processing, optical switching and optoelectronics, numerous studies have been devoted to the dynamics of such transitions in a range of (primarily semiconductor) materials [9-21]. It was considered that an understanding of gallium's ultrafast response dynamics would be important both in terms of fundamental physics, where it may provide further insight into the nature of the response mechanisms, and in relation to the development of practical switching applications [1, 2], where the response dynamics will ultimately determine a device's performance limits.

A femtosecond pump-probe reflectometer, shown schematically in Figure 3.8, was therefore assembled. The low-power 'probe' arm of this device was essentially

identical to the single-beam reflectometer shown in Figure 2.1 and described in Section 2.4. A computer-controlled corner-cube delay-line was used to vary the relative timing of the pump and probe pulses around the zero position, which was located by maximising second harmonic generation in a thin (~200 μm) KTP crystal at the sample position. Pump power was controlled using a variable attenuator.

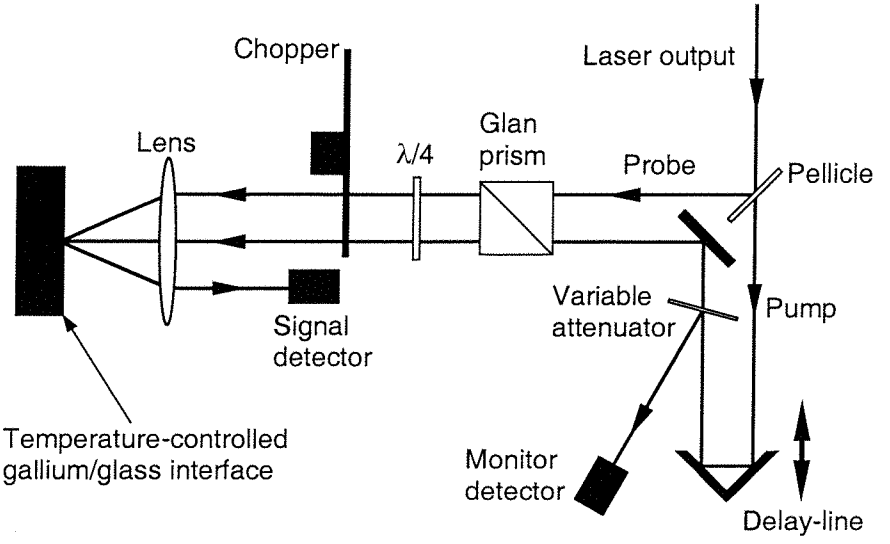

Figure 3.8: Schematic of the femtosecond pump-probe reflectometer, based on a Ti:sapphire laser, designed to study the dynamics of reflectivity switching at UPLD gallium/glass interfaces. The pump and probe were chopped at different rates to facilitate sum-frequency lock-in detection.

The Ti:sapphire laser produced pulses of ~50 fs duration at a wavelength of 810 nm with a repetition rate of ~87 MHz. Both the pump and probe were focused to ~20 μm diameter spots and made to overlap on the gallium/glass interface. The probe fluence was maintained at <4 $\mu J.cm^{-2}$. The maximum pump fluence used was ~0.1 $mJ.cm^{-2}$. (Beam diameters were measured using the pinhole technique described in Section 2.4, and fluences were calculated from measurements of average power at the sample position.)

These experiments did not detect any ultrafast pump-induced reflectivity changes. It was concluded that this may either have been because the energy of the pump pulses was not sufficient to induce any change, or because the repetition rate of the laser was too high (i.e. the probe beam saw a constant reflectivity level because there was no time for induced changes to relax between one pump pulse and the next).

A similar series of transient pump-probe reflectivity measurements was subsequently performed by our collaborative partners at the Australian National University in Canberra, and by Prof. N. I. Zheludev on one of his visits to their facility. For the purposes of these experiments, high power, low repetition rate (30 Hz) Nd:YLF and Ti:Sapphire lasers were used to produce 6 and 60 ps pulses at a wavelength of 1053 nm (Nd:YLF), and 150 fs pulses at 800 nm (Ti:Sapphire).

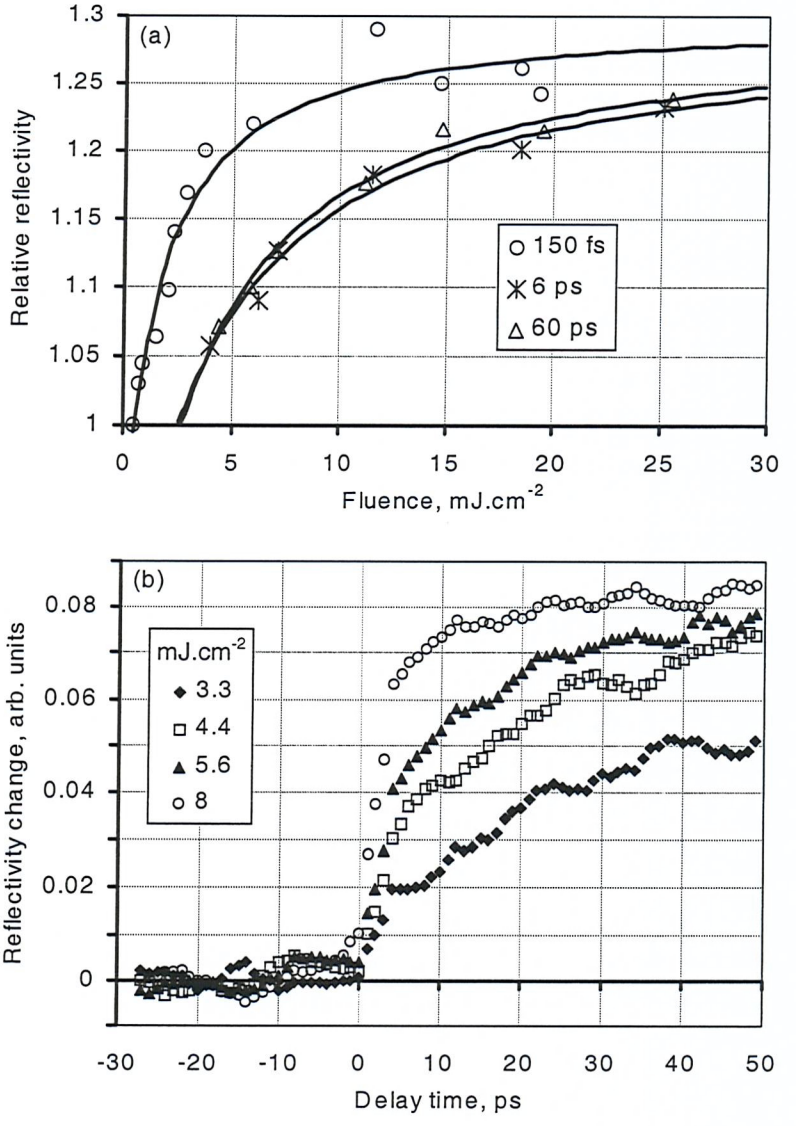

Figure 3.9: (a) Relative reflectivity of a gallium/silica interface 500 ps after 150 fs (λ = 800 nm), 6 ps and 60 ps (λ = 1053 nm) pump pulses of varying fluence. The thermostat temperature was 21°C; (b) Pump-induced reflectivity change against pump-probe delay for 150 fs pump pulses of varying fluence at a thermostat temperature of 21°C. These data, shown here for illustrative purposes, were collected at the Australian National University in Canberra by A. V. Rode and, during a visit to Canberra, by N. I. Zheludev from the University of Southampton.

In each case, a threshold pump fluence was found to be required for the observation of an induced reflectivity change, and the magnitude of the induced change was seen to saturate at a fluence of ~20 $mJ.cm^{-2}$ (Figure 3.9a). These measurements also demonstrated that the reflectivity increase is a two-stage process (See Figure 3.9b): There is an initial rapid increase, during the first 2-4 ps after excitation (only resolved by the 150 fs pulses), followed by a slower increase over the next 300 – 500 ps. The rate of change of reflectivity during the initial increase is proportional to the pump fluence but is independent of the thermostat temperature.

Gallium's response to pico- and femtosecond optical pulses may be compared with the 'ultrafast melting' processes studied in various semiconductors and metals [9-21]. Such comparison reveals that the threshold fluence for ultrafast melting of gallium is particularly low - at least an order of magnitude smaller than the threshold in materials such as silicon and gallium arsenide. This may be explained by the fact that in silicon, for example, all of the inter-atomic bonds are covalent and its enthalpy of melting is thus approximately nine times higher than that of α-gallium. Furthermore, the above-bandgap absorption depth in silicon is around ten times larger than the absorption depth in gallium, so more energy is required to melt the skin layer. The dynamics of gallium's response are broadly consistent with the ultrafast thermal melting process observed (and numerically simulated) in gallium arsenide by Sokolowski-Tinten *et al.* [10]: Immediately following the excitation pulse, the gallium at the interface is strongly overheated (i.e. the temperature of the solid exceeds the equilibrium melting temperature). Melting occurs by nucleation of the liquid phase, beginning at the interface and propagating into the solid [13]. The initial velocity of the melt front is very high (~hundreds of $m.s^{-1}$) – hence the sharp reflectivity increase during the first few picoseconds after excitation. As latent heat is consumed, the extent of overheating is greatly reduced and the velocity of the melt front (viz. the rate of change of reflectivity) falls accordingly (to just a few tens of $m.s^{-1}$).

The relaxation dynamics of the induced reflectivity changes were recorded using a cw probe beam from a He-Ne laser and a photodetector with ~10 ns resolution. The decay times are in the microsecond range (See Figure 3.10), i.e. much longer than the response times, and are strongly dependent on the thermostat temperature.

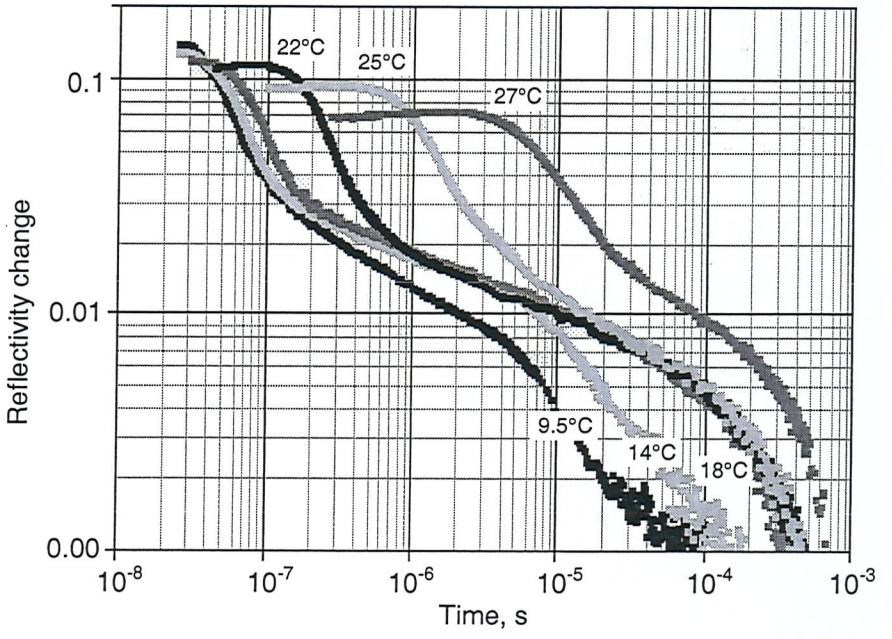

Figure 3.10: Reflectivity relaxation dynamics at various thermostat temperatures following 60 ps pump pulses with a fluence of 15 mJ.cm^{-2}. These data were collected by A. V. Rode at the Australian National University in Canberra and are shown here for illustrative purposes.

At temperatures closer to gallium's melting point more time is required before the reflectivity begins to decrease, because it takes more time for the liquid metal to cool to the solidification temperature and then begin to recrystallize. As the gallium returns to the α-phase the reflectivity of the interface falls. The rate of crystallization is determined by the rate at which heat is transferred away from the excitation region by conduction through both the gallium bulk and the silica substrate. The presence of two very different thermal conduction channels is illustrated by the complex (approximately double exponential) nature of the reflectivity decay curves.

3.7 Summary and conclusions

A pump-probe reflectometer, with an optical parametric oscillator as the light source, was used to study the response of UPLD gallium/silica interfaces to nanosecond laser pulses. In the course of this work, data were collected on the temperature, fluence and

wavelength dependencies of pump-induced reflectivity changes. The results suggested that a thermally-induced structural transition, involving a thickness of no more than a few tens of nanometres of gallium, was responsible for these changes, and a numerical simulation of the experiment strongly supported this interpretation.

This study has demonstrated that gallium/silica interfaces are sensitive to low-fluence nanosecond optical excitation at wavelengths throughout the visible spectrum. Given that such interfaces are known to show an optical response at certain wavelengths up to 2.8 μm (See references 1, 22 and 23), it would not be unreasonable to expect that the gallium/silica structure is continuously sensitive to all wavelengths in the range from the visible to mid-infrared. Furthermore, it may be anticipated that given sub-picosecond excitation pulses of sufficient energy, the ultrafast melting mechanism will yield picosecond switching times throughout this wavelength range. Figure 3.11 shows the switching contrast that might be expected from a gallium/silica mirror for wavelengths from 440 to 2200 nm.

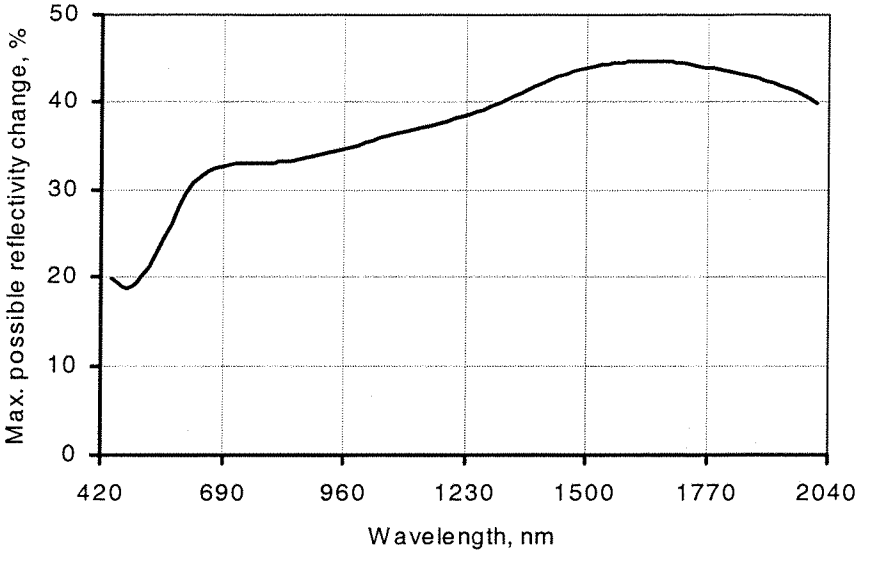

Figure 3.11: Maximum change expected in the reflectivity of a gallium/silica interface, as the result of laser-induced thermal metallization (assuming the existence of a 4 nm metallic gallium layer at the interface even in the absence of laser excitation).

In terms of applications, such a broadband response characteristic may give gallium-based devices a significant advantage over competing technologies. For example, most materials employed to passively Q-switch lasers operate at specific wavelengths or in

relatively narrow spectral ranges [24-26]. In contrast, it has already been shown [1] that the same gallium mirror can passively Q-switch fibre lasers at both 1030 and 1550 nm. However, the gallium structure's microsecond relaxation times are likely to limit its range of potential applications to those, like Q-switching, that do not necessarily require high repetition rates or sharp transitions in both directions.

3.8 References

1 P. Petropoulos, H. L. Offerhaus, D. J. Richardson, S. Dhanjal and N. I. Zheludev, Appl. Phys. Lett. **74**, 3619 (1999).

2 P. J. Bennett, S. Dhanjal, P. Petropoulos, D. J. Richardson, N. I. Zheludev and V. I. Emel'yanov, Appl. Phys. Lett. **73**, 1787 (1998).

3 S. Dhanjal, K. F. MacDonald, P. Petropoulos, D. J. Richardson and N. I. Zheludev, in *Conference on Lasers and Electro-optics 1999*, Technical digest (Opt. Soc. Am., Washington DC, USA, 1999), p. 282-283.

4 *CRC Handbook of Chemistry and Physics*, 73rd edition (CRC Press Inc., Boca Raton, 1992).

5 W. A. Harrison, in *Electronic Structure and the Properties of Solids: The Physics of the Chemical Bond* (Constable and Company, Ltd., London, 1989), p. 396-399.

6 R. Kofman, P. Cheyssac and J. Richard, Phys. Rev. B **16**, 5216 (1977).

7 V. Albanis, Ph.D. thesis, University of Southampton, 2001.

8 R. Sh. Teshev and A. A. Shebzukhov, Opt. Spectrosc. (USSR) **65**, 693 (1988).

9 Y. Siegal, E. N. Glezer, L. Huang and E. Mazur, Annu. Rev. Mater. Sci. **25**, 223 (1995).

[10] K. Sokolowski-Tinten, J. Bialkowski, M. Boing, A. Cavalleri and D. von der Linde, Phys. Rev. B **58**, R11805 (1998).

[11] C. W. Siders, A. Cavalleri, K. Sokolowski-Tinten, Cs. Toth, T. Guo, M. Kammler, M. Horn von Hoegen, K. R. Wilson, D. von der Linde and C. P. J. Barty, Science **286**, 1340 (1999).

[12] C. Guo, G. Rodriguez, A. Lobad and A. J. Taylor, Phys. Rev. Lett. **84**, 4493 (2000).

[13] N. Fabricus, P. Hermes, D. von der Linde, A. Pospieszczyk and B. Stritzker, Solid State Commun. **58**, 239 (1986).

[14] G. L. Eesley, Phys. Rev. Lett. **51**, 2140 (1983).

[15] H. E. Elsayed-Ali, T. B. Norris, M. A. Pessot and G. A. Mourou, Phys. Rev. Lett. **58**, 1212 (1987).

[16] J. G. Fujimoto, J. M. Liu, E. P. Ippen and N. Bloembergen, Phys. Rev. Lett. **53**, 1837 (1984).

[17] C. V. Shank, R. Yen and C. Hirlimann, Phys. Rev. Lett. **50**, 454 (1983).

[18] H. W. K. Tom, G. D. Aumiller and C. H. Brito-Cruz, Phys. Rev. Lett. **60**, 1438 (1988).

[19] P. Saeta, J-K. Wang, Y. Siegal, N. Bloembergen and E. Mazur, Phys. Rev. Lett. **67**, 1023 (1991).

[20] K. Sokolowski-Tinten, J. Bialkowski and D. von der Linde, Phys. Rev. B **51**, 14186 (1995).

[21] L. Huang, J. P. Callan, E. N. Glezer and E. Mazur, Phys. Rev. Lett. **80**, 185 (1998).

[22] K. F. MacDonald, V. A. Fedotov, R. W. Eason, N. I. Zheludev, A. V. Rode, B. Luther-Davies and V. I. Emel'yanov, J. Opt. Soc. Am. B **18**, 331 (2001).

[23] N. J. C. Libatique, J. D. Tafoya and R. K. Jain, in *Conference on Lasers and Electro-optics 2000*, technical digest (Opt. Soc. Am., Washington DC USA, 2000), p. 76-77.

[24] D. C. Jones and D. A. Rockwell, Appl. Opt. **32**, 1547 (1993).

[25] V. V. Ter-Mikirtychev, Opt. Commun. **119**, 109 (1995).

[26] R. Paschotta, R. Haring, E. Gini, H. Melchior, U. Keller, H. L. Offerhaus and D. J. Richardson, Opt. Lett. **24**, 388 (1999).

Chapter 4

Light-assisted self-assembly of gallium nanoparticles

4.1 Synopsis

It has been found that light can dramatically influence and regulate the nanoparticle self-assembly process: Laser illumination of a substrate exposed to a beam of gallium atoms results in the formation of gallium nanoparticles with a relatively narrow size distribution. Very low light intensities, below the threshold for thermally-induced evaporation, exert considerable control over particle formation through a combination of non-thermal processes.

Section 4.3 describes the construction of a UHV gallium deposition system that was built to enable the preparation and in-situ study of gallium interfaces. A series of experiments to establish the conditions required for the light-assisted self-assembly of gallium nanoparticles is documented in Section 4.4. The findings of these experiments made possible the development of a theory to explain the mechanisms that enable optical control of nanoparticle formation. This theory is outlined in Section 4.5.

4.2 Introduction

Given the extensive range of potential applications, in fields such as spectroscopy [1, 2], microscopy [3], data storage [4, 5], energy transport [6], sensitive infrared detection [7, 8], and

selective catalysis [9, 10], the preparation of monodisperse metallic nanoparticles is a very important process. These applications rely on the fact that the properties of such nanoparticles, both individual and collective, are very different from those of the corresponding bulk metals. Their unique properties stem from the highly confining nature of the nanoparticle geometry: The high surface-to-volume ratios lead to local field-enhancement effects and can dramatically modify a material's properties and its phase diagram [11-15].

The work reported in Chapters 2 and 3 demonstrates that the one-dimensional confinement of gallium at an interface facilitates reversible light-induced structural transitions in the metal, which lead to a substantial optical nonlinearity. The study of gallium nanoparticles, in which the metal is confined in three dimensions, is a logical progression of this work. Indeed, it may be anticipated that gallium nanoparticles will show more pronounced, or perhaps new, nonlinear characteristics that could be exploited in nanoscale photonic devices.

Self-assembly has been one of the main approaches to the preparation of spontaneously ordered and disordered nanoparticles [16-22], including particles of liquid gallium on silica [23]. However, the problem with such fabrication procedures is that they tend to produce particles with a broad range of diameters, thus obscuring the size-dependent properties that are essential to many applications. Very small clusters (<20 atoms) of well-defined size can be produced by mass-separation of charged clusters in the gas phase [24], and larger structures can be synthesised with high size-uniformity using lithographic techniques [25]. Several procedures for the manipulation of nanoparticle shape, size and size distribution, based on evaporation, desorption and fragmentation processes induced by high-power pulsed lasers, have also been reported [26-31].

This chapter details a comparatively simple 'light-assisted self-assembly' process for the production of gallium nanoparticles. By slowly depositing gallium on cryogenically cooled silica substrates and simultaneously exposing the substrates to pulses from a low-power diode laser, particles with a relatively narrow size distribution can be fabricated. Very low light intensities, below the threshold for thermally-induced evaporation, exert considerable control over nanoparticle formation through at least one, and possibly a combination of two, non-thermal processes.

4.3 UHV gallium deposition system

As discussed in Sections 2.2 and 2.3, the preparation of high-quality gallium interfaces is by no means a trivial task. Whilst a certain number of UPLD gallium/silica interfaces were available through collaboration with the Australian National University in Canberra (See Section 2.3), this arrangement did not allow for the optical properties of the interfaces to be studied during deposition or prior to removal from vacuum, nor could it provide thin film or nanoparticle samples. It was therefore decided that a dedicated gallium deposition facility would be built in Southampton.

To this end, a UHV chamber equipped with an atomic beam gallium source, cryogenically-cooled substrate holder and, importantly, provision for the use of cleaved optical fibre tips as substrates, was designed and constructed from scratch. This system, pictured in Figure 4.1 and shown schematically in Figures 4.2 and 4.3, was based around a turbomolecular pump and a small, fourteen-port 'spherical square' vacuum chamber. Atomic beam deposition was chosen in preference to other sample preparation techniques because it provides an ultimately clean and controllable means of fabricating gallium interfaces.

It was determined that the gallium source would need to operate at a temperature of approximately 1000°C to achieve a vapour pressure of about 5×10^{-3} mbar (Ref. 32). A resistively heated oven was therefore constructed along the lines of a design developed by Ross [33]: An open-topped crucible was manufactured from graphite (a material known to be suitable for use with gallium [34]) so as to be a 'slide fit' into a tantalum foil tube. Two independent heating elements, made from molybdenum wire and twin-bore alumina rods, were wrapped around this tube and held in place with a second tantalum tube. Two chromel-alumel thermocouples were incorporated into this heater assembly, one in contact with the mouth of the crucible and the other with the inner tantalum tube at the base of the crucible. Radiation shields, comprising concentric tantalum tubes spaced with carbon wool, completed the oven, which was housed in a water-cooled arm of the vacuum system. This arm could be isolated from the rest of the system using a gate valve, thus allowing for substrates and other components in the chamber to be changed without exposing the gallium source to the atmosphere.

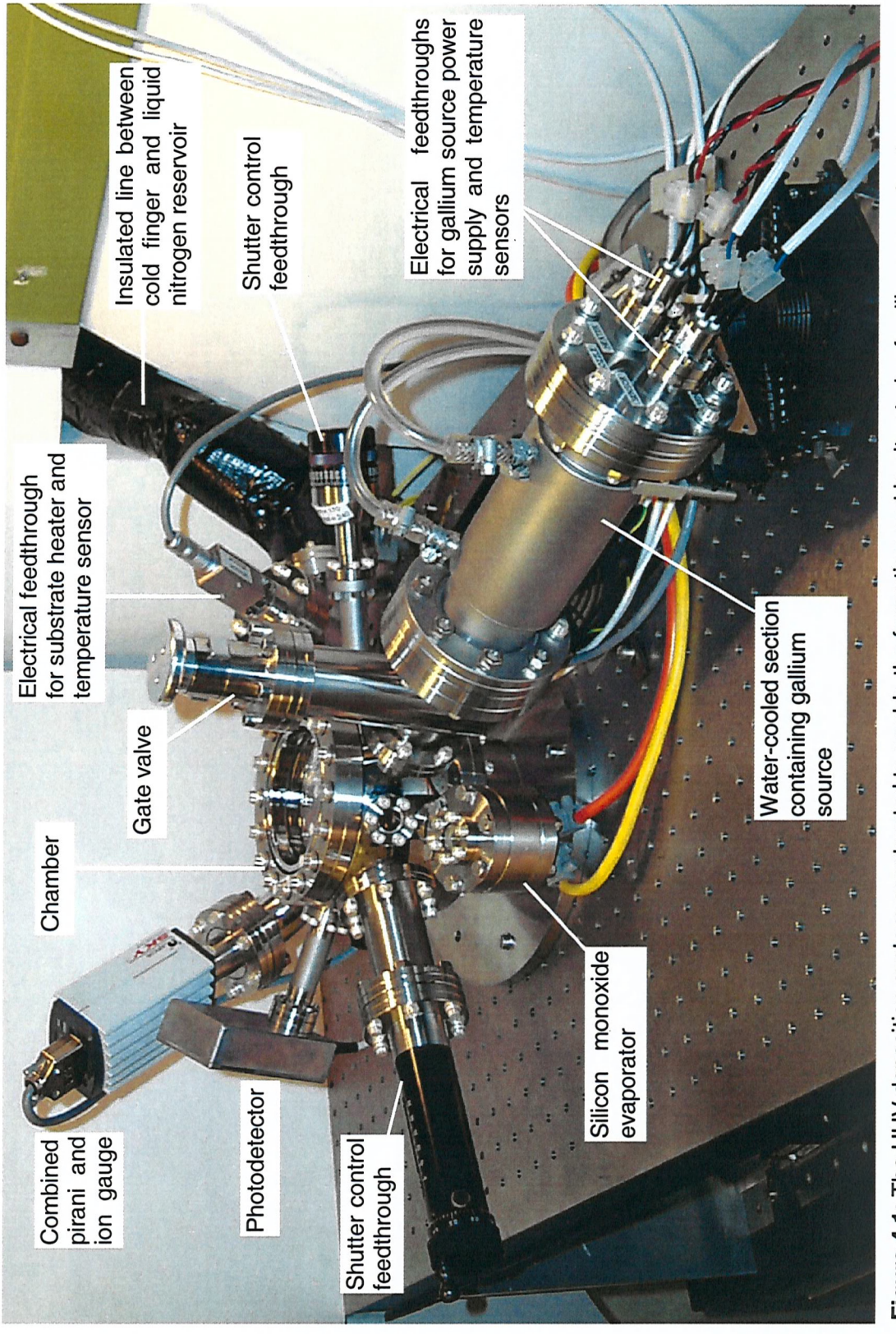

Figure 4.1: The UHV deposition system constructed to enable the formation and in-situ study of gallium nanostructures.

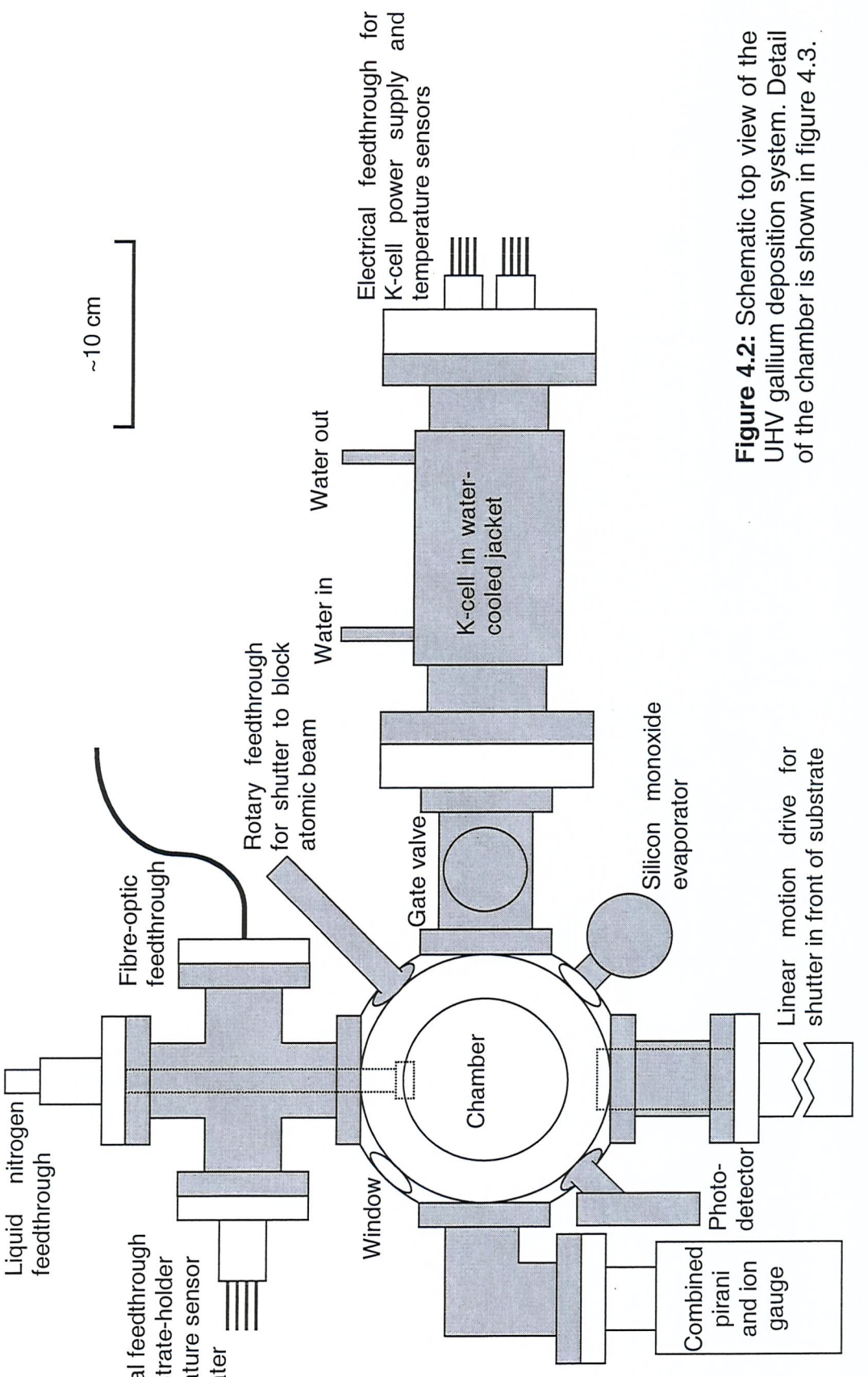

Figure 4.2: Schematic top view of the UHV gallium deposition system. Detail of the chamber is shown in figure 4.3.

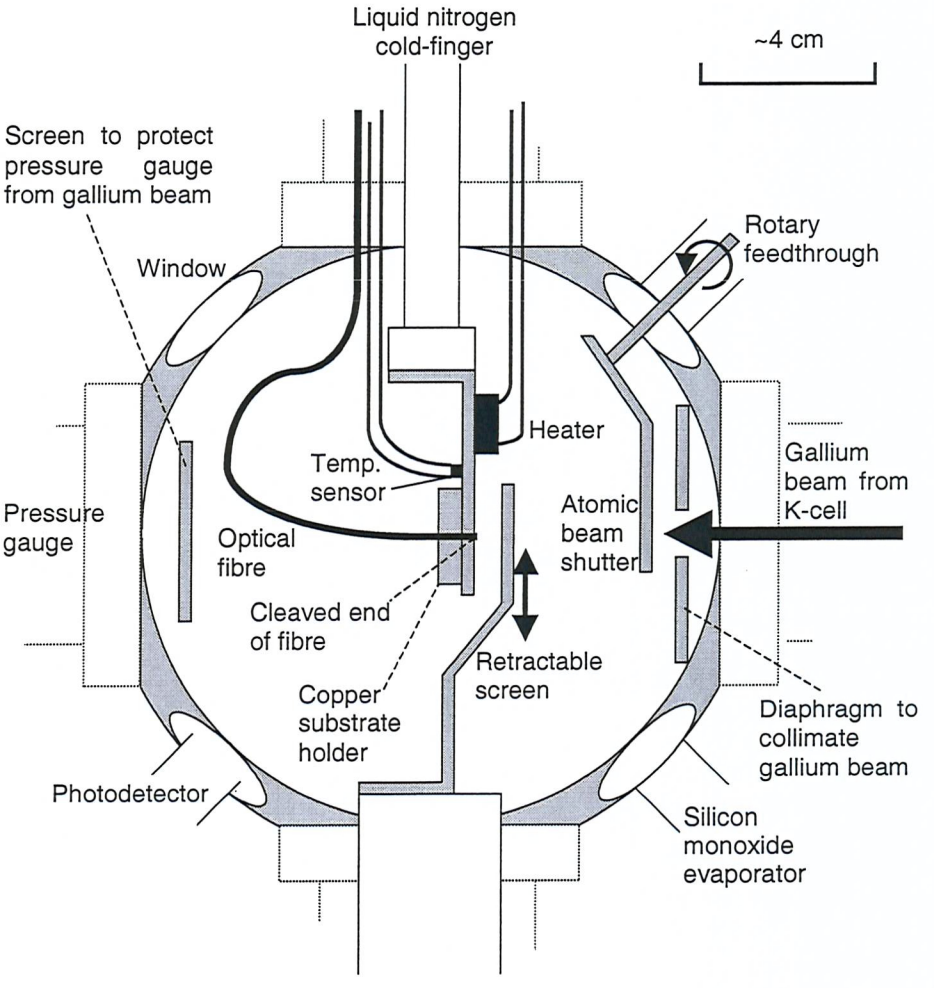

Figure 4.3: The arrangement of components in and around the main chamber of the gallium deposition system.

A substrate holder, incorporating a silicon-diode temperature sensor and a small resistive heater, was mounted on the end of a liquid-nitrogen-cooled cold-finger. It was positioned at the centre of the chamber and allowed for substrate temperatures to be controlled throughout the range from 100 to 300 K. This arm of the system also included a purpose-built fibre-optic feedthrough so that optical systems outside the chamber could be connected to fibre substrates inside, both during and after deposition, without breaking the vacuum. Other ports around the chamber accommodated the following:

- A pressure gauge covering the range from atmospheric pressure to 5×10^{-10} mbar.

- A photodetector to monitor light emerging from the fibre substrates.
- A silicon monoxide evaporator (a small alumina crucible with a built-in heating element) so that, if required, protective coatings could be applied to gallium films before their removal from vacuum.
- Mechanical shutters to block the gallium and silicon monoxide sources.

This system typically achieved pressures of ~10^{-8} mbar, rising to ~5 x 10^{-6} mbar when the gallium source was in operation. By setting the crucible temperature to 985°C at the base and 1000°C at the mouth (slightly higher at the mouth to prevent evaporated material from condensing on the walls of the crucible), a gallium deposition rate of ~0.3 nm.min^{-1} (measured using a quartz crystal microbalance) was routinely obtained.

4.4 Light-assisted nanoparticle formation - Experiments

A series of experiments was performed to establish the conditions required for the formation of gallium nanoparticles on optical fibre substrates. In each case:

- the fibres used were single-mode (at both 1.31 and 1.55 μm) silica fibres with core and cladding diameters of 9 and 125 μm respectively;
- the 'in-vacuum' ends of the fibres were cleaved and attached to the copper substrate-holder on the end of the cold-finger, such that they pointed towards the gallium source and protruded from the holder by as short a distance as possible (See Figure 4.4);
- the chamber was evacuated and the fibres were exposed to the gallium source for thirty minutes;
- the fibres were subsequently removed from the chamber and examined using optical and atomic force microscopes.

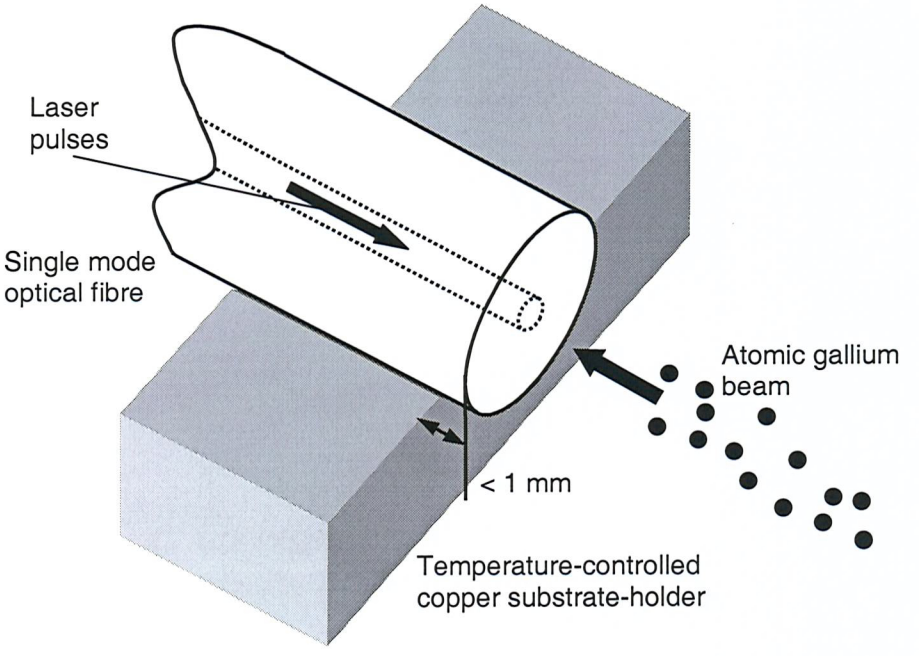

Figure 4.4: Schematic of an optical fibre on the substrate holder. The fibre was clamped in position with a second copper section.

Gallium was first deposited on fibre tips at room temperature (i.e. the cold-finger was not cooled). This led to the formation of glossy featureless mirror-like gallium layers (See Figure 4.5). Atomic force microscope (AFM) scans, with resolutions down to a few nanometres, showed that the gallium films were flat.

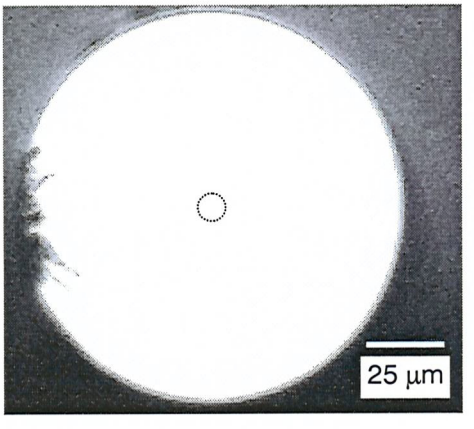

Figure 4.5: Optical microscope image of a fibre tip on which gallium was deposited whilst it was at room temperature. The dotted line indicates the position of the fibre's core. The rough edge on the left is a result of the cleaving process.

Next, deposition was performed on cryogenically cooled fibres: A continuous flow of liquid nitrogen through the cold finger maintained the substrate holder at a temperature of ~100 K during deposition. Thirty minutes of deposition under these conditions produced a uniform, rough layer of gallium (See Figure 4.6). AFM scans of the fibre

tips revealed that the gallium was in lumps of varying shape and size, from a few nanometres to several tenths of a micron.

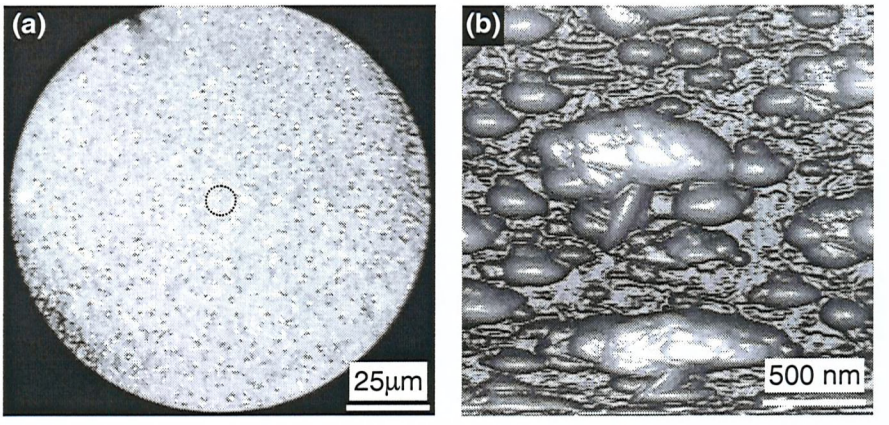

Figure 4.6: (a) Optical microscope image of a fibre tip on which gallium was deposited whilst it was at a temperature of ~100 K. The dotted line indicates the position of the core. (b) Atomic force microscope image of the irregular gallium structures on the fibre's surface.

In further experiments, the 'out-of-vacuum' ends of the fibres were connected to a diode laser operating at a wavelength of 1.55 μm and producing 1 μs pulses, with peak powers of 17 mW, at a rate of 1 kHz (average power = 17 μW, individual pulse energy = 17 nJ). Again, the fibres were cooled to ~100 K during deposition. Under these circumstances, the gallium layers formed had two distinct parts (See Figure 4.7).

For the most part, the fibres were covered with a dull, 'rough' gallium structure, like that shown in Figure 4.6. However, on the cores of the fibres, which were exposed to the laser during deposition, a highly reflective layer of gallium nanoparticles was formed. These had a typical diameter of ~80 nm* and a relatively narrow size distribution. At this stage it was found that if a fibre's tip protruded by more than ~1 mm from the front surface of the cold-finger, neither the nanoparticles nor the rough gallium structure were formed. Instead, a featureless layer of gallium developed, as if the fibre had not been cooled during deposition.

* As measured from the AFM image taken at room temperature and pressure. To obtain the true particle size, the dimensions of the AFM tip must be taken into account (See Appendix B).

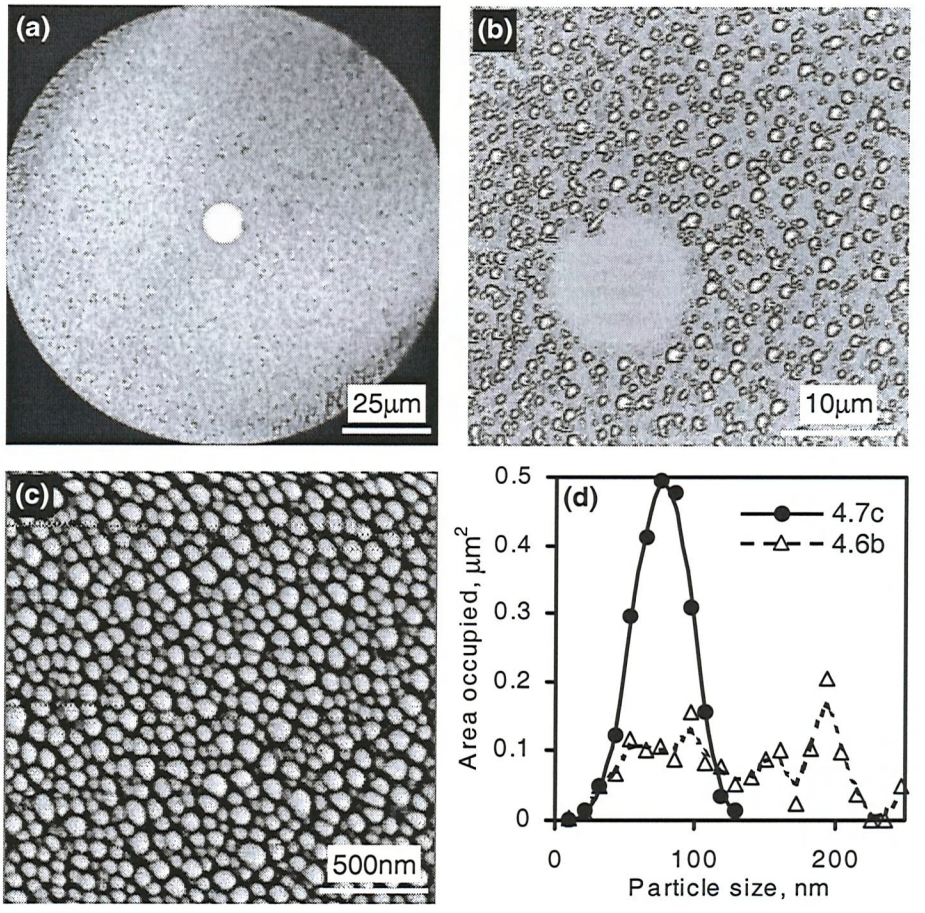

Figure 4.7: (a) Optical microscope image of a fibre tip on which gallium was deposited whilst it was at a temperature of ~100 K with laser pulses present in the core. It should be noted that this is a reflection image. There was no light emanating from the fibre's core when it was taken. The core appears bright because the gallium there is more reflective than that on the rest of the surface; (b) Atomic force microscope image of an area encompassing the fibre's core, which is clearly visible as a crater-like formation; (c) Atomic force microscope image showing the nanoparticle structure formed on the surface of the fibre's core; (d) Area occupied by particles as a function of their size for image c (—•—) and, for comparison, image 4.6b (- Δ -). The nanoparticles on the fibre's core have a relatively narrow size distribution centred at ~80 nm (sizes were measured directly from the image, i.e. without accounting for the finite size of the probe tip).

To determine whether the light-assisted nanoparticle formation took place during deposition or during the process of bringing the gallium-coated fibres from ~100 K back to room temperature after deposition, two further sets of experiments were performed. In the first, the laser was switched on only while gallium was being deposited. In the second the laser remained off until the end of deposition and was then switched on while the fibre was warmed to room temperature. Only under the first set

of conditions, where laser pulses were present during deposition, was a well-defined reflective area of nanoparticles formed on the cores of the fibres.

To summarise, this series of experiments illustrates that efficient cooling of the fibre tip and the presence of laser pulses during deposition are essential for the creation of gallium nanoparticles on the core of a fibre.

In an additional experiment, gallium was deposited more slowly (at ~0.1 rather than 0.3 $nm.min^{-1}$) but for much longer than normal (six hours rather than thirty minutes) on a cooled fibre connected to the pulsed laser. The mass of gallium deposited in this experiment (four times the 'normal' quantity) was such that in areas not exposed to laser light it coagulated into large blobs (probably during warming) and on the fibre's core, it formed particles with diameters ~230 nm (See Figure 4.8).

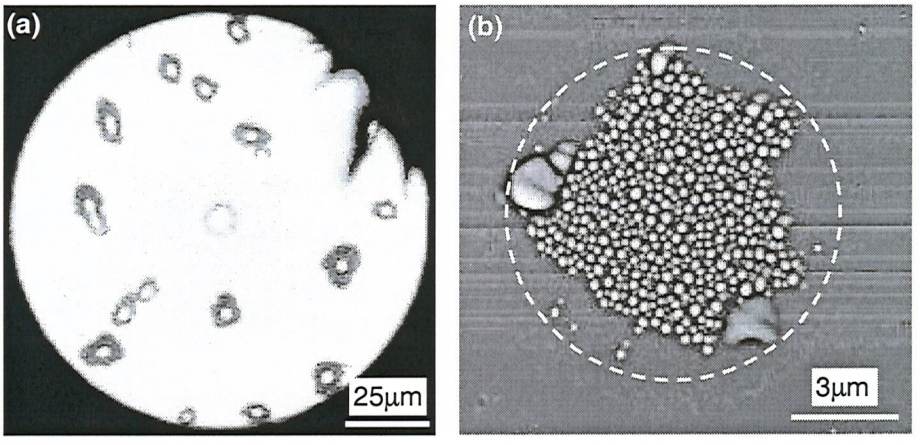

Figure 4.8: (a) Optical microscope image of a fibre tip on which gallium was deposited very slowly (~0.1 $nm.min^{-1}$) for six hours whilst it was at a temperature of ~100 K with laser pulses present in the core. Most of the gallium has coagulated into large blobs; (b) Atomic force microscope image of an area encompassing the fibre's core (dashed line). The nanoparticles have diameters of ~230 nm.

4.5 Light-assisted nanoparticle formation – Microscopic mechanisms

Having established the conditions required for the light-assisted self-assembly of gallium nanoparticles, consideration could be given to the mechanisms underlying this novel particle formation process.

Section 4.2 mentioned that several methods for manipulating the shape, size or size distribution of nanoparticles using lasers have been reported. However, only one of these involves actually controlling the growth of the particles [31]. (The others employ lasers to modify the characteristics of particles after they have been formed.) This control, over the axial ratio of silver nanoparticles on quartz, was achieved through laser-induced thermal evaporation of atoms from the particles' surfaces, initiated by nanosecond pulses with peak intensities in the $MW.cm^{-2}$ range.

In contrast, the mechanisms that control the growth of gallium nanoparticles must be non-thermal because the temperature increase in the particles, resulting from absorption of laser radiation, is too small for evaporation (thermal desorption) to be significant: By approximating the gallium nanoparticles to cylinders and numerically solving their thermal conductivity equation using the Green's function technique [35], V. A. Fedotov calculated that the maximum laser-induced temperature increase for the experimental conditions described above would be ~80 K (ignoring radiation losses and conduction in the plane of the substrate). The rate of thermal desorption is proportional to $\exp\{-E_g/k_bT\}$, where E_g is the activation energy for atomic desorption [36]. Given that the maximum value of k_bT is more than two orders of magnitude smaller than the activation energy for gallium (~2.7 eV) [37], laser heating has little effect on the evaporation rate.

The results of the experiments described in Section 4.4 therefore suggest that the following sequence of events takes place during the formation of gallium nanoparticles in a laser-illuminated area:

- Slow deposition of gallium on a cold silica substrate initially leads to the creation of small clusters through surface diffusion and nucleation [17, 38].

- The conditions (substrate temperature, deposition rate, gallium/silica wetting characteristics, etc.) are such that the clusters grow preferentially across the surface [17, 18, 39-41], increasing their aspect ratio (diameter:height) and filling factor (fraction of silica surface covered).

- As their volume and aspect ratio increase, those particles on the fibre's core interact more strongly with the laser radiation emanating from the core. The direction of their growth is subsequently controlled by non-thermal, laser-induced desorption [42-45].

To substantiate this theory, the optical absorption characteristics of the nanoparticles were numerically simulated, again using the model of cylindrical nanoparticles (See inset to Figure 4.9a), by V. A. Fedotov. Due to depolarization effects [46] and collective dipole-dipole interactions between the particles and the substrate [47, 48], the absorption cross-section of the nanoparticles [49] depends on the dielectric properties of both the substrate and the particle bulk material. It is also a function of the particles' size, filling factor and in particular, shape (i.e. aspect ratio). Absorption cross-sections were thus calculated for ensembles of cylindrical gallium particles on silica (See Figure 4.9). The phase of gallium in which the nanoparticles exist is not known but their dielectric parameters must lie between those of semi-metallic α-gallium, the stable bulk phase under normal conditions, and those of the amorphous solid phase, which is essentially a free-electron metal. Cross-sections were therefore calculated for these two limiting cases using dielectric coefficients for α-gallium from Kofman *et al.* [50], and for free-electron gallium from Hunderi and Ryberg [51]. (For α-gallium, the covalently bound dimers were assumed to be perpendicular to the substrate, as described in Section 2.5, although the results of these calculations were largely unaffected by changing the dimer orientation.)

In both cases, the absorption cross-section at 1.55μm increases rapidly with aspect ratio. Consequently, infrared laser excitation will couple more strongly to particles with larger aspect ratios, leading to an increased rate of atomic desorption from these particles.

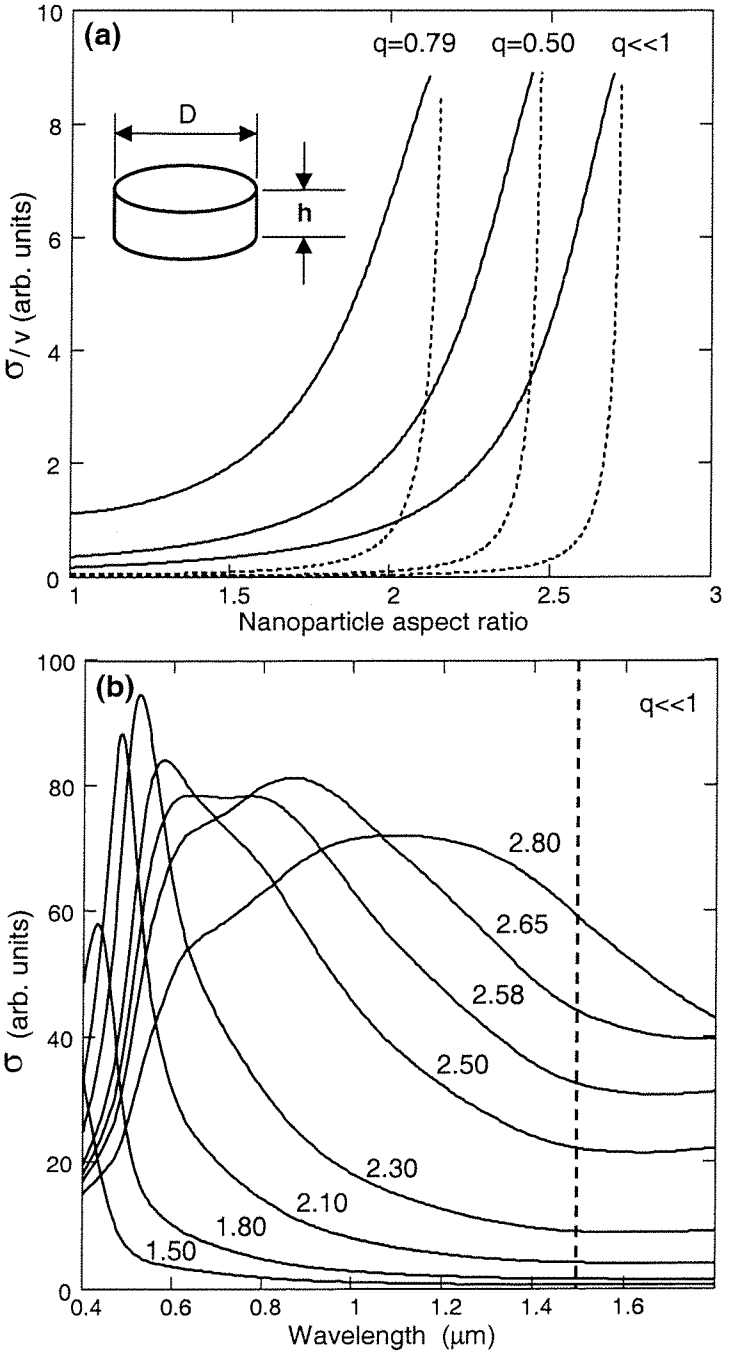

Figure 4.9: (a) Calculated optical absorption cross-section σ per unit volume V at 1.55 μm for cylindrical gallium particles on a silica substrate, plotted as a function of aspect ratio D/h (see inset) for different filling factors q. The solid and dashed lines correspond to the limiting cases of α- and free-electron gallium respectively; (b) Calculated spectral dependencies of the optical absorption cross-section σ of cylindrical α-gallium particles on a silica substrate. The different lines correspond to different aspect ratios for particles of a fixed height. Calculations were performed by V. A. Fedotov, the results are shown here for illustrative purposes.

In addition to this dependence on particle shape, the rate of non-thermal atomic desorption from metallic particles is known to be a function of particle size [42, 52]. This is because it depends on the electromagnetic field at a particle's surface, which in turn depends on the interplay between the particle's radius and the wavelength of the incident radiation [53]. Other factors (themselves dependent on particle shape and size) which can also affect the rate of desorption include the availability of desorption sites on the surface of a particle [42, 44, 54-56] and competition between desorption and other relaxation channels [42, 44]. Atoms are desorbed preferentially from low co-ordination number sites on a surface (edges, steps and other defects) where the excitation can overcome an atom's binding energy. As such sites are depleted, the rate of desorption falls dramatically. Furthermore, as a particle's morphology evolves, the proportion of the energy absorbed from a laser pulse that leads to desorption may change. For example, if a particle is of a certain size or aspect ratio, the energy may be converted more efficiently to heat and subsequently lost to the substrate by thermal conduction.

So, as the deposition of gallium proceeds in the presence of laser pulses and the small, low-aspect-ratio clusters grow, competition between the rates of deposition and desorption places constraints on their shape and size. A comparison of Figures 4.7c and 4.8b, wherein the particles are of roughly the same shape but different sizes, suggests that a shape (aspect ratio) limit is reached even within a half-hour deposition period, but that the particles can continue to increase in size for much longer.

One might ask what happens when deposition stops but laser excitation continues, and the balance between desorption and deposition is disturbed. Reflectivity measurements indicate that there is a small change in the optical properties of the nanoparticles during the minutes immediately after the atomic beam source is shut off (See Section 5.4). This suggests that desorption continues for a short time until the particles achieve a shape and size for which the rate of desorption is negligible if not zero. The complete process of desorption-controlled nanoparticle growth is summarised in Figure 4.10.

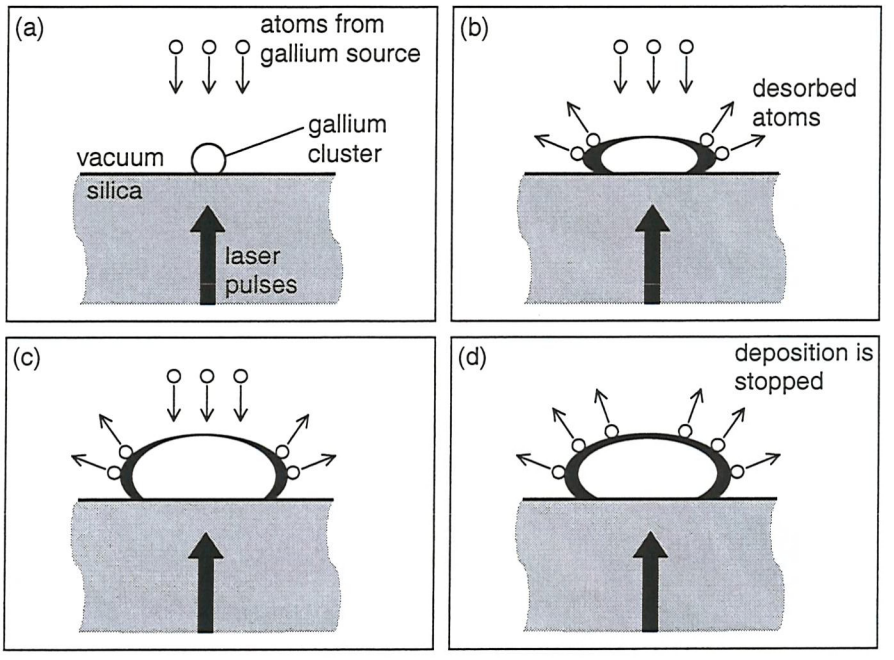

Figure 4.10: Schematic of the desorption-controlled growth process for gallium nanoparticles. (a) Initially, small, low-aspect-ratio clusters form. Their absorption cross-section is such that they interact very weakly, if at all, with the laser radiation. (b) The clusters grow across the substrate surface. As their aspect-ratio increases they interact more strongly with the laser pulses and the rate of desorption increases. Atoms are desorbed preferentially from the edges of the particle, thus limiting the aspect-ratio. (c) The particles continue to increase in size at a rate determined by the balance struck between the rates of deposition and desorption. (d) Deposition stops. Desorption continues for some time until the particles achieve a form for which the rate of desorption is close to (if not actually) zero.

The final shape of the nanoparticles is established when the fibre is removed from the vacuum chamber. At this stage, the gallium particles melt and atmospheric gases are adsorbed on their surfaces. As a result, they undergo morphological changes, evidenced by changes in the reflectivity of the fibre/nanoparticle interface (See Section 5.5), and adopt a shape determined by the gallium/air interfacial energy and the contact angle between liquid gallium and silica [57-60].

The non-thermal laser-induced desorption of atoms and ions from various metal and semiconductor particles, thin-films and surfaces has been extensively studied, and numerous models of the underlying microscopic mechanisms have been proposed [42-45, 53, 56, 61-64]. The consensus from these publications is that the absorption of photons leads to localised excitations at surface defect sites, from where desorption subsequently occurs.

The presence of covalently bound dimers and chains within gallium's α and β crystalline structures [65] may make it particularly susceptible to non-thermal laser-induced desorption. (Under normal conditions the β phase is metastable, but evidence suggests that it may be the preferred solid phase in nanoparticles [14].) The local stability of the crystalline structure can be significantly reduced by optical excitation of the covalent structures' bonding-antibonding transition. (They have an exceptionally broad absorption line [66], encompassing the 1.55 μm wavelength used in these experiments.) This may be expected to decrease the activation energy for desorption. Moreover, the presence of covalent structures could make gallium uniquely susceptible to another growth-control mechanism - 'laser-induced adsorption suppression', whereby the probability that new atoms (arriving from the atomic beam) will 'stick' to a particle is reduced when the crystalline structure at the particle's surface is in an optically excited state.

4.6 Summary and conclusions

A UHV gallium deposition system has been designed and constructed to enable the preparation and in-situ study of gallium interfaces. A series of deposition experiments have established that under certain conditions, the formation of gallium nanoparticles can be influenced by very low intensity light through non-thermal laser-induced desorption and/or adsorption suppression during the growth process.

It is expected that by changing the deposition conditions (atomic beam flux, substrate temperature, etc.) and laser excitation parameters (wavelength, power, etc.), the size, shape and spatial distribution of the nanoparticles could be controlled. Such experiments may provide some insight into the mechanisms of the growth-control processes. However, to gain a full understanding a dedicated study based on direct measurements of desorption rates and the kinetic energy distributions of desorbed atoms would be required.

If it does transpire that the light-assisted self-assembly process can produce gallium particles according to pre-determined size or spatial distribution requirements, they may find numerous and diverse applications (See Section 4.2), depending on their electrical, optical (See Chapter 5) and physical properties. Moreover, assuming that non-thermal laser-induced desorption is the main growth control mechanism, there is no apparent reason why the process could not be applied to other metal or semiconductor materials.

4.7 References

1 D. J. Maxwell, J. T. Krug II and S. Nie, Proc. SPIE **3913**, 112 (2000).

2 C. Sonnichsen, S. Geier, N. E. Hecker, G. von Plessen, J. Feldmann, H. Ditlbacher, B. Lamprecht, J. R. Krenn, F. R. Aussenegg, V. Z-H. Chan, J. P. Spatz and M. Moller, Appl. Phys. Lett. **77**, 2949 (2000).

3 L. Ansheng, A. Rahmani, G. W. Bryant, L. J. Richter and S. J. Stranick, J. Opt. Soc. Am. A **18**, 704 (2001).

4 S. Kirkpatrick, M. E. McHenry, M. DeGraef, P. A. Smith, Y. Nakamura, D. E. Laughlin, E. M. Brunsman, J. H. Scott and S. A. Majetich, Scr. Metall. Mater. **33**, 1703 (1995).

5 H. Ditlbacher, J. R. Krenn, B. Lamprecht, A. Leitner and F. R. Aussenegg, Opt. Lett. **25**, 563 (2000).

6 M. Quinten, A. Leitner, J. R. Krenn and F. R. Aussenegg, Opt. Lett. **23**, 1331 (1998).

7 H. R. Stuart and D. G. Hall, Appl. Phys. Lett. **69**, 2327 (1996).

8 H. R. Stuart and D. G. Hall, Appl. Phys. Lett. **73**, 3815 (1998).

[9] M. Haruta, Catal. Today **36**, 153 (1997).

[10] G. A. Somorjai, Appl. Surf. Sci. **121/122**, 1 (1997).

[11] J-P. Borel, Surf. Sci. **106**, 1 (1981).

[12] R. Garrigos, P. Cheyssac and R. Kofman, Z. Phys. D **12**, 497 (1989).

[13] A. A. Shvartsburg and M. F. Jarrold, Phys. Rev. Lett. **85**, 2530 (2000).

[14] A. Di Cicco, Phys. Rev. Lett. **81**, 2942 (1998).

[15] V. N. Bogomolov, A. I. Zadorozhnii, A. A. Kapanadze, E. L. Lutsenko and V. P. Petranovskii, Sov. Phys. Solid State **18**, 1777 (1976).

[16] V. A. Shchukin and D. Bimberg, Rev. Mod. Phys. **71**, 1125 (1999).

[17] H. Brune, Surf. Sci. Rep. **31**, 125 (1998).

[18] E. Sondergard, R. Kofman, P. Cheyssac and A. Stella, Surf. Sci. **364**, 467 (1996).

[19] A. Taleb, V. Russier, A. Courty and M. P. Pileni, Phys. Rev. B **59**, 13350 (1999).

[20] M. M. R. Evans and J. Nogami, Phys. Rev. B **59**, 7644 (1999).

[21] H. Brune, M. Giovannini, K. Bromann and K. Kern, Nature (London) **394**, 451 (1998).

[22] Z. Suo and W. Lu, J. Nanopart. Res. **2**, 333 (2000).

[23] D. Tonova, M. Patrini, P. Tognini, A. Stella, P. Cheyssac and R. Kofman, J. Phys.: Condens. Matter **11**, 2211 (1999).

[24] S. H. Baker, S. C. Thornton, A. M. Keen, T. I. Preston, C. Norris, K. W. Edmonds and C. Binns, Rev. Sci. Instrum. **68**, 1853 (1997).

[25] T. R. Jensen, M. D. Malinsky, C. L. Haynes and R. P. Van Duyne, J. Phys.

Chem. B **104**, 10549 (2000).

[26] F. Gonella, G. Mattei, P. Mazzoldi, E. Cattaruzza, G. W. Arnold, G. Battaglin, P. Calvelli, R. Polloni, R. Bertoncello and R. F. Haglund Jr., Appl. Phys. Lett. **69**, 3101 (1996).

[27] H. Kurita, A. Takami and S. Koda, Appl. Phys. Lett. **72**, 789 (1998).

[28] S. Y. Park, T. Isobe, M. Senna, R. A. Weeks and R. A. Zuhr, Appl. Phys. Lett. **73**, 2687 (1998).

[29] A. L. Stepanov, D. E. Hole, A. A. Bukharaev, P. D. Townsend and N. I. Nurgazizov, Appl. Surf. Sci. **136**, 298 (1998).

[30] J. Bosbach, D. Martin, F. Stietz, T. Wenzel and F. Trager, Appl. Phys. Lett. **74**, 2605 (1999).

[31] T. Wenzel, J. Bosbach, A. Goldmann, F. Stietz and F. Trager, Appl. Phys. B **69**, 513 (1999).

[32] *CRC Handbook of Chemistry and Physics*, 73rd edition (CRC Press Inc., Boca Raton, 1992).

[33] K. J. Ross, Vacuum **44**, 863 (1993).

[34] K. J. Ross and B Sonntag, Rev. Sci. Instrum. **66**, 4409 (1995).

[35] H. S. Carslaw and J. C. Jaeger, *Conduction of Heat in Solids*, 2nd edition (Clarendon Press, Oxford, 1959).

[36] M. Vollmer and F. Trager, Surf. Sci. **187**, 445 (1987).

[37] P. G. Strupp, A. L. Alstrin, B. J. Korte and S. R. Leone, J. Vac. Sci. Technol. A **10**, 508 (1992).

[38] B. Muller, L. Nedelmann, B. Fischer, H. Brune and K. Kern, Phys. Rev. B **54**, 17858 (1996).

[39] T. Wenzel, J. Bosbach, F. Stietz and F. Trager, Surf. Sci. **432**, 257 (1999).

[40] L. Holland, in *Vacuum deposition of thin films* (Chapman and Hall Ltd., London, 1963), p. 199-246.

[41] C. R. Henry, C. Chapon, C. Duriez and S. Giorigo, Surf. Sci. **253**, 177 (1991).

[42] W. Hoheisel, M. Vollmer and F. Trager, Phys. Rev. B **48**, 17463 (1993).

[43] I. Lee, T. A. Callcott and E. T. Arakawa, Phys. Rev. B **47**, 6661 (1993).

[44] J. R. Manson, M. Renger and H-G. Rubahn, Phys. Lett. A **224**, 121 (1996).

[45] D. P. Taylor and H. Helvajian, Surf. Sci. **451**, 68 (2000).

[46] V. I. Emel'yanov, E. M. Zemskov and V. N. Seminogov, Phys. Chem. Mech. Surf. **3**, 381 (1985).

[47] T. Yamaguchi, S. Yoshida and A. Kinbara, Thin Solid Films **21**, 173 (1974).

[48] T. Yamaguchi, S. Yoshida and A. Kinbara, Thin Solid Films **18**, 63 (1973).

[49] C. F. Bohren and D. R. Huffman, *Absorption and Scattering of Light by Small Particles* (Wiley, New York, 1983).

[50] R. Kofman, P. Cheyssac and J. Richard, Phys. Rev. B **16**, 5216 (1977).

[51] O. Hunderi and R. Ryberg, J. Phys. F **4**, 2096 (1974).

[52] M. Vollmer, R. Weidenauer, W. Hoheisel, U. Schulte and F. Trager, Phys. Rev. B **40**, 12509 (1989).

[53] R. Monreal and S. P. Apell, Phys. Rev. B **41**, 7852 (1990).

[54] T. Gotz, M. Bergt, W. Hoheisel, F. Trager and M. Stuke, Appl. Surf. Sci. **96-98**, 280 (1996).

[55] K. Ishikawa, J. Kanasaki, K. Tanimura and Y. Nakai, Solid State Commun. **98**, 913 (1996).

[56] K. Hattori, A. Okano, Y. Nakai and N. Itoh, Phys. Rev. B **45**, 8424 (1992).

[57] H. Graoui, S. Giorgio and C. R. Henry, Surf. Sci. **417**, 350 (1998).

[58] A-C. Shi, Phys. Rev. B **36**, 9068 (1987).

[59] S. Yoshida, T. Yamaguchi and A. Kinbara, J. Opt. Soc. Am. **61**, 463 (1971).

[60] M. Hida, A. Sakakibara and H. Kamiyabu, J. Jpn. Inst. Met. **53**, 1263 (1989).

[61] F. Blazer, R. Gerlach, J. R. Manson and H-G. Rubahn, J. Chem. Phys. **106**, 7995 (1997).

[62] Z. Wu, Phys. Lett. A **131**, 486 (1988).

[63] L. Chen, V. Liberman, J. A. O'Neill, Z. Wu and R. M. Osgood Jr., J. Vac. Sci. Technol. A **6**, 1426 (1988).

[64] G. S. Khoo, C. K. Ong and N. Itoh, Phys. Rev. B **47**, 2031 (1993).

[65] M. Bernasconi, G. L. Chiarotti and E. Tosatti, Phys. Rev. B **52**, 9988 (1995).

[66] X. G. Gong, G. L. Chiarotti, M. Parrinello and E. Tosatti, Phys. Rev. B **43**, 14277 (1991).

Chapter 5

Optical nonlinearity resulting from a light-induced structural transition in gallium nanoparticles

5.1 Synopsis

It has been found that gallium nanoparticles, prepared by light-assisted self-assembly, show a nonlinear response to low-power infrared optical excitation. Reversible reflectivity changes of several percent result from a light-induced structural transformation in the metal. The evidence suggests that both thermal and non-thermal excitation mechanisms contribute to the effect and that the 'ground-state' phase of the nanoparticles is not α-gallium.

In Section 5.3, the techniques used to investigate the optical properties of nanoparticles, both during and after the deposition process, are described. The results of these studies are presented in Sections 5.4 and 5.5. In light of these results, the potential mechanisms of nanoparticle metallization are discussed in Section 5.6.

5.2 Introduction

The study of metallic nanoparticles has a considerable history in linear and nonlinear optics [1], with current emphasis on the study of ultrafast response dynamics, size- and shape-dependent properties and collective optical effects [2-10]. As noted in Section 4.2,

confinement can significantly modify a material's properties and as such, given the right materials, the nanoparticle geometry has the potential to enable the development of nanoscale photonic devices [11]. Gallium may be one such material: Chapters 2 and 3 describe how, when the metal is confined at an interface with silica and held at a temperature close to its melting point, it responds dramatically to low-power optical excitation. Intensities of just a few $kW.cm^{-2}$ can reversibly modulate the intensity and phase of reflected light, by more than 30% and by several degrees respectively [12-15], as the result of a light-induced structural transition occurring in a layer of gallium just a few tens of nanometres thick. It may be that the modification of properties brought about by confining the metal in three dimensions rather than one (i.e. in nanoparticles rather than at an interface) could significantly improve the characteristics of gallium-based all-optical devices.

Experiments are described in this chapter that demonstrate for the first time that a light-induced structural transformation is the source of a large, and strongly temperature-dependent optical nonlinearity in gallium nanoparticles. The data indicate that the transformation does not involve gallium's α phase (the stable solid form of the bulk metal) but nevertheless leads to reflectivity changes of several percent in response to light intensities some four orders of magnitude smaller than those required for the observation of an ultrafast electronic nonlinearity [4]. The induced changes are fully reversible with a typical relaxation time of ~0.5 μs.

5.3 Measurement techniques

Previous experience with gallium suggested that any nonlinear optical response associated with light-induced metallization of gallium nanoparticles would be revealed by reflective pump-probe measurements. It was also anticipated that the evolution of the particles' linear and nonlinear optical properties with time and temperature might highlight the occurrence of significant changes in their morphology, reveal their phase composition and provide some insight into the mechanisms of any metallization

processes. Gallium nanoparticles, prepared directly on the ends of optical fibres using the light-assisted self-assembly process detailed in Chapter 4, were therefore subjected to such pump-probe measurements both during deposition, and in the temperature range from 100 to 320 K after deposition (without breaking the vacuum or physically disturbing the fibres in any way).

As described in Chapter 4, the growth of gallium nanoparticles was controlled by 1 μs, 17 nJ pulses from a 1.55 μm diode laser. By introducing a low power (0.8 mW at the input to the chamber), 1.31 μm cw diode laser alongside the pulsed laser (See Figure 5.1), it was possible to continuously probe the reflectivity of the fibre/nanoparticle interface. Reflectivity measurements were normalized against variations in laser output (via the laser's built-in monitor photodiode) and calibrated, using the reflectivity of the cleaved fibre tip as a reference point (the reflectivity of a silica/vacuum interface at 1.31 μm is 3.3%), prior to each deposition. In light of the considerable birefringence displayed by some of gallium's bulk crystalline phases, polarization controllers for both lasers were included in this fibre-optic reflectometer.

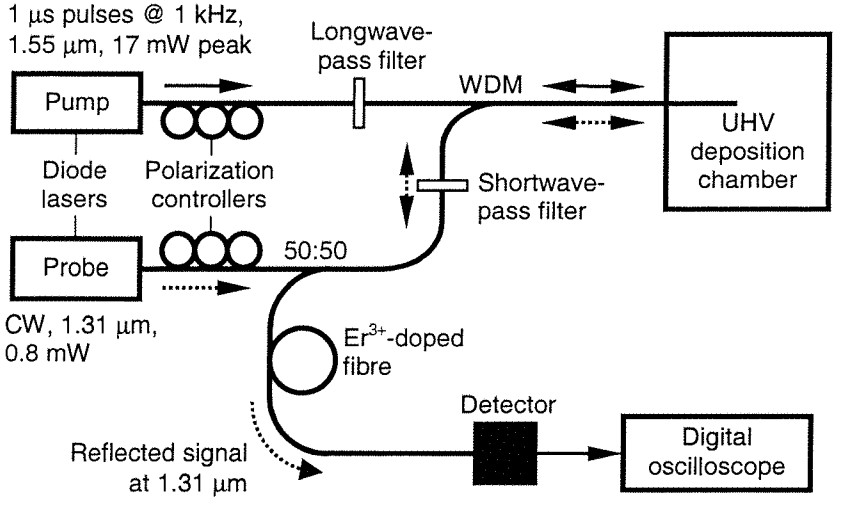

Figure 5.1: Schematic of the diode-laser/fibre-optic arrangement for light-assisted self-assembly of gallium nanoparticles and simultaneous interrogation of their optical properties. The WDM (Wavelength-Division Multiplexer) combines/splits signals at different wavelengths. The filters protect each laser from damage by reflected light from the other laser (built-in isolators protect them at their own wavelength). The combination of shortwave-pass filter and erbium-doped fibre stops reflected pump light from reaching the detector (Er^{3+} absorbs light at 1.55 μm).

Whilst controlling the growth of the nanoparticles, the pulsed laser also acted as a 'pump' - inducing changes in the particles' optical properties that manifested themselves as transient modulations of the reflected 1.31 μm signal intensity. This signal was separated from reflected pump light using a wavelength-division multiplexer, isolated further using optical filters (the 'pump leakage' signal generated at the detector was below the probe noise level), and recorded in real time using a digital storage oscilloscope. Data from the oscilloscope were collected alongside information on deposition time, substrate temperature and the reflectivity of the fibre tip by a purpose-written computer program. Details of the magnitude and relaxation time of pump-induced reflectivity changes were later derived from the oscilloscope traces (See Figure 5.2). The detection system had an overall bandwidth of 125 MHz.

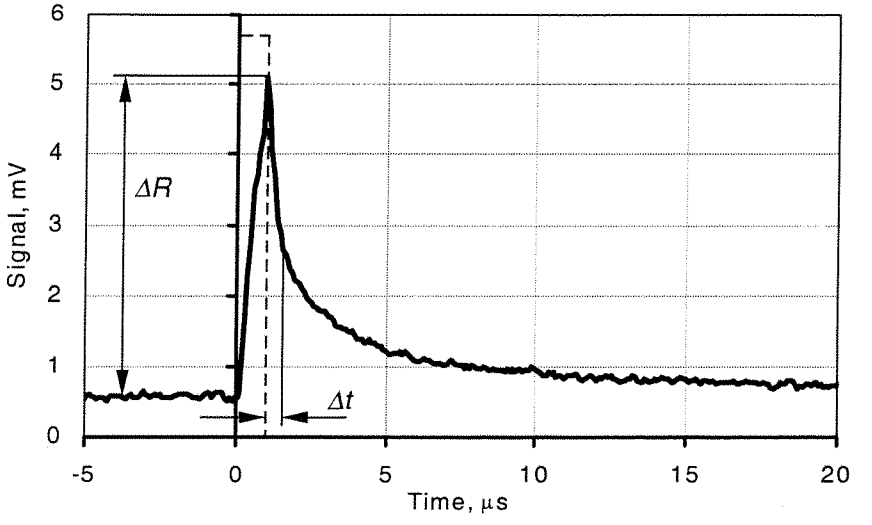

Figure 5.2: Typical oscilloscope trace showing pump-induced reflectivity change. The timing of the pump pulse is indicated by the dashed line. The magnitude (ΔR) and half-maximum relaxation time (Δt) are measured as shown.

5.4 Changes in optical properties during deposition

The numerical modelling of nanoparticle cross-sections described in Section 4.5 illustrates the fact that the particles' optical properties are highly dependent on their

shape and size. Consequently, the optical properties can be used as a diagnostic of particle development during the deposition process.

In a 'standard' particle formation experiment, gallium was deposited at a rate of ~0.3 nm.min^{-1} on fibres cooled to ~100 K for a period of 30 minutes. During this time the reflectivity of the fibre tip increases from 3.3 % to ~7 %, as shown in Figure 5.3.

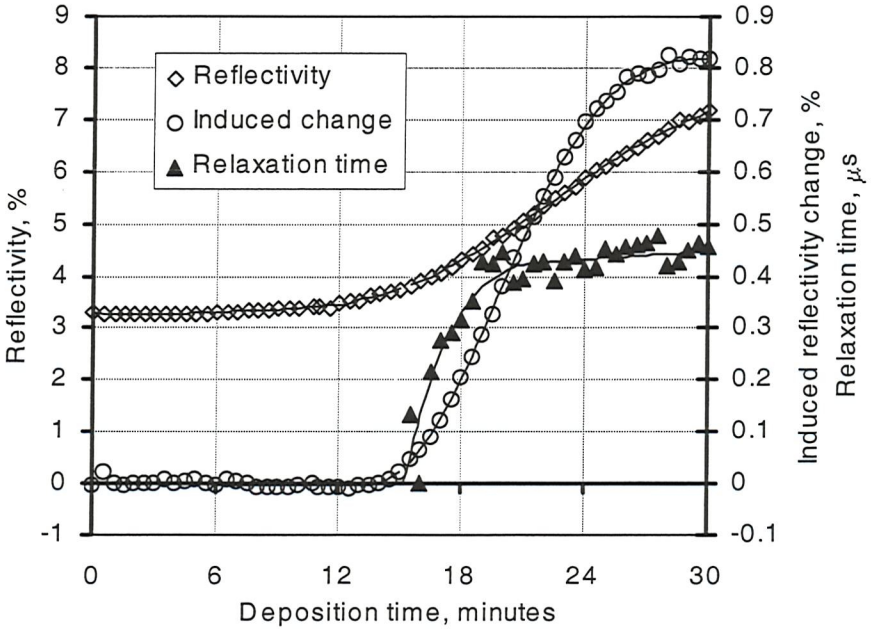

Figure 5.3: Reflectivity, pump-induced reflectivity change, and relaxation time of the induced change as functions of deposition time for a thirty minute period of gallium deposition undertaken at a rate of ~0.3 nm.min^{-1} on a fibre cooled to ~100K under vacuum (~10^{-6} mbar).

The reflectivity begins to increase as soon as gallium deposition begins. However, it is not until about fifteen minutes into the deposition that a pump-induced change in reflectivity is seen. At this point, the reflectivity also begins to increase more rapidly. These observations would both appear to support the theory (outlined in Section 4.5) that the particles must reach a certain size before they can interact with the laser radiation. The magnitude of the pump-induced change typically reaches ~0.8 % of the absolute reflectivity level. The sample oscilloscope trace in Figure 5.2 shows that the change is a cumulative effect, increasing throughout the duration of the pump pulse. After termination of the pulse, the change relaxes rapidly to its original level. This relaxation is a non-exponential process consisting of an initial sharp drop in reflectivity during the first few hundred nanoseconds, followed by a more gradual decrease over

several microseconds. The relaxation time, measured at half-maximum, is a strong function of the gallium layer's mass-thickness: When the induced change first emerges, about fifteen minutes into the deposition, the relaxation time is very short, beyond the instrumental resolution. Then, as the magnitude of the induced change increases, its relaxation time increases and assumes an almost constant value of ~0.5 μs. This behaviour may indicate the occurrence of subtle changes in the form of the particles: The shortest relaxation times are associated with particles whose size/shape is such that they only just give a nonlinear optical response. At this relatively early stage in their development, it may be that the particles' optical response places their crystalline structure under a certain amount of mechanical stress, which drives the relaxation process to occur faster than it otherwise would. As the size of the particles' increases and their shape evolves, this stress factor diminishes and the relaxation times increase [16].

Immediately after the end of deposition, when the gallium source is blocked but substrate temperature is maintained and pump-probe measurements continue, there is a very slight drop in the reflectivity of the fibre tip over a period of several minutes, after which it achieves a constant level. Such behaviour is almost imperceptible after just thirty minutes of deposition but is more clearly seen when a greater quantity of gallium is deposited over a period of several hours (Figure 5.4).

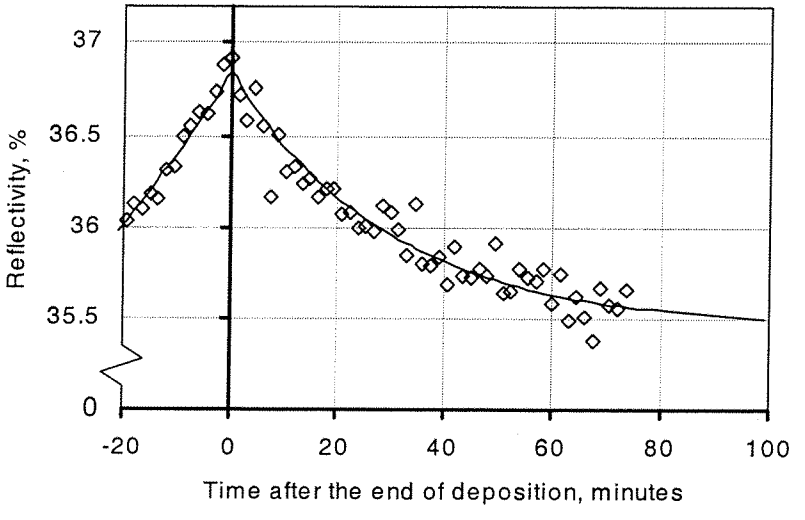

Figure 5.4: Reflectivity of a fibre/nanoparticle interface as a function of time after the end of a six-hour period of gallium deposition (deposition rate ~0.1 nm.min^{-1}).

This continued evolution of the reflectivity after termination of the atomic beam supports the hypothesis (described in Section 4.5) that desorption continues after deposition until the nanoparticles achieve a certain size or shape. This post-deposition reflectivity decrease leads to a proportionate small increase in the magnitude of the pump-induced reflectivity change. Relaxation times are unaffected.

5.5 Temperature-dependence of optical properties

After completion of the deposition process, the nanoparticles' optical properties continue to act as an indicator of changes in their morphology and phase composition. Without breaking the vacuum, the particles' temperature was scanned back and forth across the range between 100 and 320 K in anticipation of the fact that data on the temperature dependencies of the particles' reflectivity and nonlinear response would provide some insight into the microscopic mechanisms responsible for their behaviour.

The temperature was first increased from 100 K (the substrate temperature during deposition) to 320 K. During this heating process the reflectivity of the fibre tip increases erratically to a maximum at ~245 K then decreases slightly (See Figure 5.5a). At the same time, the magnitude ΔR of the pump-induced reflectivity change increases considerably, reaching a peak at ~170 K before falling to zero at ~200 K (Figure 5.5b). The relaxation time Δt (Figure 5.5c) also peaks at ~170 K, where it reaches ~16 μs, and then falls back to a fraction of a microsecond. The peaks in ΔR and Δt coincide with the point at which reflectivity begins to increase most rapidly with temperature, and the ΔR signal disappears as this rapid increase comes to an end.

The reflectivity changes are a consequence of both the nanoparticles' melting (i.e. the simple fact that liquid gallium is more reflective than the metal's solid phases [17, 18]) and the associated changes in their shape and surface filling-factor [19-23].

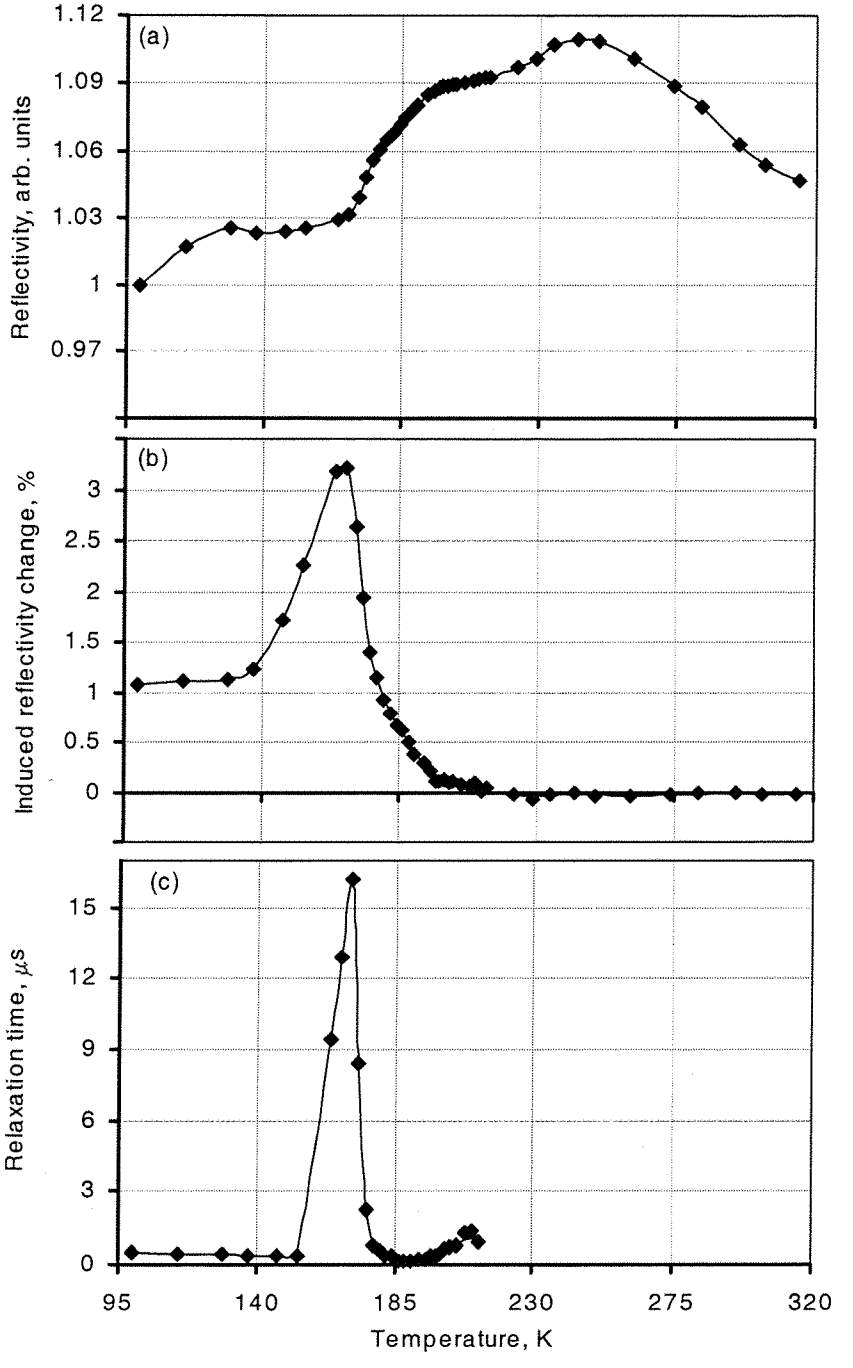

Figure 5.5: Temperature dependencies of (a) reflectivity, (b) induced reflectivity change and (c) relaxation time of the induced change during the first heating run after deposition.

After this 'first melting', a stable nanoparticle structure is formed and its properties behave in a reproducible manner as the temperature is cycled across the range from 100 to 320 K. Such cycling reveals that the reflectivity, the light-induced reflectivity change and its relaxation time all show hysteretic behaviour (see Figure 5.6).

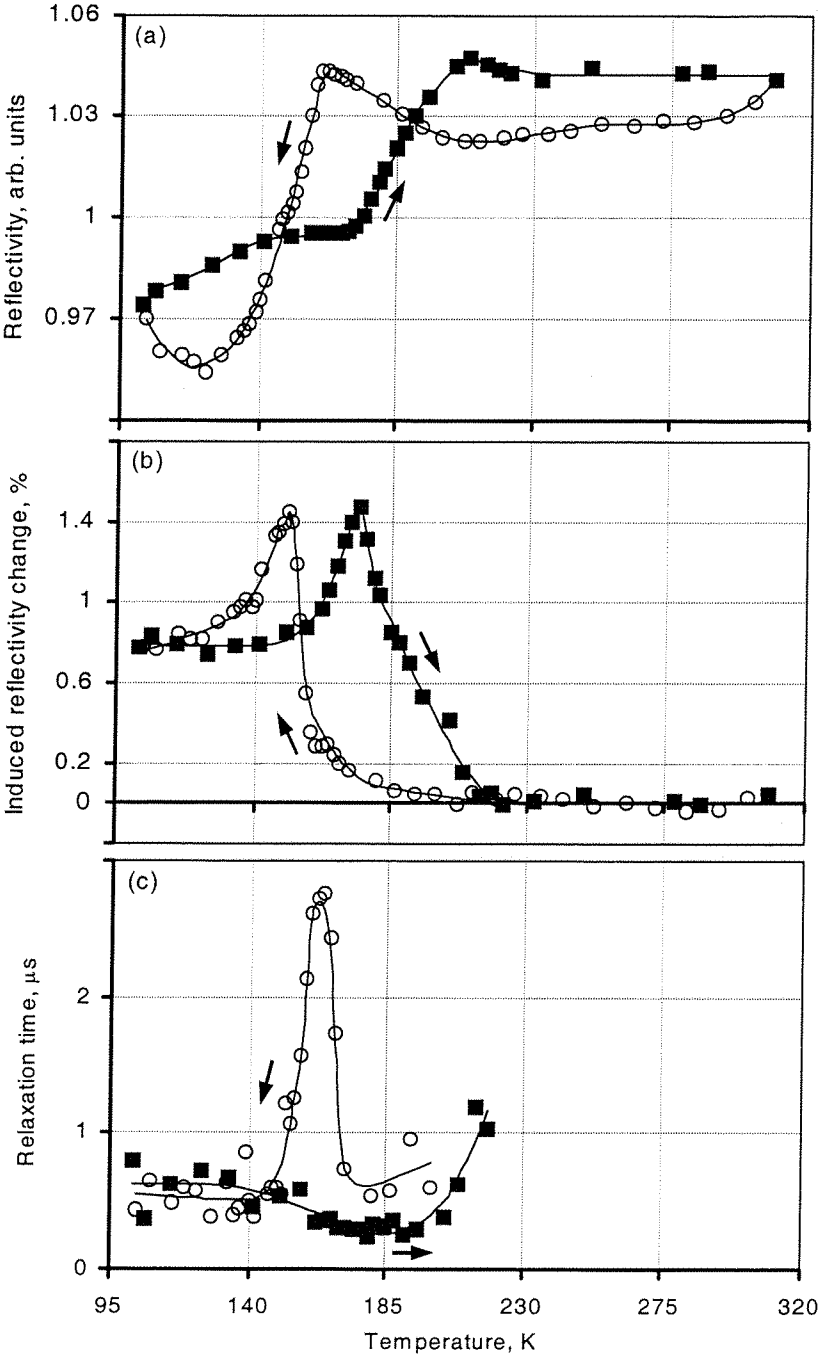

Figure 5.6: Typical temperature dependencies of (a) reflectivity, (b) induced reflectivity change and (c) relaxation time of the induced change for a complete temperature cycle after the first post-deposition heating run.

The reflectivity hysteresis observed during these temperature cycles (Figure 5.6a) is reminiscent of that seen around the solid-liquid transition point of bulk α-gallium at an interface with silica [12, 13]. However, there are some marked differences: Firstly, bulk α-gallium melts at 303 K and re-solidifies at ~300 K, giving a hysteresis with a width

of just a few degrees. In contrast, Figure 5.6a shows that the nanoparticles display a much wider hysteresis (~30 degrees) with smoother transitions at much lower temperatures (~185 and 155 K). It is known that the confinement of a material can suppress its melting and solidification temperatures (although not necessarily to the same extent) [24-27]. However, calculations (based on references 24 and 25) indicate that the melting point of gallium would only be suppressed by about 12 degrees in 50 nm particles - not enough to account for the observed value. Another difference between the properties of the nanoparticles and those of bulk α-gallium films is the height of the hysteresis loop: There is a 40% change in reflectivity (at 1.31 μm) when a bulk α-gallium film melts but Figure 5.6a indicates that the reflectivity of the nanoparticles changes by no more than ~7%. This discrepancy is too large to be accounted for simply by the fact that the nanoparticle layer is very thin, and suggests that α-gallium is not the ground-state (low-temperature) phase of the nanoparticles. Indeed, x-ray studies have detected the presence of several different crystalline phases in gallium nanoparticles [28]. A phase known as β-gallium was found to be the most abundant, and the metastable γ and δ phases were also seen to be present. All of these phases have lower bulk melting temperatures than α-gallium (β = 255 K, γ = 241 K and δ = 253 K) [29] and are more metallic (i.e. have optical properties closer to those of liquid gallium) [18]. Consequently, they are better able to account for the low transition temperatures and shallow hysteresis observed in the present study. The detailed form of the hysteresis curve is determined by factors such as the following:

- The nanoparticles' size distribution: Particles of different sizes will have different transition temperatures.

- The fact that the first order phase transitions of bulk materials become dynamic equilibria, more akin to second order transitions, in confined geometries [30]: In gallium's case, the hysteretic behaviour characteristic of first order transitions is still present but the abrupt structural transformations associated with such transitions are replaced by continuous evolutionary changes.

- Gallium's exceptional polymorphism: It is likely that the transition involves more than two phases [31]. Indeed, it has been suggested that even the melting of bulk gallium is in fact a sequence of transitions through different phases [32].

The pump-induced reflectivity change also shows a temperature hysteresis (Figure 5.6b), with pronounced peaks in both the increasing and decreasing temperature parts that coincide with the steepest sections of the corresponding reflectivity vs. temperature plot. This suggests that the induced changes are the consequence of a light-induced transition between the phases responsible for the reflectivity hysteresis. As discussed in Chapters 2 and 3, the optical nonlinearity of bulk gallium/silica interfaces is the result of light-induced interface metallization. The data presented above indicate that a similar process occurs in nanoparticles, i.e. optical excitation converts a relatively non-metallic solid phase, such as α- or β-gallium, to a more metallic phase, like the liquid. This metallization may take place on the nanoparticles' surfaces (leading to the formation of a metallic skin layer), or within the particles (creating metallic inclusions), or both (See Figure 5.7). The degree of metallization, and consequently the particles' reflectivity, is a function of temperature and incident light intensity.

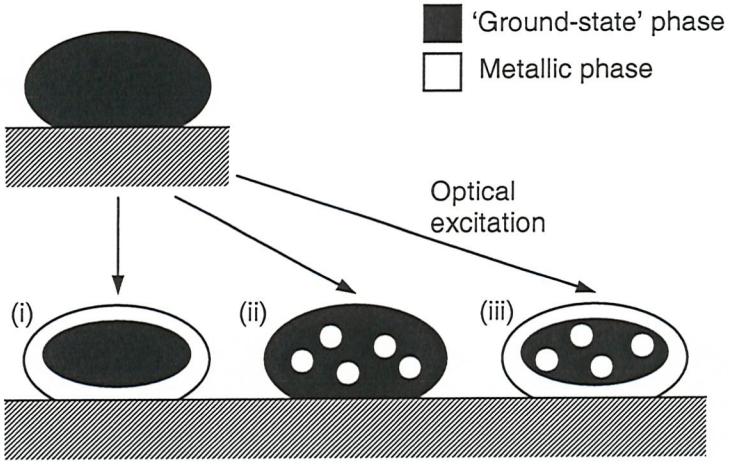

Figure 5.7: Schematic of possible nanoparticle metallization processes. Optical excitation may lead to the formation of: (i) a metallic shell; (ii) metallic inclusions; or (iii) both.

Changing the polarization state of the pump and probe beams was found to have no effect on the reflectivity of the fibre/nanoparticle interface or on the magnitude of pump-induced reflectivity changes. This implies either that the nanoparticles exist in

isotropic phases at all temperatures, or that if they are in an anisotropic phase at any stage, the crystalline structure is oriented differently in different particles such that collectively they are isotropic.

5.6 Mechanisms of nanoparticle metallization

The results presented in Sections 5.4 and 5.5 constitute the first observation of an optical nonlinearity associated with a light-induced structural transformation in gallium nanoparticles. The data collected have enabled the development of some ideas as to the microscopic mechanisms underlying the phenomenon.

Light-induced heating of the nanoparticles is possibly the most obvious potential explanation for their metallization. To make a simple assessment of this mechanism, one can plot the reflectivity change that would result from a laser-induced temperature increase ΔT.

Figure 5.8 demonstrates that this most basic model can reproduce many of the features seen in the experimental data. The position and magnitude of these features depend on the assumed value of ΔT, and best fits to the experimental peak magnitudes were obtained by using values of 7.55 K and 3.85 K for the increasing and decreasing temperature parts of the cycle respectively. The lower value of ΔT for decreasing temperatures may be expected because when they are in the highly-reflective liquid phase the particles absorb less of the incident energy.

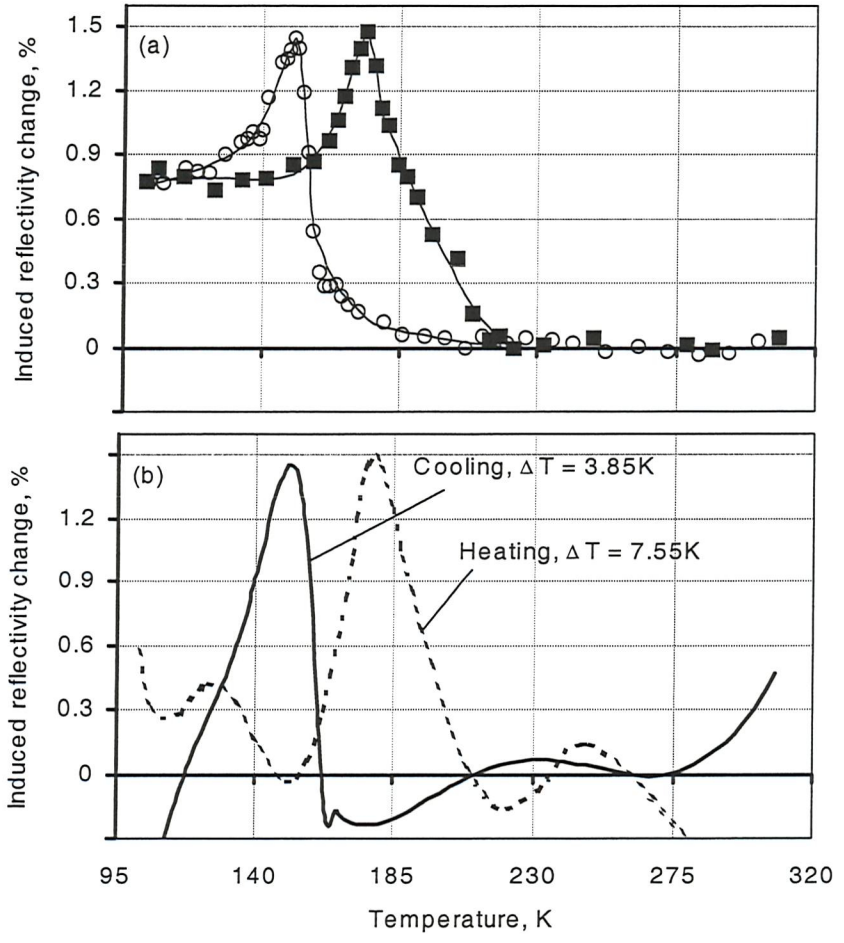

Figure 5.8: (a) Temperature dependence of induced reflectivity change for a complete temperature cycle, as shown in figure 5.6b; (b) Reflectivity change that would result from a laser-induced temperature increase ΔT. These curves are derived from the reflectivity data, shown in figure 5.6a, for the second heat-cool cycle after deposition.

These calculations demonstrate that a thermal mechanism can account for most of the experimental results, and the values of ΔT are not inconsistent with an upper estimate of 80 K for the laser-induced temperature increase (See Section 4.5). However, there are clear discrepancies between Figures 5.8a and b, primarily at low temperatures, where the magnitude of the induced change is constant but non-zero. This suggests that another, temperature-independent, non-thermal excitation mechanism may also be contributing to the effect.

The relaxation time data (Figure 5.6c) also indicate that there may be two metallization processes at work: Away from the phase transition temperatures the relaxation time (of

~0.5 μs) is independent of temperature and may be interpreted as the relaxation time of the non-thermal effect. However, near the transition points the relaxation times increase, indicating a more complex relaxation process. Similar behaviour is observed in gallium films (See Section 2.6) where it relates to the motion of the boundary between the metallic layer and the α phase. In nanoparticles it may relate to the motion of the interface between the particles' solid core and liquid shell. In Chapters 2 and 3 it was shown that the formation of a liquid gallium layer just a few nanometres thick can change the reflectivity of a bulk α-gallium/silica interface by several percent. It may be assumed that a liquid shell of similar thickness would produce changes in the reflectivity of solid nanoparticles comparable to those seen in the present experiment. The observed relaxation times, of between 0.5 and 3 μs, would therefore imply recrystalization velocities of around 1 $mm.s^{-1}$, a value consistent with previous experimental measurements [33, 34].

5.7 Summary and conclusions

A fiberized pump-probe reflectometer has been developed, for use in conjunction with the UHV deposition system described in Section 4.3, to study the optical properties of gallium nanoparticles formed by light-assisted self-assembly on the ends of optical fibres. The data, collected both during the deposition process and whilst varying the nanoparticles' temperature, have demonstrated for the first time that gallium nanoparticles show an optical nonlinearity as the result of a light-induced structural phase transition in the metal.

Like the nonlinearity observed at bulk gallium/silica interfaces, the effect has a hysteretic dependence on temperature and is enhanced near to the phase transition points. However, in contrast to the bulk geometry, where α-gallium is the 'ground-state' solid phase, the evidence suggests that in nanoparticles the α phase does not play a part, its place being taken by one (or a mixture) of gallium's other solid phases.

If conditions can be found under which the nanoparticles' nonlinear optical response is optimised, and they can be prepared in such a way that their properties are stable over extended periods of time (preferably at room temperature and pressure), they may find numerous applications in nanoscale photonic devices. The fact that the particles are inherently coupled to an optical waveguide (by virtue of the light-assisted self-assembly process) may prove to be an advantage when it comes to developing such applications, as might their lack of any (collective) polarization-dependent properties.

5.8 References

1 U. Kreibig and M. Vollmer, *Optical Properties of Metal Clusters* (Springer-Verlag, Berlin Heidelberg, 1995).

2 F. Stietz, J. Bosbach, T. Wenzel, T. Vartanyan, A. Goldmann and F. Trager, Phys. Rev. Lett. **84**, 5644 (2000).

3 M. Perner, S. Gresillon, J. Marz, G. von Plessen and J. Feldmann, Phys. Rev. Lett. **85**, 792 (2000).

4 M. Nisoli, S. Stagira, S. De Silvestri, A. Stella, P. Tognini, P. Cheyssac and R. Kofman, Phys. Rev. Lett. **78**, 3575 (1997).

5 K. Puech and W. J. Blau, J. Nanopart. Res. **3**, 13 (2001).

6 C. Voisin, D. Christofilos, N. Del Fatti, F. Vallee, B. Prevel, E. Cottancin, J. Lerme, M. Pellarin and M. Broyer, Phys. Rev. Lett. **85**, 2200 (2000).

7 T. V. Shahbazyan, I. E. Perakis and J-Y. Bigot, Phys. Rev. Lett. **81**, 3120 (1998).

8 B. Lamprecht, J. R. Krenn, A. Leitner and F. R. Aussenegg, Phys. Rev. Lett. **83**, 4421 (1999).

[9] T. Klar, M. Perner, S. Grosse, G. von Plessen, W. Spirkl and J. Feldmann, Phys. Rev. Lett. **80**, 4249 (1998).

[10] A. Taleb, V. Russier, A. Courty and M. P. Pileni, Phys. Rev. B **59**, 13350 (1999).

[11] N. I. Zheludev, Contemp. Phys., (In press).

[12] P. J. Bennett, S. Dhanjal, P. Petropoulos, D. J. Richardson, N. I. Zheludev and V. I. Emel'yanov, Appl. Phys. Lett. **73**, 1787 (1998).

[13] K. F. MacDonald, V. A. Fedotov, R. W. Eason, N. I. Zheludev, A. V. Rode, B. Luther-Davies and V. I. Emel'yanov, J. Opt. Soc. Am. B **18**, 331 (2001).

[14] K. F. MacDonald, V. A. Fedotov, N. I. Zheludev, B. V. Zhdanov and R. J. Knize, Appl. Phys. Lett. **79**, 2375 (2001).

[15] P. Petropoulos, H. S. Kim, D. J. Richardson, V. A. Fedotov and N. I. Zheludev, Phys. Rev. B **64**, 193312 (2001).

[16] V. I. Emel'yanov (private communication).

[17] N. R. Comins, Phil. Mag. **25**, 817 (1972).

[18] M. Bernasconi, G. L. Chiarotti and E. Tosatti, Phys. Rev. B **52**, 9988 (1995).

[19] J. C. Heyraud and J. J. Metois, Surf. Sci. **128**, 334 (1983).

[20] M. Hida, A. Sakakibara and H. Kamiyabu, J. Jpn. Inst. Met. **53**, 1263 (1989).

[21] S. Yoshida, T. Yamaguchi and A. Kinbara, J. Opt. Soc. Am. **61**, 463 (1971).

[22] C. Jayaram, R. Ravi and R. P. Chhabra, Chem. Phys. Lett. **341**, 179 (2001).

[23] C. F. Bohren and D. R. Huffman, *Absorption and Scattering of Light by Small Particles* (Wiley, New York, 1983).

[24] Ph. Buffat and J-P. Borel, Phys. Rev. A **13**, 2287 (1976).

[25] E. V. Charnaya, C. Tien, K. J. Lin and Yu. A. Kumzerov, J. Phys.: Condens. Matter **10**, 7273 (1998).

[26] G. L. Allen, R. A. Bayles, W. W. Gile and W. A. Jesser, Thin Solid Films **144**, 297 (1986).

[27] R. S. Berry, J. Jellinek and G. Natanson, Chem. Phys. Lett. **107**, 227 (1984).

[28] A. Di Cicco, Phys. Rev. Lett. **81**, 2942 (1998).

[29] L. Bosio, J. Chem. Phys. **68**, 1221 (1978).

[30] R. S. Berry and B. M. Smirnov, J. Chem. Phys. **113**, 728 (2000).

[31] Y. Oshima and K. Takayanagi, Z. Phys. D **27**, 287 (1993).

[32] H. G. von Schnering and R. Nesper, Acta Chem. Scand. **45**, 870 (1991).

[33] V. T. Borisov and Yu. E. Matveev, Sov. Phys. Crystallogr. **14**, 765 (1970).

[34] S. D. Peteves and R Abbaschian, Met. Trans. **22A**, 1259 (1991).

Chapter 6

Summary and future work

6.1 Summary

The nonlinear optical response of bulk α-gallium/glass interfaces, prepared by ultrafast pulsed laser deposition, has been studied under pulsed and quasi-cw laser excitation regimes at a range of wavelengths (See Chapters 2 and 3). Reflectivity changes of up to 35% are observed in response to continuous excitation intensities of just a few $kW.cm^{-2}$ or pulse energies of a few $mJ.cm^{-2}$. Femtosecond pump-probe measurements have demonstrated that the fastest component of the nonlinearity has a response time of ~4 ps. The nonlinearity is a consequence of light-induced, surface-assisted metallization of α-gallium at the interface and the results of these experiments have enabled the development of quantitative theories to describe the microscopic processes underlying the effect. Two mechanisms contribute to the metallization of gallium, one thermal and one non-thermal: For excitation pulses lasting less than a few nanoseconds, thermal diffusion does not have enough time to remove heat from the skin layer during the pulse. The temperature at the excitation point increases, inevitably leading to thermal melting of the metal. For longer pulses and cw excitation, laser-induced heating is insufficient to cause melting and metallization occurs through optical excitation of the bonding-antibonding transition associated with gallium dimers in the α structure.

A novel, light-assisted self-assembly technique for the preparation of gallium nanoparticles has been developed (See Chapter 4). Particles with a relatively narrow

size distribution can be formed by illuminating substrates with low intensity laser light during deposition. Control over nanoparticle size and shape is achieved through a combination of non-thermal light-induced processes. This technique has been employed in a purpose-built UHV system to grow gallium nanoparticles directly on the ends of optical fibres, so that their optical properties could be studied in-situ, both during and after the deposition process. These studies have shown that, as in bulk α-gallium films, a light-induced structural transformation can form the basis of a significant optical nonlinearity in gallium nanoparticles (See Chapter 5). Reversible reflectivity changes of several percent are induced by $kW.cm^{-2}$ light intensities. As in bulk gallium films, the magnitude of this effect shows a temperature hysteresis and is enhanced near the phase transition points. The experimental results suggest that both thermal and non-thermal metallization processes contribute to the response, and that the 'ground state' solid phase of the particles is not α-gallium but rather one, or a mixture, of the metal's other crystalline phases.

6.2 Future work

Following the success of the broadband nanosecond pump-probe experiments preformed in collaboration with the US Air Force Academy, the research group in Southampton has gained funding from the EPSRC to perform a comprehensive study of the spectral characteristics and nanosecond dynamics of gallium's nonlinearity. This project will concentrate on gallium/semiconductor rather than gallium/glass interfaces because they promise much larger contrast ratios between the high and low reflectivity states.

Numerous avenues of investigation may be followed in relation to the light-assisted self-assembly of gallium nanoparticles. A systematic study of the way in which the various deposition and laser excitation parameters affect the resulting nanostructures may provide some insight into the mechanisms through which control of particle growth is achieved. Beyond this, the technique might be applied to different materials

or implemented in different geometrical configurations. These approaches may, for example, enable the formation of single particles or the preparation of nanoparticles directly on the surfaces of optoelectronic components (e.g. the output surface of a diode laser).

The optical nonlinearity of gallium nanoparticles is the subject of ongoing investigations. The phenomenon will have to be investigated under various regimes of optical excitation, across a broad range of temperatures, and perhaps at several different wavelengths, if the phase composition and metallization processes are to be understood. Having demonstrated that gallium nanoparticles formed by light-assisted self-assembly show a nonlinear optical response, the research team in Southampton has also won funding from the EPSRC to study this effect in single nanoparticles, and to develop the theoretical understanding of nonlinearities resulting from light-induced structural transitions in nanoparticles.

Appendix A

Calculating metallic film thickness from reflectivity data

The thickness of the metallic gallium layer present at an α-gallium/glass interface was calculated from experimental reflectivity data using an iterative process based on an expression, derived by Bennett [1] (and subsequently corrected for typographic errors), for the normal-incidence reflectivity of a layered structure (see figure A1).

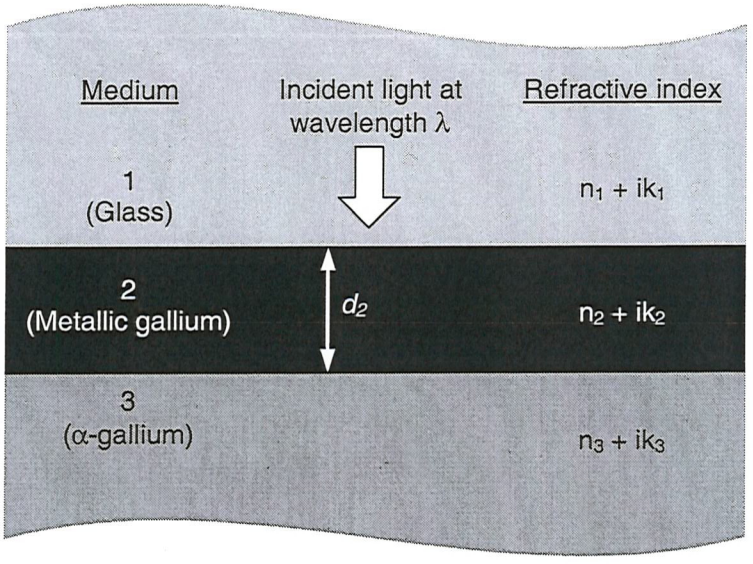

Figure A1: Layered structure for which normal-incidence reflectivity is calculated in terms of the components' refractive indices.

$$\text{Reflectivity, } R = \frac{Ae^{\frac{4\pi d_2 k_2}{\lambda}} + Be^{\frac{-4\pi d_2 k_2}{\lambda}} - 2\sqrt{AB}\cos C}{e^{\frac{4\pi d_2 k_2}{\lambda}} + ABe^{\frac{-4\pi d_2 k_2}{\lambda}} - 2\sqrt{AB}\cos E}$$

Where:
$$A = \frac{(n_1 - n_2)^2 + (k_1 - k_2)^2}{(n_1 + n_2)^2 + (k_1 + k_2)^2}$$

$$B = \frac{(n_2 - n_3)^2 + (k_2 - k_3)^2}{(n_2 + n_3)^2 + (k_2 + k_3)^2}$$

$$C = \arctan\left(\frac{2(n_1 k_2 - n_2 k_1)}{(n_1^2 - n_2^2 + k_1^2 - k_2^2)}\right) - \arctan\left(\frac{2(n_2 k_3 - n_3 k_2)}{(n_2^2 - n_3^2 + k_2^2 - k_3^2)}\right) + \frac{4\pi\, d_2 n_2}{\lambda}$$

$$E = \arctan\left(\frac{2(n_1 k_2 - n_2 k_1)}{(n_1^2 - n_2^2 + k_1^2 - k_2^2)}\right) + \arctan\left(\frac{2(n_2 k_3 - n_3 k_2)}{(n_2^2 - n_3^2 + k_2^2 - k_3^2)}\right) - \frac{4\pi\, d_2 n_2}{\lambda}$$

A computer program was composed to calculate values of d_2 (to the nearest 0.1 nm) from experimental reflectivity data R_{exp}, according to the following iterative algorithm:

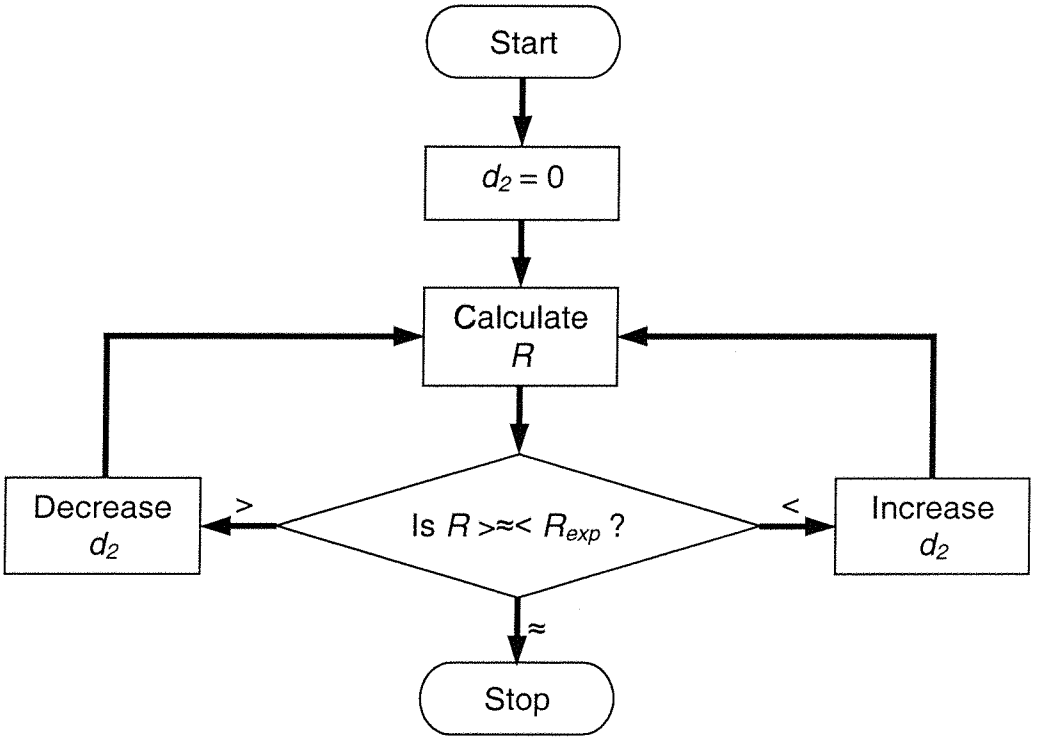

References

1 P. J. Bennett, Ph.D. thesis, University of Southampton, 1998.

Appendix B

Atomic force microscopy

The essential elements of an atomic force microscope are shown in Figure B1. A sharp tip on the end of a cantilever spring is raster-scanned across the surface of a sample and the cantilever deflects in response to atomic force variations between the tip and the sample. The deflection is monitored using a laser beam (reflected from the top of the cantilever) and a segmented detector. By plotting deflection against tip position, a topographical map of the sample is built up.

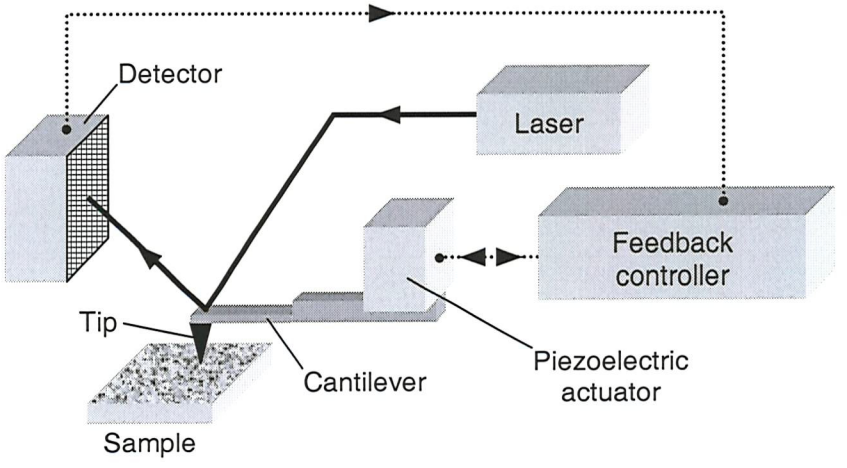

Figure B1: Schematic diagram of the essential components of the atomic force microscope.

AFM images should however be used with caution. The dimensions of the tip are comparable to, if not larger than, those of the structures being probed. Consequently, the dimensions of structures can be significantly overestimated in the plane of the sample surface, as shown by Figure B2.

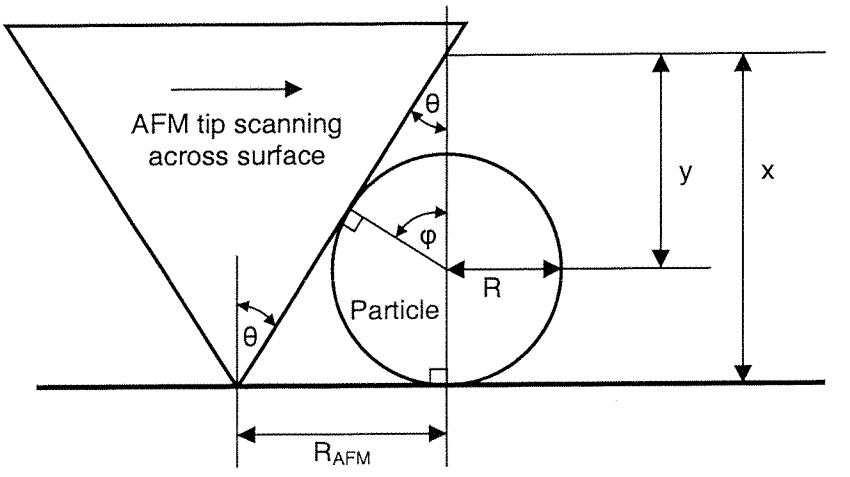

Figure B2: Schematic of pyramidal AFM tip interaction with a spherical particle of radius R. Due to the shape and finite size of the tip, the AFM "sees" a roughly hemispherical particle with radius R_{AFM}.

The extent to which dimensions are exaggerated can be estimated as follows:

From Figure B2: $\tan\theta = \frac{R}{x}$, $x = r + y$ and $\sin\theta = \frac{r}{y}$

So $$\tan\theta = \frac{R}{r+y} = \frac{R}{r+\frac{r}{\sin\theta}} = \frac{R}{r\left(1+\frac{1}{\sin\theta}\right)}$$

Therefore $$\frac{R}{r} = \tan\theta\left(1+\frac{1}{\sin\theta}\right)$$

The studies of gallium nanostructures reported in Chapter 4 were performed using Burleigh Vista non-contact silicon probes. These have pyramidal tips with a height:base ratio of 1:1 and an end radius of ~0.1 nm, giving θ a value of ~26.6°. Particle diameters are subsequently overestimated by a factor of ~1.6. So, for example, the 80 nm particles shown in Figure 4.7c actually have diameters of ~50 nm. In spite of this instrumental problem, particle size distributions can still be determined accurately and the images are an invaluable diagnostic tool.

Appendix C

Refereed publications

Reprints of the following articles are included in this appendix by permission of the relevant copyright holders (See individual citations).

1. **Optical control of gallium nanoparticle growth.**
   K. F. MacDonald, V. A. Fedotov, S. Pochon, K. J. Ross, G. C. Stevens, N. I. Zheludev, W. S. Brocklesby and V. I. Emel'yanov, *Applied Physics Letters* **80**, 1643-1645 (2002). Copyright (2002) by the American Institute of Physics.

2. **Structural phase transition as a mechanism for broadband, low-threshold reflectivity switching in gallium.**
   K. F. MacDonald, V. A. Fedotov, N. I. Zheludev, B. V. Zhdanov and R. J. Knize, *Applied Physics Letters* **79**, 2375-2377 (2001). Copyright (2001) by the American Institute of Physics.

3. **Nanosecond dynamics of a gallium mirror's light-induced reflectivity change.**
   V. Albanis, S. Dhanjal, V. A. Fedotov, K. F. MacDonald, N. I. Zheludev, P. Petropoulos, D. J. Richardson and V. I. Emel'yanov, *Physical Review B* **63**, 165207 (2001). Copyright (2000) by the American Physical Society.

4. **Dynamics of light-induced reflectivity switching in gallium films deposited on silica by pulsed laser ablation.**
   A. V. Rode, M. Samoc, B. Luther-Davies, E. G. Gamaly, K. F. MacDonald, and N. I. Zheludev, *Optics Letters* **26**, 441-443 (2001). Copyright (2001) by the Optical Society of America.
   N.B. Throughout this paper, 'Si' should be read as 'silica'.

5. **Light-induced metallization in laser-deposited gallium films.**
   K. F. MacDonald, V. A. Fedotov, R. W. Eason, N. I. Zheludev, A. V. Rode, B. Luther-Davies, and V. I. Emel'yanov, *Journal of the Optical Society of America B* **18**, 331-334 (2001). Copyright (2001) by the Optical Society of America.

6. **Light-induced structural transformations and optical nonlinearity in gallium nano-films and self-assembled nanoparticles.** (Invited)
   K. F. MacDonald, V. A. Fedotov, G. Stevens, S. Pochon, V. I. Emel'yanov, W. S. Brocklesby and N. I. Zheludev, in *XVII International Conference on Coherent and Nonlinear Optics, Technical digest* (2001), paper WK2.

7. **Optical switching with self-assembled gallium nanoparticles on the tip of an optical fiber.**
   K. F. MacDonald, W. S. Brocklesby, V. A. Fedotov, S. Pochon, K. J. Ross, G. Stevens and N. I. Zheludev, in *CLEO/Europe-EQEC Focus Meetings 2001, Conference Digest* (European Physical Society, 2001), p. 177.

8. **Nanoscale light-induced phase transformation in alpha-gallium as the source of a broadband optical nonlinearity.**
   K. F. MacDonald, V. A. Fedotov, N. I. Zheludev, B. V. Zhdanov and R. J. Knize, in *Conference on Lasers and Electro-optics 2001, Technical digest* (Optical Society of America, Washington D. C., 2001), paper CTuP4. Copyright (2001) by the Optical Society of America.

9. **Gigantic broadband optical nonlinearity in gallium films deposited by ultrafast laser ablation.**
V. Albanis, V. A. Fedotov, K. F. MacDonald, V. I. Emel'yanov, N. I. Zheludev, R. J. Knize, B. V. Zhdanov and A. V. Rode, in *CLEO/Europe 2000, Technical digest* (IEEE, 2000), paper QTuE28. Copyright (2000) by the IEEE.

10. **Gigantic optical nonlinearity in laser-deposited gallium films on the verge of a structural phase transition.** (Invited)
K. F. MacDonald, N. I. Zheludev, K. Puech, L. Lefort, D. C. Hanna, A. V. Rode, B. Luther-Davies and V. I. Emel'yanov, in *Quantum Electronics and Laser Science 2000, Technical Digest* (Optical Society of America, Washington D. C., 2000), paper QThG3. Copyright (2000) by the Optical Society of America.

11. **The light-induced structural phase transition in confining gallium and its photonic applications.**
V. Albanis, S. Dhanjal, K. F. MacDonald, P. Petropoulos, H. L. Offerhaus, D. J. Richardson, A. V. Rode and N. I. Zheludev, in *Proceedings of the International Conference on Luminescence 1999*, Journal of Luminescence **87-89**, 646-648 (2000). Copyright (2000) by Elsevier Science.

12. **Broadband optical switching in confined gallium at milliwatt power levels.**
S. Dhanjal, K. F. MacDonald, P. Petropoulos, D. J. Richardson and N. I. Zheludev, in *Conference on Lasers and Electro-optics 1999, Technical digest* (Optical Society of America, Washington D. C., 1999), paper CWF50. Copyright (1999) by the Optical Society of America.

The following published papers were included in the bound thesis. These have not been digitised due to copyright restrictions, but their doi or reference are provided.

MacDonald, K. F., Fedotov, V. A., Pochon, S., Ross, K. J., Stevens, G. C., Zheludev, N. I., … Emel'yanov, V. I. (2002). Optical control of gallium nanoparticle growth. Applied Physics Letters, 80(9), 1643–1645. Available at: http://dx.doi.org/10.1063/1.1456260

MacDonald, K. F., Fedotov, V. A., Zheludev, N. I., Zhdanov, B. V., & Knize, R. J. (2001). Structural phase transition as a mechanism for broadband, low-threshold reflectivity switching in gallium. Applied Physics Letters, 79(15), 2375–2377. Available at: http://dx.doi.org/10.1063/1.1409335

Albanis, V., Dhanjal, S., Fedotov, V. A., MacDonald, K. F., Zheludev, N. I., Petropoulos, P., … Emel'yanov, V. I. (2001). Nanosecond dynamics of a gallium mirror's light-induced reflectivity change. Physical Review B, 63(16). Available at: http://dx.doi.org/10.1103/physrevb.63.165207

Rode, A. V., Samoc, M., Luther-Davies, B., Gamaly, E. G., MacDonald, K. F., & Zheludev, N. I. (2001). Dynamics of light-induced reflectivity switching in gallium films deposited on silica by pulsed laser ablation. Optics Letters, 26(7), 441. Available at: http://dx.doi.org/10.1364/ol.26.000441

MacDonald, K. F., Fedotov, V. A., Eason, R. W., Zheludev, N. I., Rode, A. V., Luther-Davies, B., & Emel'yanov, V. I. (2001). Light-induced metallization in laser-deposited gallium films. Journal of the Optical Society of America B, 18(3), 331. Available at: http://dx.doi.org/10.1364/josab.18.000331

MacDonald, K.F., Fedotov, V.A., Stevens, G.C., Pochon, S., Emel'yanov, V.I., Brocklesby, W.S. and Zheludev, N.I. (2001) Light-induced structural transformations and optical nonlinearity in gallium nano-films and self-assembled nanoparticles. At ICONO 2001: XVII International Conference on Coherent and Nonlinear Optics ICONO 2001: XVII International Conference on Coherent and Nonlinear Optics, Belarus. 26 Jun - 01 Jul 2001.

MacDonald, K.F., Brocklesby, W.S., Fedotov, V.A., Pochon, S., Ross, K.J., Stevens, G.C. and Zheludev, N.I. (2001) Optical switching with self-assembled gallium nanoparticles on the tip of an optical fiber. At Conference on Lasers and Electro-Optics - Europe / European Quantum Electronics Conference Conference on Lasers and Electro-Optics - Europe / European Quantum Electronics Conference, Germany.

MacDonald, K.F., Fedotov, V.A., Zheludev, N.I., Zhdanov, B.V. and Knize, R.J. (2001) Nanoscale light-induced phase transformation in alpha-gallium as the source of a broadband optical nonlinearity. At Conference on Lasers and Electro-Optics '01

Conference on Lasers and Electro-Optics '01, United States. 06 - 11 May 2001. Available at: http://dx.doi.org/10.1109/cleo.2001.947720

Albanis, V., Fedotov, V. A., MacDonald, K. F., Emelyanov, V. I., Zheludev, N. I., Knize, R. J., … Rode, A. V. (n.d.). Gigantic broadband optical nonlinearity in gallium films deposited by ultrafast laser ablation. Conference Digest. 2000 International Quantum Electronics Conference (Cat. No.00TH8504). Available at: http://dx.doi.org/10.1109/iqec.2000.907841

MacDonald, K.F., Zheludev, N.I., Puech, K., Lefort, L., Hanna, D.C., Rode, A.V., Luther-Davies, B. and Emelyanov, V.I. (2000) Gigantic optical nonlinearity in laser-deposited gallium films on the verge of a structural phase transition. At *Quantum Electronics and Laser Science 2000* Quantum Electronics and Laser Science 2000. 07 - 12 May 2000. Available from: https://eprints.soton.ac.uk/16963/1/14968.pdf

Albanis, V., Dhanjal, S., MacDonald, K., Petropoulos, P., Offerhaus, H. ., Richardson, D. ., … Zheludev, N. . (2000). The light-induced structural phase transition in confining gallium and its photonic applications. Journal of Luminescence, 87-89, 646–648. Available at: http://dx.doi.org/10.1016/s0022-2313(99)00340-3

Dhanjal, S., MacDonald, K. F., Petropoulos, P., Richardson, D. J., & Zheludev, N. I. (n.d.). Broadband optical switching in confined gallium at milliwatt power levels. Technical Digest. Summaries of Papers Presented at the Conference on Lasers and Electro-Optics. Postconference Edition. CLEO '99. Conference on Lasers and Electro-Optics (IEEE Cat. No.99CH37013). Available at: http://dx.doi.org/10.1109/cleo.1999.834194